Doctoral Dissertation

Numerical Computation and Analysis for Hydroelasticity of Ship with Forward Speed by Using Orthogonal Polynomials and Cubic B-spline Functions

HONG YANG

June 2022

Dept. of Naval Architecture & Ocean Engineering
Division of Global Architecture
Graduate School of Engineering
Osaka University

Abstract

In the past decade, larger ships have been built with increasing commercial needs of ocean transport and keep relatively high sail speed balanced between economic effectiveness and environmental protection so that ships become more flexible and associated accidents are prone to occur because higher encounter wave frequency approaches the natural frequency of elastic ship motions. A linear spectral approach just for rigid-body motions no longer gives a reliable prediction of fatigue load, since wave-induced vibrations, commonly referred to as springing and whipping, can aggravate the fatigue damage of very large ships. Therefore, to compute wave-induced hydroelastic responses with sufficient accuracy gradually becomes of practical importance in naval engineering. For hydroelastic analysis, the structural deflection and hydrodynamic response of flexible ships or VLFS are fully coupled. An analysis of structural deflection is widely applied to define a special set of natural mode shapes, which correspond to the actual elastic deflections of the body in a specified physical context with free ends. This is difficult for hydroelastic analysis, where the mode shapes are affected by the hydrodynamic pressure field and cannot be specified in advance. This problem can be avoided if the structural deflection is represented instead by a superposition of simpler mathematical mode shapes which are sufficiently general and complete to express the physical motion.

In this study, Legendre polynomials and Chebyshev polynomials are adopted as simpler mode functions to replace the dry eigenmodes of the Euler-Bernoulli and Timoshenko beam, and the B-spline element method is used as another supplement. Then the mode-expansion method is applied to prove that a superposition of orthogonal mathematical functions can represent the flexural deflection of a ship in waves, despite the fact that each of these mathematical functions does not satisfy the required boundary conditions and has no physical meaning. For the forward speed case, by means of the Rankine panel method, validation in a wide range of wave frequencies is performed through a comparison of computed results for the modified Wigley model between dry eigenmodes and orthogonal polynomials used as the mode function. From this comparison, the rationality of consistency in the proposed method is proven and availability in various engineering fields can be expected. The ratio of flexural and shearing rigidities is intentionally increased for numerical study to see the effect of shearing force on various related quantities using Legendre polynomials. B-spline methods as supplement can predict total deflection and natrual modes of ship precisely. The merit and demerit of each method are discussed in detail.

Keywords: Hydroelasticity, Rankine panel method, Frequency domain, Mode functions, Timoshenko beam, Orthogonal polynomials, B-spline method.

Acknowledgements

I would like to dedicate this paper to those who have helped me along the way.

The special English program for foreign students is accomplished in the International Program of Maritime and Urban Engineering of Osaka University, which is fully supported by the Japan International Cooperation Agency (JICA) Innovative Asia program. Thank MEXT scholarship for helping me reduce the burden on my family. Not only can this program choose courses from other majors for interdisciplinary credit, but also participate in seminars with students from other majors to experience the knowledge and inspiration gained from interdisciplinary learning.

First and foremost, it is an honor to express my heartfelt gratitude to my supervisor, Professor Masashi Kashiwagi, whose expertise, perseverance, and vision made the completion of this dissertation possible in the end. I am indebted too much for his generosity and kindness during my study. His prodigious thought and continuous encouragement are inspiringly a lot to my study. Thank him for choosing me to be his last Ph.D. student. From being surprised by the huge size and beautiful writing of 'Kashiwagi Notes' at first, to the beautiful formulas introduced in textbooks, it is hard for me not to admire or respect him. Thank him for helping me complete the graduation requirements before his retirement and replying to me the email even at midnight discussing the problem. I may be like a frog in the well who knows nothing of the great ocean and even have no courage to look at the outside world if I did not study in Japan. All because the professor gave me the chance and I just had enough luck to meet him.

I would also like to give thanks to some faculty members in our laboratory, I am indebted and thankful to professor Munehiko Minoura. I learned a lot from his sea-keeping lecture and receive critical and constructive comments during the lab meeting. I still remember we talked about anything like movies or culture and he would explain everything in English with patience when he noticed I may not able to understand Japanese. He cares a lot about my research progress, the difficulties I faced and also gave me very positive encouragement, especially after Professor Kashiwagi's retirement. Thanks to assistant professor Iida for helping me answer the question about program and wave theory. I also want to thank Ms. Miyabe who did a lot of help in many affairs and applications.

I would like to thanks to professor Guanghua He. Without his recommendation and encouragement, I never have had an opportunity to know this special English program.

Special thanks to professor Zhang Jie who gave me much help with my study and life. We always discuss and share ideas that broaden my viewpoint. He also gave me a lot of help and advice in my job hunting. He is like a real brother that always cares about me.

I am delighted to belong to a fantastic laboratory with enjoyment and supporting members. I should appreciate considerably the positive atmosphere of pursuing a graduate study. To all lab members and university colleagues, I would like to thank them for their lively friendship.

Thanks to Ms. Yuxuan Cheng, Mr. Siyu Chan, and Ms. Ziyun Chen for being with me through my hardest time. It's the power of friends that saves me from loneliness and despair. It is so lucky to have them.

In the end of the foremost important, I am always indebted to my dearest parents and other family members who always sacrificed themselves and supported me without hesitation. They endure the loneliness of their child far away from home and respect any decision I made as long as I can move forward.

After all, I should acknowledge every single individual whose contribution is worth mentioning. I sincerely thank everyone without exception.

Sincerely yours.

Osaka, August 2022

HONG YANG

Contents

List of Figures

List of Tables

Chapter 1

Introduction

1.1 Background

In the past decade, larger ships have been built with increasing commercial needs of ocean transport and keep relatively high sail speed balanced between economic effectiveness and environmental protection so that ships become more flexible and associated accidents are prone to occur because higher encounter wave frequency approaches the natural frequency of elastic ship motions. A linear spectral approach just for rigid-body motions no longer gives a reliable prediction of fatigue load, since wave-induced vibrations, commonly referred to as springing and whipping, can aggravate the fatigue damage of very large ships. An underestimated fatigue load will cause frequent maintenance and lead to damage that cannot be belittled. Therefore, to compute wave-induced hydroelastic responses with sufficient accuracy gradually becomes of practical importance in naval engineering. In particular, for flexible bodies like ultra-large ships, it is required to analyze the wave loads and induced vibration as a coupled hydroelastic problem.

For hydroelastic analysis, the structural deflection and hydrodynamic response of flexible ships are fully coupled. A fundamental concept of the hydroelastic problem and its analysis was first developed using the strip theory to predict the elastic motion in waves by Bishop and Price (1979)[1], which is widely used by researchers. Jensen and Dogliani (1996) [2] calculated the nonlinear springing load using a second-order strip theory. Malenica et al. (2003)[3] proposed a hybrid method combining the frequency-domain 3D boundary integral-equation method (BIEM) with the 1D finite element method (FEM) for non-uniform beam, results of which were compared successfully with experimental data. Kim and Kim (2012)[4] computed the springing phenomena of a fast ship with forward speed in waves using the time-domain Rankine panel method and 3D FEM. Melenica and Derbanne (2012)[5] presented hydro-structural issues in ship design using the so-called weakly nonlinear approach. Recently, hydroelastic characteristics of flexible containership with forward speed are discussed through a series of experiments

by Kim and Kim(2016)[6]. Park et al.(2017)[7] discussed the added resistance characteristics of a flexible ship by numerical computations. Jiao et al(2020) et al. [8] investigated the nonlinear hydroelastic motion and load responses on a large flexible ship advancing in harsh irregular waves for the prediction of ship motions, deformations, and wave loads in long-crested irregular waves.

Unlike other types of ships, container ships have much lower torsional natural frequencies due to large hatch openings on deck. To analyze this torsional response, Dvorkin et al.(1989)[9] improved a finite element based on the Vlasov beam theory for thin-walled open section beam structures and proved its effectiveness since only one element can exactly model simple cases of nonuniform torsion without the requirement of numerical integration. Kim et al.(2009a) [10] and Kim et al.(2009b)[11] used a higher-order B-spline Rankine panel method to present the effects of fluid motion on a flexible seagoing vessel and employed a finite element formulation based on Vlasov beam for the torsional response. Shin et al.(2009) [12] investigated the importance of modeling approaches in the global symmetric and anti-symmetric responses of a 16,000 TEU large container ship using the Vlasov beam theory in the 2D linear problem.

Because the Euler-Bernoulli beam model tends to slightly overestimate the natural frequencies of elastic motions and this problem is exacerbated for higher elastic modes, the Timoshenko beam is adopted as a more advanced model which takes the shear deformation and rotary inertia into account and provides a better prediction for a blunt ship. For the research using the Timoshenko beam, Bokaian (1988) [13] studied the free vibration of axially loaded Timoshenko beams, and Farchaly and Shebl (1995) [14] studied the eigenfrequencies and associated more shapes of Timoshenko beams with intermediate fixities and elastic end supports. Majkut (2009) [15] solved the vibration of Timoshenko beams by the Green's function method. Senjanović et al.(2014) [16] developed an advanced thin-walled girder theory based on the modified Timoshenko-beam theory for the analysis of coupled horizontal and torsional ship hull vibrations. Datta and Siddiqui (2016) [17] presented a hydroelastic analysis of an axially loaded uniform Timoshenko beam undergoing bottom slamming,

In the structural analysis, it is common to define a special set of natural mode shapes, which correspond to the actual flexural deflections of a body in a specified physical context. Nevertheless, providing those natural mode shapes may be difficult in hydroelastic problems, because the mode shapes must satisfy the edge boundary conditions and are specified in advance. Normally the FEM may be used for providing complicated mode shapes. However, it was noted by Newman (1994)[18] that this difficulty can be avoided if the structural deflection is represented instead by a superposition of simpler orthogonal mathematical functions that are sufficiently general and complete to represent the physical motions of a body.

Following the idea of Newman (1994), many researchers have also chosen different mode functions using the modal superposition method to represent the total elastic deformation. Zhou et al.

(2002)[19] used the Chebyshev polynomials to analyze the 3-dimension vibration of thick rectangular plates. Kim and Kim (2001) [20] presented the frequency-domain expressions for the Euler-Bernoulli beam with generally restrained boundary conditions by using the Fourier series. Kashiwagi (1998) [21] used a direct method for calculating hydroelastic responses of a very large floating structure is investigated with two different numerical schemes. The direct method means solving the integral equation for the pressure distribution beneath a structure simultaneously with the vibration equation of a freely-floating plate. Lin and Takaki (1998)[22] estimated the hydroelastic response of a very large floating structure in waves by using the B-spline element functions. Hong and Hong (2007)[23] employed Legendre polynomials as admissible functions to represent the assumed modes of the VLFS with pinned-free-boundary conditions.

In Newman's paper (1994), the effectiveness of Legendre polynomials is proven but data is only at one wave frequency, which is maybe lack completeness and the theoretical explanation was not given for that fungibility. As for the Chebyshev polynomials used in that paper, there is no relevant data and no information is given concerning whether or how to use the orthogonality relation of Chebyshev polynomials due to the existence of the weight function in the relation. Although the orthogonality of Chebyshev polynomials cannot be embodied without the weight function, Zhou et al. (2002) noted that the Chebyshev polynomials are sets of complete and orthogonal series but there is no weight function applied in computation, which may be perplexing to the reader.

In the present study, dry eigenmodes of the Timoshenko beam, Legendre polynomials, Chebyshev polynomials of the first and second kind are adopted for the structural deflection of a ship in waves using the modal superposition method, even though each of these alternative polynomials does not satisfy required free-edge boundary conditions. Since the dry eigenmodes of the Timoshenko beam are relatively complicated and non-orthogonal, we cannot take advantage of the modal expansion method for computation. Thus, the present research is directed to prove that a superposition of polynomial functions can satisfy eventually the required boundary conditions in the process of transformation of the stiffness matrix with partial integration, and computed results are in good agreement with the results obtained by using the conventional dry eigenmodes of a uniform free-free beam. The advantages of the present calculation method are also discussed in the accuracy, the rate of convergence, the computation time, and the applicability to other problems. Whether the weight function is used in the orthogonality relation of Chebyshev polynomials will also be explained and obtained results will be compared with those using the other mode functions. The cubic B-spline method is also adopted as another supplement. Modal analysis and direct method are both used to imply further that although dry modes are fitting by segment lines using cubic B-spline functions, they still obtain accurate results without satisfying the free-end boundary conditions.

1.2 Objective

In **Chapter 2**, three-dimensional seakeeping performance theory was applied to predict the ship motions with high accuracy by considering the mutual interference between constant flow and forward speed effect. For hydrodynamic analysis, potential flow theory with several boundary conditions was satisfied by the method of Rankine panel method to impose the Rankine source. Complicated free surface boundary conditions and ship hull boundary conditions were derived including Reyleigh's artificial friction coefficient to satisfy radiation conditions. The complicity is mainly since there are many interactive items because of forward speed. Then, the radiation and diffraction problems were denoted after pressure analysis carefully, so that added mass and damping coefficient are induced here. Ranke panel method was used to express the potential by using Rankine source over ship hull and boundary condition and Rankine source strength can be obtained when imposing them into boundary conditions. The Rankine shift method (numerical technique) was applied to satisfy the boundary condition at infinity for Rankine panel method.

In **Chapter 3**, the deduction of natural modes of Timoshenko beam with shear effect and introduction of several numerical orthogonal polynomials to replace natural modes reasonably were elucidated. The orthogonality of natural modes of Timoshenko beam was discussed compared with Euler beam and orthogonal polynomials like Legendre and Chebyshev polynomials. Cubic B-spline methods including modal analysis method and direct method were also adopted to prove the correct conclusion even the dry modes are presented as piecewise curves using cubic B-spline basis functions.

In **Chapter 4**, it describes the formulation of motions of Timoshenko beam including rigid and elastic modes using the mode expansion method by integration over ship hull with weights into matrix form. Appropriate boundary conditions were introduced and adopted into the stiffness matrix to obtain the final conventional motion equations. The spatial part of the distribution of external force acting on a transverse cross-section of the ship and the shear-deformation force were adopted. The matrices of mass, stiffness, and shearing are denoted and the form of restoring force was derived.

In **Chapter 5**, the convergence study at forward speed for a total displacement of a ship by a superposition of all modes of motion was conducted. The modified Wigley model was used as a calculated object in Rankine panel method. The figures of non-dimensional added mass, damping coefficient, and exciting force were illustrated and compared with different mode functions. The values were defined to check the convergence of total deflection of the ship displacement at the ship bow. The reason for the different speeds of convergence was discussed. Supplementary proof of convergence using Legendre polynomials was raised by analyzing the satisfied boundary condition to prove five bending modes are enough from which the number of the demanded bending mode can be decreased. The effect of shearing force in Timoshenko beam was studied

by changing the ratio of flexural and shear rigidities artificially. The merits and demerits of each mode function were pointed out.

In **Chapter 6** concludes the present research about the hydroelastic forces on a ship with specified bending mode shapes and the resulting flexural deflection of a ship in waves by using Rankine panel method combined with the modal superposition method in terms of mode functions.

Chapter 2

Hydrodynamic Analysis

Three-dimensional seakeeping performance theory is applied to predict the ship motions with high accuracy by considering the mutual interference between constant flow and forward speed effect. Besides, flow is assumed as an ideal flow that is incompressible and inviscid with irrotational motion so that potential flow theory is adopted in this study that vector velocity with three parameters can be represented as one scalar potential.

This section introduces the coordinate system for hydrodynamic analysis and potential flow theory with several boundary conditions satisfied by the method of Rankine panel method to impose the Rankine source. Complicated free surface boundary conditions and ship hull boundary conditions are derived including Reyleigh's artificial friction coefficient to satisfy radiation conditions. The complicity is mainly because that there are many interactive items because of forward speed. Then, the radiation and diffraction problems are denoted after pressure analysis carefully, so that added mass and damping coefficient are induced here. Ranke panel method is adopted to express the potential by using Rankine source over ship hull and boundary condition and Rankine source strength can be obtained when imposed them into boundary conditions. The Rankine shift method (numerical technique) is used to satisfy the boundary condition at infinity for Rankine panel method.

2.1 Coordinate System and Potential Flow Theory

The 3-dimensional coordinate system in hydrodynamic analysis is illustrated as Fig.2.1, the moving coordinate o-xyz with constant speed is applied that shifts with ship forward speed U but not the ship generalized movements. Encounter wave angle β by incident wave comes from the negative x-axis and $\beta = 2\pi$ means head wave from the right ahead whereas $\beta = 0$ is following wave. Ship-fixed coordinate system $\overline{o}$-$\overline{xyz}$ is presented in Fig.2.2, which expresses the location

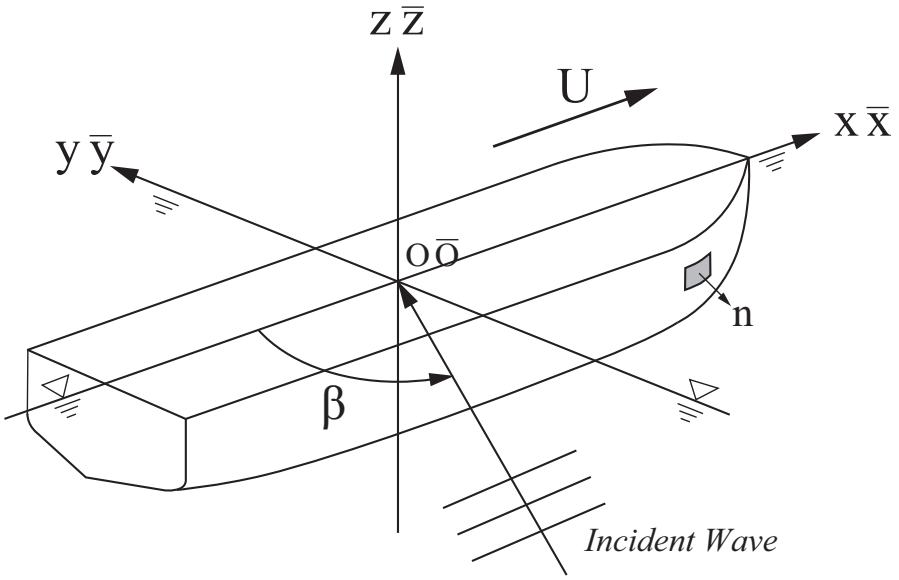

FIGURE 2.1: 3-dimensional coordinate system in hydrodynamic analysis.

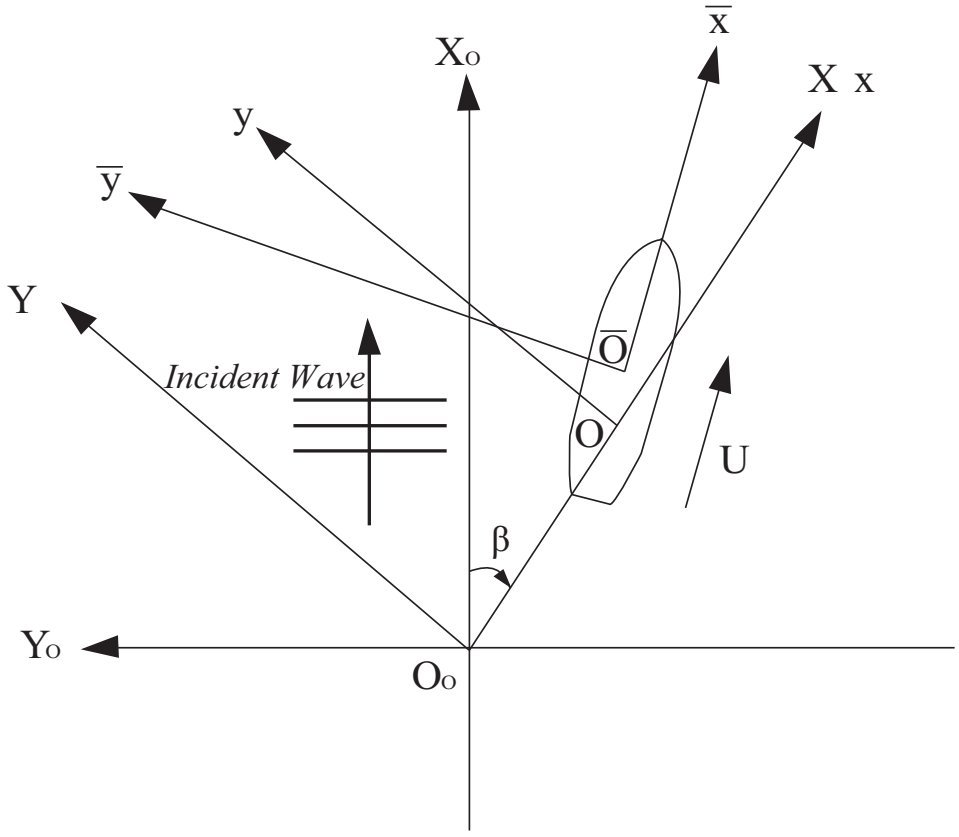

FIGURE 2.2: Coordinate system relationship.

vector $\bar{\boldsymbol{x}} = (\bar{x}, \bar{y}, \bar{z})$ of ship hull. Coordinates $O\text{-}X_0Y_0Z_0$ and $O\text{-}XYZ$ with angle β are space-fixed coordinates. The relation between space-fixed coordinate and moving coordinate can be expressed as

$$X_0 = (x + Ut)\cos\beta + y\sin\beta. \tag{2.1}$$

The case of a ship advancing at forward speed U and angle β in the regular wave is considered and the wave amplitude ζ_a, wavenumber k_0, wavelength $\lambda = 2\pi/k_0$ and circular wave frequency $\omega_0 = \sqrt{gk_0}$ are adopted under the assumption of the infinite depth water.

The incident wave potential $\Phi_I(\boldsymbol{x}; t)$ in infinit depth water can be expressed as

$$\Phi_I(\boldsymbol{x}; t) = \Re\left[\frac{ig\zeta_a}{\omega_0}\phi_I(\boldsymbol{x})e^{i\omega_e t}\right], \quad \phi_I(\boldsymbol{x}) = e^{k_0 z - ik_0(x\cos\beta + y\sin\beta)} \tag{2.2}$$

where "$\Re$" means the real part of expression to be taken, and

$$\omega_e = \omega_0 - k_0 U\cos\beta, \quad k_0 = \omega_0^2/g, \tag{2.3}$$

Vector $\boldsymbol{x}$ is the coordinate (x, y, z) of moving coordinate with constant speed and ω_e is called the circular frequency of encounter which considers the forward speed U. The parameter $ig\zeta_a/\omega_0$ is obtained by satisfying the continuity equation (or Laplace equation), free surface boundary condition, and infinitely deep bottom condition at the same time:

$$\left.\begin{array}{lll} \text{[L]} & \dfrac{\partial^2\Phi_I}{\partial x^2} + \dfrac{\partial^2\Phi_I}{\partial z^2} = 0 & \text{for} \quad z \le 0 \\ \text{[F]} & \dfrac{\partial^2\Phi_I}{\partial t^2} + g\dfrac{\partial\Phi_I}{\partial z} = 0 & \text{on} \quad z = 0 \\ \text{[B]} & \dfrac{\partial\Phi_I}{\partial z} = 0 & \text{on} \quad z = -\infty \end{array}\right\}. \tag{2.4}$$

Then, the velocity potentials are introduced, and the total velocity potential $\Phi(\boldsymbol{x}; t)$ including incident potential refer to Eq.(2.2) is written as follows:

$$\Phi(\boldsymbol{x}; t) = U\left[\Phi_D(\boldsymbol{x}) + \phi_w(\boldsymbol{x})\right] + \Phi_U(\boldsymbol{x}; t), \tag{2.5}$$

where on the right-hand side, terms in brackets with speed U outside are the time-independent constant flow potentials. Double-body flow potential $\Phi_D(\boldsymbol{x})$ is treated as basis flow expressed in Eq.(2.6) including uniform flow $-x$ and influence flow potential ϕ_D caused by the existence of ship hull (the flow should bypass the ship hull not pass through it).

$$\Phi_D(\boldsymbol{x}) = -x + \phi_D. \tag{2.6}$$

$\phi_w(\boldsymbol{x})$, also called wavy wave, is disturbing waves on basis flow which is negligible in most cases. The difference between double-body flow and uniform flow is illustrated in Fig.2.3 and arrows mean the streamlines that demonstrate the fluid motion. The function of influence flow potential ϕ_D that makes streamlines crooked can be understood clearly. The second term $\Phi_U(\boldsymbol{x};t)$ on right-hand side of Eq.(2.5) is time-dependent velocity potential (or unsteady velocity potential) including the incident wave potential. With the assumption of time harmonic oscillation

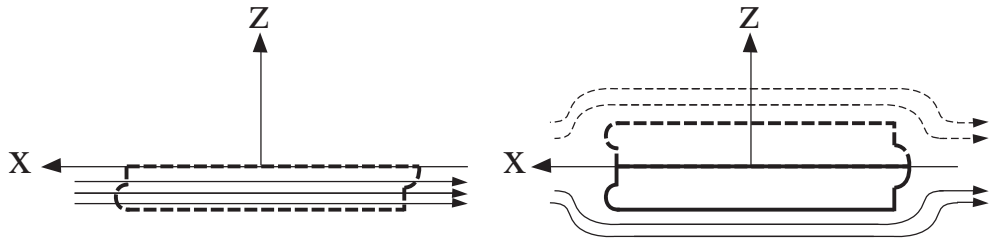

(a) uniform flow (b) double-body flow

FIGURE 2.3: Two kinds of basis flow.

in the unsteady component, the time-dependent part of unsteady quantities is expressed as $e^{i\omega_e t}$, and then the unsteady velocity potential $\Phi_U(\boldsymbol{x};t)$ can be written as

$$\Phi_U(\boldsymbol{x};t) = \Re\left[\phi(\boldsymbol{x})e^{i\omega_e t}\right], \tag{2.7}$$

$\phi(\boldsymbol{x})$ is the spatial part of the unsteady velocity potential which can be written in the linear theory by a linear superposition as follow:

$$\phi(\boldsymbol{x}) = \frac{ig\zeta_a}{\omega_0}\{\phi_I(\boldsymbol{x}) + \phi_S(\boldsymbol{x})\} + i\omega_e \sum_{j=1}^{N} \boldsymbol{X}_j \phi_j(\boldsymbol{x}), \tag{2.8}$$

where $\phi_I(\boldsymbol{x})$ is the part of incident wave velocity potential, already given by Eq.(2.6) and $\phi_S(\boldsymbol{x})$ is the scattering wave. $\phi_j(\boldsymbol{x})$ is the radiation velocity potential of the j-th motion and it is notable that j-th mode is the generalized motion, not only rigid motions but also elastic motions. X_j denotes the complex amplitude of the j-th motion. General periodic ship motions with time variables can be expressed as

$$\begin{aligned} \xi_j(t) &= \Re\left[\boldsymbol{X}_j e^{i\omega_e t}\right] = \Re\left[(X_{jc} + iX_{js})e^{i\omega_e t}\right] \\ &= \Re\left[|\boldsymbol{X}_j|e^{i\delta_j}e^{i\omega_e t}\right] = |\boldsymbol{X}_j|\cos(\omega_e t + \delta_j) \end{aligned} \tag{2.9}$$

where

$$|\boldsymbol{X}_j| = \sqrt{X_{jc}^2 + X_{js}^2}, \quad \delta_j = \tan^{-1}(X_{js}/X_{jc}), \tag{2.10}$$

$|X_j|$ is amplitude and δ_j is phase, so the complex amplitude can also be rewritten as $\boldsymbol{X}_j = |\boldsymbol{X}_j|e^{i\delta_j}$.

2.2 Free Surface Boundary Conditions

Double-body flow Φ_D represents a velocity potential of flow field when ship hull and its mirror (that why call double-body) advance in an infinite flow. Since the infinite flow has no free surface and the flow potential should be symmetric about the x-axis and the flow should move to surround the double-body, the free surface boundary condition (there is no velocity perpendicular to x-axis) and ship hull boundary condition (there is no speed perpendicular to hull) can be gained as

$$\frac{\partial \Phi_D}{\partial z} = 0 \quad \text{on} \quad z = 0, \quad \frac{\partial \Phi_D}{\partial n} = 0 \quad \text{on} \quad S_H. \tag{2.11}$$

Substituting Eq.(2.6) into Eq.(2.11), the boundary conditions could be derived as

$$\frac{\partial \phi_D}{\partial z} = 0 \quad \text{on} \quad z = 0, \quad \frac{\partial \phi_D}{\partial n} = n_1 \quad \text{on} \quad S_H, \tag{2.12}$$

where n_1 is the first part of normal vector of ship hull $\boldsymbol{n} = (n_1, n_2, n_3)$.

To begin with, Bernoulli's pressure equation is developed from Euler's equation and continuity equation. The velocity of irrotational flow (vector with three parameters) can be represented as Eq.(2.13) from one scalar function φ that is velocity potential,

$$\boldsymbol{u} = \nabla\varphi, \tag{2.13}$$

where ∇ express the differential operator :

$$\nabla = \frac{\partial}{\partial x}\boldsymbol{e}_1 + \frac{\partial}{\partial y}\boldsymbol{e}_2 + \frac{\partial}{\partial z}\boldsymbol{e}_3, \tag{2.14}$$

and is called the nabla. $\boldsymbol{e}_1, \boldsymbol{e}_2, \boldsymbol{e}_3$ are the unit vectors along axis of Cartsian coordinate system. Continuity equation derived from conservation of mass and Euler's equation from conservation of momentum are shown as

$$\nabla \cdot \boldsymbol{u} = 0, \quad \nabla \cdot \nabla\varphi = \nabla^2\varphi = 0, \tag{2.15}$$

$$\frac{\partial \boldsymbol{u}}{\partial t} + \boldsymbol{u} \cdot \nabla\boldsymbol{u} = -\frac{1}{\rho}\nabla p + \boldsymbol{K}. \tag{2.16}$$

The second equation in Eq.(2.15) is a continuity equation using scalar velocity potential which is widely named Laplace's equation. The right-hand side of Eq.(2.16) $\boldsymbol{K}$ is the external force

acting on per mass flow. Normally, the gravity force is the only consideration, and gravity acceleration g can be expressed as $\boldsymbol{K} = (0, 0, -g)$ because vertical upward is the positive direction of z-axis. With assumption of irrotational flow $\nabla \times \boldsymbol{u}$, Euler's equation can be derived as Eq.(2.17) using velocity potential φ.

$$\nabla \left[\frac{\partial \varphi}{\partial t} + \frac{1}{2} \nabla \varphi \cdot \nabla \varphi + \frac{p}{\rho} + gz \right] = 0, \tag{2.17}$$

so that

$$\frac{\partial \varphi}{\partial t} + \frac{1}{2} \nabla \varphi \cdot \nabla \varphi + \frac{p}{\rho} + gz = f(t). \tag{2.18}$$

Eq.(2.18) is Bernoulli's pressure equation and right-hand side $f(t)$ can be arbitrary time-dependent function. Beside, Rayleigh's artificial friction coefficient is introduced in the external force $\boldsymbol{K}$ for satisfying the radiation condition which is explained in detail by Wehausen and Laitone (1960) [24]. Suppose there is a friction force that is proportional to the speed. This friction force acts in the opposite direction of the fluid velocity, and its proportionality coefficient is μ. The external force K is:

$$\boldsymbol{K} = -g\boldsymbol{e}_3 - \mu \boldsymbol{u}. \tag{2.19}$$

Then there is one more term $\mu\varphi$ added on the left-hand side of Eq.(2.18) as:

$$\frac{\partial \varphi}{\partial t} + \frac{1}{2} \nabla \varphi \cdot \nabla \varphi + \frac{p}{\rho} + gz + \mu\varphi = f(t). \tag{2.20}$$

Now, Eq.(2.20) is our Bernoulli's pressure equation with Reyleigh's artificial friction coefficient to satisfy radiation conditions. The free surface points far from ship hull is considered in the equation, and on right-hand side of Eq.(2.20), we set $f(t) = p_a/\rho + U^2/2$ where p_a is standard atmospheric pressure and based on that, pressure $P(\boldsymbol{x}; t) \equiv p - p_a$. The total velocity mentioned before is substituted into Bernoulli's pressure equation, the equation can be rewritten further as:

$$-\frac{P(\boldsymbol{x}; t)}{\rho} = -\frac{U^2}{2} + gz + \frac{\partial \Phi}{\partial t} + \frac{1}{2} \nabla \Phi \cdot \nabla \Phi + \mu(U\phi_w + \Phi_U). \tag{2.21}$$

There is no wave transferring far away for double-body flow potential which does not participate in friction term. Specifically,

$$\left.\begin{aligned} \frac{\partial \Phi(\boldsymbol{x}; t)}{\partial t} &= \frac{\partial}{\partial t} \left\{ U \left[\Phi_D(\boldsymbol{x}) + \phi_w(\boldsymbol{x}) \right] + \Phi_U(\boldsymbol{x}; t) \right\} = \frac{\partial}{\partial t} \Phi_U(\boldsymbol{x}; t) \\ \nabla \Phi(\boldsymbol{x}; t) &= U \nabla (\Phi_D(\boldsymbol{x}) + \phi_w(\boldsymbol{x}) + \nabla \Phi_U(\boldsymbol{x}; t) = U\boldsymbol{V}(\boldsymbol{x}) + \nabla \Phi_U(\boldsymbol{x}; t) \end{aligned}\right\}, \tag{2.22}$$

and $\boldsymbol{V}(\boldsymbol{x}) = \nabla(\Phi_D(\boldsymbol{x}) + \phi_w(\boldsymbol{x}))$ is the normalized velocity vector in constant flow. The variables $\boldsymbol{x}$ and t are omitted in what follows for brevity, then,

$$\left.\begin{aligned} &\frac{1}{2}\nabla\Phi\cdot\nabla\Phi = \frac{1}{2}(U\boldsymbol{V}+\nabla\Phi_U)^2 = \frac{1}{2}U^2\boldsymbol{V}^2 + U\boldsymbol{V}\nabla\Phi_U + \frac{1}{2}\nabla\Phi_U\cdot\nabla\Phi_U \\ &\boldsymbol{V}^2 = \nabla\Phi_D\cdot\nabla\Phi_D + 2\nabla\Phi_D\cdot\nabla\phi_w\nabla\phi_w\cdot\nabla\phi_w \end{aligned}\right\}. \tag{2.23}$$

Among the parts in above equations, the right-hand side of Eq.(2.21) can be separated into gravity term, steady term, unsteady term, and friction term shown as follows,

$$-\frac{P(\boldsymbol{x};t)}{\rho} = gz - \frac{P^S(\boldsymbol{x})}{\rho} - \frac{P^U(\boldsymbol{x};t)}{\rho} + \mu(U\phi_w + \Phi_U). \tag{2.24}$$

where

$$\begin{aligned} \frac{P^S(\boldsymbol{x})}{\rho} &= \frac{U^2}{2}(1-\boldsymbol{V}\cdot\boldsymbol{V}) \\ &= \frac{U^2}{2}(1-\nabla\Phi_D\cdot\nabla\Phi_D - 2\nabla\Phi_D\cdot\nabla\phi_w) + O(\phi_w^2) \qquad (2.25) \\ \frac{P^U(\boldsymbol{x};t)}{\rho} &= -(\frac{\partial}{\partial t} + U\boldsymbol{V}\cdot\nabla)\Phi_U - \frac{1}{2}\nabla\Phi_U\cdot\nabla\Phi_U \\ &= -(\frac{\partial}{\partial t} + U\nabla\Phi_D\cdot\nabla)\Phi_U + O(\phi_w\Phi_U, \Phi_U^2) \qquad (2.26) \end{aligned}$$

Then, the wave elevation $\zeta(x,y;t)$ of the free surface is considered, and the condition $P = 0$ is adopted when $z = \zeta$ expressed as

$$\zeta(x,y;t) = -\frac{1}{g}\left(\frac{\partial\Phi}{\partial t} + \frac{1}{2}\nabla\Phi\cdot\nabla\Phi - \frac{U^2}{2}\right) \quad \text{on} \quad z = \zeta \tag{2.27}$$

The total potential Φ is substituted into the above equation and estimated on still surface $z = 0$ using Taylor expansion method with higher-order terms $O(\phi_w^2, \phi_w\Phi_U, \Phi_U^2)$ neglected and condition $\partial\Phi_D/\partial z = 0$ is applied as follows:

$$\zeta(x,y;t) = \zeta^{(0)}(x,y) + \zeta^{(1)}(x,y;t) \quad \text{on} \quad z = 0, \tag{2.28}$$

where,

$$\left.\begin{aligned} \zeta^{(0)} &= \frac{U^2}{2g}\left(1 - \nabla\Phi_D\cdot\nabla\Phi_D - 2\nabla\Phi_D\cdot\nabla\phi_w\right) \\ \zeta^{(1)} &= -\frac{1}{g}\left(\frac{\partial}{\partial t} + U\nabla\Phi_D\cdot\nabla\right)\Phi_U \equiv \Re\left[\zeta_w(x,y)e^{i\omega_e t}\right] \\ \zeta_w &= -\frac{1}{g}\left(i\omega_e + U\nabla\Phi_D\cdot\nabla\right)\phi \end{aligned}\right\}. \tag{2.29}$$

The wave elevation is also separated into time-independent steady wave elevation expressed as $\zeta^{(0)}$ and time-dependent unsteady wave elevation as $\zeta^{(1)}$ concerning the linear term of Φ_U.

The pressure at the fluid particle on the free surface is always equal to the standard atmospheric pressure, so the substantial derivative of the pressure is always equal to zero as shown in the form of

$$\frac{D}{Dt}\left(-\frac{P}{\rho}\right)=\left(\frac{\partial}{\partial t}+\nabla\Phi\cdot\nabla\right)\left[gz-\frac{P^S}{\rho}-\frac{P^U}{\rho}+\mu(U\phi_w+\Phi_U)\right]=0 \quad \text{on} \quad z=\zeta. \tag{2.30}$$

The first term in brackets is the static pressure term gz:

$$\begin{aligned}\left(\frac{\partial}{\partial t}+\nabla\Phi\cdot\nabla\right)gz &= U\nabla\Phi_D\cdot\nabla(gz)+U\nabla\phi_w\cdot\nabla(gz)+\nabla\Phi_U\cdot\nabla(gz)\\ &= Ug\frac{\partial\phi_w}{\partial z}+g\frac{\partial\Phi_U}{\partial z}.\end{aligned} \tag{2.31}$$

Sencondly, the steady term $-\frac{P^S}{\rho}$ is:

$$\begin{aligned}\left(\frac{\partial}{\partial t}+\nabla\Phi\cdot\nabla\right)\left(-\frac{P^S}{\rho}\right) &= \frac{U^3}{2}\nabla\Phi_D\cdot\nabla\left(\nabla\Phi_D\cdot\nabla\Phi_D\right)+U^3\nabla\Phi_D\cdot\nabla\left(\nabla\Phi_D\cdot\nabla\phi_w\right)\\ &+ \frac{U^3}{2}\nabla\phi_w\cdot\nabla\left(\nabla\Phi_D\cdot\nabla\Phi_D\right)+U^3\nabla\phi_w\cdot\nabla\left(\nabla\Phi_D\cdot\nabla\phi_w\right)\\ &+ \frac{U^2}{2}\nabla\Phi_U\cdot\nabla\left(\nabla\Phi_D\cdot\nabla\Phi_D\right)+U^2\nabla\Phi_U\cdot\nabla\left(\nabla\Phi_D\cdot\nabla\phi_w\right).\end{aligned} \tag{2.32}$$

Then, the third term is unsteady term $-\frac{P^U}{\rho}$ shown as:

$$\begin{aligned}\left(\frac{\partial}{\partial t}+\nabla\Phi\cdot\nabla\right)\left(-\frac{P^U}{\rho}\right) &= \frac{\partial^2}{\partial t^2}\Phi_U+U\nabla\Phi_D\cdot\nabla(\frac{\partial}{\partial t}\Phi_U)\\ &+ U\nabla\phi_w\cdot\nabla(\frac{\partial}{\partial t}\Phi_U)+\nabla\Phi_U\cdot\nabla(\frac{\partial}{\partial t}\Phi_U)\\ &+ U^2\nabla\Phi_D\cdot\nabla(\nabla_D\cdot\nabla\Phi_U)+U^2\nabla\phi_w\cdot\nabla(\nabla_D\cdot\nabla\Phi_U)\\ &+ U\nabla\Phi_U\cdot\nabla(\nabla_D\cdot\nabla\Phi_U).\end{aligned} \tag{2.33}$$

The last term is the radiation condition term $\mu(U\phi_w+\Phi_U)$:

$$\begin{aligned}\left(\frac{\partial}{\partial t}+\nabla\Phi\cdot\nabla\right)\left[\mu(U\phi_w+\Phi_U)\right] &= \mu(\frac{\partial}{\partial t}\Phi_U+U\nabla\Phi_D\cdot\nabla\Phi_U+U\nabla\phi_w\cdot\nabla\Phi_U\\ &+ \nabla\Phi_U\cdot\nabla\Phi_U+U^2\nabla\Phi_D\cdot\nabla\phi_w\\ &+ U^2\nabla\phi_w\cdot\nabla\phi_w+U\nabla\Phi_U\cdot\nabla\phi_w)\end{aligned} \tag{2.34}$$

The time-independent terms of free surface boundary conditions are considered for the steady term. Talyor expansion method is adopted to estimate steady wave elevation $\zeta^{(0)}$ and the ϕ_w

terms of higher than second order are neglected. Then, we have

$$\frac{U^2}{2}\nabla\Phi_D\cdot\nabla(\nabla\Phi_D\cdot\nabla\Phi_D)+U^2\nabla\Phi_D\cdot\nabla(\nabla\Phi_D\cdot\nabla\phi_w)+\frac{U^2}{2}\nabla(\nabla\Phi_D\cdot\nabla\Phi_D)\cdot\nabla\phi_w$$
$$+g\frac{\partial\phi_w}{\partial z}+\mu U\nabla\Phi_D\cdot\nabla\phi_w=0\quad\text{on}\quad z=0 \tag{2.35}$$

Eq.(2.35) could become free surface boundary condition cited from Dawson (1977) [25] without the artificial friction term.

The time-dependent terms of free surface boundary conditions for the unsteady problem are shown in Eq.(2.36). It is estimated to unsteady wave elevation $\zeta^{(1)}$ using the Talyor expansion method and terms Φ_U^2, $\phi_w\Phi_U$ are neglected.

$$-\omega_e^2\phi+2iU\omega_e\nabla\Phi_D\cdot\nabla\phi+U^2\nabla\Phi_D\cdot\nabla(\nabla\Phi_D\cdot\nabla\phi)$$
$$+\frac{U^2}{2}\nabla(\nabla\Phi_D\cdot\nabla\Phi_D)\cdot\nabla\phi+U\nabla^2\Phi_D(i\omega_e+U\nabla\Phi_D\cdot\nabla)\phi$$
$$+g\frac{\partial\phi}{\partial z}+\mu(i\omega_e+U\nabla\Phi_D\cdot\nabla)\phi=0\quad\text{on}\quad z=0. \tag{2.36}$$

The equation could be free surface boundary condition cited from Sclavounos and Nakos (1990) [26] if the last term about radiation condition is excluded.

Eq.(2.35) and Eq.(2.36) are free surface condition approximations of double-body flow. Wavy flow potential ϕ_w in steady problem and radiation potential ϕ in unsteady problem can be solved separately. The terms whose orders are higher than the interference term between the steady flow field and the unsteady flow field are also considered by Bertram (1990) [27]. In that case, steady flow influence term ϕ_w presents in unsteady boundary condition so that steady and unsteady problems cannot be solved as independent problems. In other words, ϕ_w and ϕ are solved in coupled problem.

2.3 Ship Hull Boundary Condition

The boundary conditions of the surface of the floating body can be obtained by solving the kinematics conditions. As long as know the shape of the ship hull, its substantial differential should be considered equal to zero. Usually, the floating body is treated as a rigid body, the floating body in the ship-fixed coordinate system is not changed with time. It is noted that in hydroelastic problem, the ship is treated as a deformable body with rigid and elastic motions and the fixed-coordinate moves with the ship movements including elastic modes, so its substantial differential still is set to equal zero.

Slight defomations and movements of floating body are assumed, the relationship between the position vector in the moving coordinate $\boldsymbol{x}=(x,y,z)$ and in the ship-fixed coordinate $\bar{\boldsymbol{x}}=$

$(\overline{x}, \overline{y}, \overline{z})$ is

$$\boldsymbol{x} = \overline{\boldsymbol{x}} + \boldsymbol{H}(t). \tag{2.37}$$

In the modal superposition method, the total ship displacement $\boldsymbol{H}(\boldsymbol{x}; t)$ is expressed by a superposition of mode funtions as follows:

$$\boldsymbol{H}\,(\boldsymbol{x}; t) = (H_x, H_y, H_z) = \sum_{j=1}^{N} \xi_j(t)\boldsymbol{h}^j(\boldsymbol{x}) = \Re\left[\sum_{j=1}^{N} X_j \boldsymbol{h}^j(\boldsymbol{x}) e^{i\omega_e t}\right], \tag{2.38}$$

where index j donotes the mode number, and $\xi_j(t)$ is the time-dependent amplitude of the j-th mode of motion. $j = 1 \sim 6$ and $j = 7 \sim N$ correspond to the rigid-body motions and the elastic motions, respectively, and N is the total number of modes to be considered. The mode functions for rigid-body motions can be expressed as

$$\boldsymbol{h}^j = \begin{cases} \boldsymbol{e}_j & (j = 1 \sim 3) \\ \boldsymbol{e}_{j-3} \times \boldsymbol{x} & (j = 4 \sim 6) \end{cases}, \tag{2.39}$$

where $\boldsymbol{e}_j$ is the unit vector along axis of the Cartesian coordinate system. Commonly, notation j is used as subscript to express the serial number of motions, there are exceptions on $\boldsymbol{h}^j$ that j is adopted as superscript. Mode function $\boldsymbol{h}^j$ is a vector that has three componets in three directions and needs subscript to point its components like following equation. Also, this superscript is aim to distinguish the vector from complex values. The mode function for the j-th elastic motion is written in a general form

$$\boldsymbol{h}^j = (h_x^j, h_y^j, h_z^j) = (h_1^j, h_2^j, h_3^j) \quad (j = 7 \sim N). \tag{2.40}$$

As an example, we can write in the case of vertical bending as

$$h_x^j = -\frac{dw_j(x)}{dx}(z - z_N), \quad h_y^j = 0, \quad h_z^j = w_j(x), \tag{2.41}$$

where $w_j(x)$ is the vertical displacement in the j-th mode of motion, h_x^j is the horizontal displacement due to the inclination of the neutral axis by the elastic deflection, and z_N is the vertical position of the neutral axis. h_x^j is reasonable in the Euler beam due to Bernoulli's assumption that cross-sections remain perpendicular to the neutral axis of the beam. h_x^j should be slightly modified to $h_x^j = -(\frac{dw_j(x)}{dx} - \theta)(z - z_N)$ theoretically because of shearing force considered in Timoshenko beam. However, the product of shear angle and vertical position is relatively small, and deciding the shear angle is not easy to calculate, so it still follows the Eq.(2.41) in the case of Timoshenko beam. The concept map of the Timoshenko beam and Euler-Bernoulli beam is shown in Fig.3.1 next chapter.

Back to the substantial differential of ship hull, interference from time-independent steady flow to time-dependent unsteady flow is considered here also. Shape of ship hull can be expressed as $F(\overline{\boldsymbol{x}}) = 0$ and partial differential operator $\overline{\nabla}$ concerning about $\overline{\boldsymbol{x}}$ is included in substantial differential shown as

$$\frac{DF(\overline{\boldsymbol{x}})}{Dt} = \left(\frac{\partial}{\partial t} + \nabla\Phi(\boldsymbol{x};t)\cdot\nabla\right)F(\overline{\boldsymbol{x}}) = \overline{\nabla}F(\overline{\boldsymbol{x}})\cdot\frac{\partial\overline{\boldsymbol{x}}}{\partial t} + \nabla\Phi(\boldsymbol{x};t)\cdot \left\{\left(\overline{\nabla}F(\overline{\boldsymbol{x}})\cdot\frac{\partial\overline{\boldsymbol{x}}}{\partial x}\right)\boldsymbol{e}_1 + \left(\overline{\nabla}F(\overline{\boldsymbol{x}})\cdot\frac{\partial\overline{\boldsymbol{x}}}{\partial y}\right)\boldsymbol{e}_2 + \left(\overline{\nabla}F(\overline{\boldsymbol{x}})\cdot\frac{\partial\overline{\boldsymbol{x}}}{\partial z}\right)\boldsymbol{e}_3\right\} = 0. \tag{2.42}$$

The specific derivation process of the partial derivative with respect to time for the first term is:

$$\frac{\partial}{\partial t}F(\overline{\boldsymbol{x}}) = \frac{F(\overline{\boldsymbol{x}})}{\partial\overline{x}}\cdot\frac{\partial\overline{x}}{\partial t} + \frac{F(\overline{\boldsymbol{x}})}{\partial\overline{y}}\cdot\frac{\partial\overline{y}}{\partial t} + \frac{F(\overline{\boldsymbol{x}})}{\partial\overline{z}}\cdot\frac{\partial\overline{z}}{\partial t} = \overline{\nabla}F(\overline{\boldsymbol{x}})\cdot\frac{\partial\overline{\boldsymbol{x}}}{\partial t}. \tag{2.43}$$

From Eq.(2.37), the relations can be obtained as

$$\begin{cases} \dfrac{\partial\boldsymbol{x}}{\partial t} = \dfrac{\partial\overline{\boldsymbol{x}}}{\partial t} + \dfrac{\partial\boldsymbol{H}(t)}{\partial t} = 0 \\ \dfrac{\partial\boldsymbol{x}}{\partial x_j} = \dfrac{\partial\overline{\boldsymbol{x}}}{\partial x_j} + \dfrac{\partial\boldsymbol{H}(t)}{\partial x_j} = \boldsymbol{e}_j \\ (x_1, x_2, x_3) = (x, y, z) \end{cases}, \tag{2.44}$$

and substituting the above relations into Eq.(2.42), we can derive to

$$-\dot{\boldsymbol{H}}(t)\cdot\overline{\nabla}F(\overline{\boldsymbol{x}}) + \nabla\Phi(\boldsymbol{x};t)\cdot\overline{\nabla}F(\overline{\boldsymbol{x}}) - [(\nabla\Phi(\boldsymbol{x};t)\cdot\nabla)\boldsymbol{H}(t)] \cdot\overline{\nabla}F(\overline{\boldsymbol{x}}) = 0 \quad \text{on} \quad F(\overline{\boldsymbol{x}}) = 0. \tag{2.45}$$

Divided $|\overline{\nabla}F(\overline{\boldsymbol{x}})|$ both sides of the above equation, normal vector on ship-fixed coordinate can be defined as

$$\overline{\boldsymbol{n}} = \frac{\overline{\nabla}F(\overline{\boldsymbol{x}})}{|\overline{\nabla}F(\overline{\boldsymbol{x}})|}. \tag{2.46}$$

Using the definition of the normal vector, Eq.(2.45) can be simplified as

$$-\dot{\boldsymbol{H}}(t)\cdot\overline{\boldsymbol{n}} + \nabla\Phi(\boldsymbol{x};t)\cdot\overline{\boldsymbol{n}} - [(\nabla\Phi(\boldsymbol{x};t)\cdot\nabla)\boldsymbol{H}(t)]\cdot\overline{\boldsymbol{n}} = 0 \quad \text{on} \quad F(\overline{\boldsymbol{x}}) = 0. \tag{2.47}$$

From Eq.(2.5),

$$\nabla\Phi(\boldsymbol{x};t) = U\boldsymbol{V}(\boldsymbol{x}) + \nabla\Phi_U(\boldsymbol{x};t), \tag{2.48}$$

velocity vectors $\boldsymbol{V}$ and Φ_U are expanded around $\boldsymbol{x} = \overline{\boldsymbol{x}}$ using Talyor expansion method:

$$\boldsymbol{V}(\boldsymbol{x}) = \boldsymbol{V}(\overline{\boldsymbol{x}} + \boldsymbol{H}(t)) = \boldsymbol{V}(\overline{\boldsymbol{x}}) + (\boldsymbol{H}(t) \cdot \nabla)\boldsymbol{V}(\overline{\boldsymbol{x}}) + O(\boldsymbol{H}^2) \tag{2.49}$$

$$\nabla\Phi_U(\boldsymbol{x}; t) = \nabla\Phi_U(\overline{\boldsymbol{x}} + \boldsymbol{H}(t); t) = \nabla\Phi_U(\overline{\boldsymbol{x}}; t) + (\boldsymbol{H}(t) \cdot \nabla)\nabla\Phi_U(\overline{\boldsymbol{x}}; t) + O(\boldsymbol{H}^2). \tag{2.50}$$

Substituting Eqs.(2.48)-(2.50) into Eq.(2.47), steady terms and unsteady terms are separated same as before and only the linear terms are extracted. Here, the slight difference between $\boldsymbol{x}$ and $\overline{\boldsymbol{x}}$, $\boldsymbol{n}$ and $\overline{\boldsymbol{n}}$ are neglected so that $\boldsymbol{x}$ and $\boldsymbol{n}$ are used in following expressions. Firstly, the linear terms in steady problem are:

$$\boldsymbol{V} \cdot \boldsymbol{n} = \nabla(\Phi_D + \phi_w) \cdot \boldsymbol{n} = \frac{\partial \Phi_D}{\partial n} + \frac{\partial \phi_w}{\partial n} = \frac{\partial \phi_w}{\partial n} = 0 \quad \text{on} \quad S_H. \tag{2.51}$$

Then, the linear terms in unsteady problem are extracted as

$$\nabla\Phi_U \cdot \boldsymbol{n} = \frac{\partial \Phi_U}{\partial n} = \dot{\boldsymbol{H}}(t) \cdot \boldsymbol{n} + U\left[(\boldsymbol{V} \cdot \nabla)\boldsymbol{H}(t) - (\boldsymbol{H}(t) \cdot \nabla)\boldsymbol{V}\right] \cdot \boldsymbol{n} \quad \text{on} \quad S_H. \tag{2.52}$$

Adopting Eq.(2.7) and Eq.(2.38) into the above unsteady problem and eliminating the time variable on both sides, the boundary condition can be simplified further. The left side of the above equation can be rewritten as:

$$\frac{\partial \Phi_U}{\partial n} = \Re\left[\left\{\frac{ig\zeta_a}{\omega_0}\frac{\partial}{\partial n}\left\{\phi_I(\boldsymbol{x}) + \phi_S(\boldsymbol{x})\right\} + i\omega_e \sum_{j=1}^{N} \boldsymbol{X}_j \frac{\partial}{\partial n}\phi_j(\boldsymbol{x})\right\} e^{i\omega_e t}\right]. \tag{2.53}$$

The velocity vectors of incident wave and scattering wave should be cancelled on the ship hull surface so that

$$\frac{\partial}{\partial n}\phi_I(\boldsymbol{x}) = -\frac{\partial}{\partial n}\phi_S(\boldsymbol{x}) \quad \text{on} \quad S_H. \tag{2.54}$$

The first term on right-hand side of Eq.(2.52) can be expressed as:

$$\dot{\boldsymbol{H}}(t) \cdot \boldsymbol{n} = \Re\left[\left\{i\omega_e \sum_{j=1}^{N} X_j \boldsymbol{h}^j \cdot \boldsymbol{n}\right\} e^{i\omega_e t}\right], \tag{2.55}$$

and the second terms are:

$$\begin{aligned} U \quad & \left[(\boldsymbol{V} \cdot \nabla)\boldsymbol{H}(t) - (\boldsymbol{H}(t) \cdot \nabla)\boldsymbol{V}\right] \cdot \boldsymbol{n} = \\ \Re \quad & \left[U\left\{(\boldsymbol{V} \cdot \nabla)\sum_{j=1}^{N} X_j h^j \cdot \boldsymbol{n} - (\sum_{j=1}^{N} X_j \boldsymbol{h}^j \cdot \nabla)\boldsymbol{V} \cdot \boldsymbol{n}\right\} e^{i\omega_e t}\right]. \end{aligned} \tag{2.56}$$

Combining and observing the above four formulae, the neat boundary condition can be derived as follows when eliminating the time variable and common terms on both sides.

$$\begin{aligned} \frac{\partial}{\partial n}\phi_j &= \boldsymbol{h}^j \cdot \boldsymbol{n} + \frac{U}{i\omega_e}\left\{(\boldsymbol{V}\cdot\nabla)\boldsymbol{h}^j \cdot \boldsymbol{n} - (\boldsymbol{h}^j\cdot\nabla)\boldsymbol{V}\cdot\boldsymbol{n}\right\} \\ &= \widetilde{n}_j + \frac{U}{i\omega_e}\widetilde{m}_j \quad , \end{aligned} \tag{2.57}$$

where,

$$\begin{cases} \widetilde{n}_j = \boldsymbol{h}^j \cdot \boldsymbol{n} = h^j_k n_k \\ \widetilde{m}_j = n_l\left(V_k \dfrac{\partial}{\partial x_k}\right) h^j_l - h^j_l\left(n_k \dfrac{\partial}{\partial x_k}\right) V_l \end{cases} . \tag{2.58}$$

It is noteworthy that $\widetilde{n}_j$ and $\widetilde{m}_j$ are extended definitions of n_j and m_j for the case of rigid-body motions to the general modes including elastic deflections. V_k denotes the k-th component of the steady velocity vector $\boldsymbol{V}$ induced by the double-body flow. $\widetilde{m}_j$ (called m-term) calculated from the steady velocity vector expresses the interference effect of the steady flow on the unsteady flow. The expression of $\widetilde{m}_j$ is cited from Kashiwagi et al.2015[28] and its derivation can also be found in Heo and Kashiwagi (2019) [29]. The summation signs with respect to k and l are deleted in Eq.(2.58) with the convention that any term containing the same index twice in the inner product should be summed over that index (k and $l = 1 \sim 3$).

The neat ship hull boundary condition can be expressed as follows,

$$\begin{cases} \dfrac{\partial}{\partial n}\phi = i\omega_e \displaystyle\sum_{j=1}^{N} X_j\left(\widetilde{n}_j + \frac{U}{i\omega_e}\widetilde{m}_j\right) \\ \dfrac{\partial}{\partial n}\phi_I = -\dfrac{\partial}{\partial n}\phi_S \end{cases} \quad \text{on} \quad S_H. \tag{2.59}$$

In conclusion, the flow field around the ship hull is separated into the steady flow and unsteady flow that is linearized. For steady flow field, free surface boundary condition Eq.(2.35) and ship hull boundary condition Eq.(2.51) are obtained when double-body flow as basis flow. Moreover, these boundary conditions satisfy the additional boundary conditions of infinite depth water $\partial\phi_w/\partial n = 0$ on S_B and consider the radiation condition at infinity by Rayleigh's artificial friction coefficient. These boundary condition problems without time variable are called the steady problem. On the other hand, Eq.(2.36) and Eq.(2.59), and ϕ_D is the free surface and hull surface boundary conditions of the unsteady flow field in the unsteady problem satisfying water bottom and radiation boundary conditions as well.

2.4 Pressure on Ship Hull

Knowing the pressure formula shown as Eq.(2.24), the pressure integration over ship hull moving timely with the amplitude $\boldsymbol{H}(t)$ at average position $\boldsymbol{x} = \overline{\boldsymbol{x}}$ needs to be calculated. Similarly, Taylor expansion method is adopted around $\boldsymbol{x} = \overline{\boldsymbol{x}}$ and the second-order or higher terms are ignored. The expression of Eq.(2.24) can be organized as follows,

$$P(\boldsymbol{x};t) = -\rho g\bar{z} + P^C(\overline{\boldsymbol{x}};t) + P^{(0)}(\overline{\boldsymbol{x}}) + P^{(1)}(\overline{\boldsymbol{x}};t) \quad \text{on} \quad S_H, \tag{2.60}$$

where the first term on the right-hand side is the surface pressure under the stationary condition of the ship, and the buoyancy and moment obtained after integration along the hull surface cancel each other out with the gravity force and moment of the ship.

$$P^C(\overline{\boldsymbol{x}};t) = -\rho g(z - \bar{z}), \tag{2.61}$$

$P^C(\overline{\boldsymbol{x}};t)$ is the fluctuating component when the ship hull is shaking or moving which is also caused by hydrostatic pressure, and the time variable can be separated. The restoring force matrix can be obtained by the force and moment though integrating the surface pressure on the hull surface. The third term is time-independent constant pressure and is shown as

$$P^{(0)}(\overline{\boldsymbol{x}}) = \frac{\rho U^2}{2}\left[1 - \boldsymbol{V}(\overline{\boldsymbol{x}}) \cdot \boldsymbol{V}(\overline{\boldsymbol{x}})\right] = \frac{\rho U^2}{2}(1 - \nabla\Phi_D \cdot \nabla\Phi_D - 2\nabla\Phi_D \cdot \nabla\phi_w). \tag{2.62}$$

$P^{(1)}(\overline{\boldsymbol{x}};t)$ is the first-order unsteady pressure on hull surface and its expression can be presented as

$$P^{(1)}(\overline{\boldsymbol{x}};t) = -\rho\left(\frac{\partial}{\partial t} + U\boldsymbol{V}(\overline{\boldsymbol{x}}) \cdot \nabla\right)\Phi_U(\overline{\boldsymbol{x}};t) - \frac{\rho U^2}{2}\left(\boldsymbol{H}(t) \cdot \nabla\right)\left[\boldsymbol{V}(\overline{\boldsymbol{x}}) \cdot \boldsymbol{V}(\overline{\boldsymbol{x}})\right]. \tag{2.63}$$

The first term on the right-hand side of Eq.(2.63) is the expanded term of P_U by the Taylor expansion method. The second is adopted by Taylor expansion on P^S, which is proportional to movement amplitude $\boldsymbol{H}(t)$. It is the restoring force caused by constant flow and it turns to zero when basis flow is uniform flow.

2.5 Radiation Problem and Diffraction Problem

From the view of ship hull boundary conditions, the unsteady problem can be separated into radiation problem and diffraction problem. Observing from the first formula in Eq.(2.59), the ship hull boundary condition is explained that ship hull moves at a unit speed including all general modes with forward speed at the same time. The radiation problem illustrated as Fig.2.4 is the wave-making problem caused by the periodic motions of the ship with forward speed

whereas the diffraction problem illustrated as Fig.2.5 concerns about wave-making problem caused by the incident wave on the movement-fixed ship with forward speed from the second formula.

The lineazied first-order unsteady pressure $P^{(1)}$ is shown in Eq.(2.63), and right-hand side can be separated into two pressure terms on diffraction problem and radiation problem, respectively. Substituting Eqs.(2.7),(2.8), and (2.38) into Eq.(2.63), the first-order unsteady pressure is rewritten as the follows cancelling the time variable on the both sides.

$$P^{(1)}(\boldsymbol{x};t) = \Re\left[\{p_D(\boldsymbol{x}) + p_R(\boldsymbol{x})\}\, e^{i\omega_e t}\right]. \tag{2.64}$$

where

$$\begin{cases} p_D = \rho g \zeta_a \dfrac{\omega_e}{\omega_0}\left(1 + \dfrac{U}{i\omega_e}\boldsymbol{V}\cdot\nabla\right)(\phi_I + \phi_S) \\ p_R = -\rho(i\omega_e^2)\displaystyle\sum_{j=1}^{N} X_j \left\{\left(1 + \dfrac{U}{i\omega_e}\boldsymbol{V}\cdot\nabla\right)\phi_j - \dfrac{1}{2}\left(\dfrac{U}{\omega_e}\right)^2 (\boldsymbol{h}^j\cdot\nabla)(\boldsymbol{V}\cdot\boldsymbol{V})\right\} \end{cases}. \tag{2.65}$$

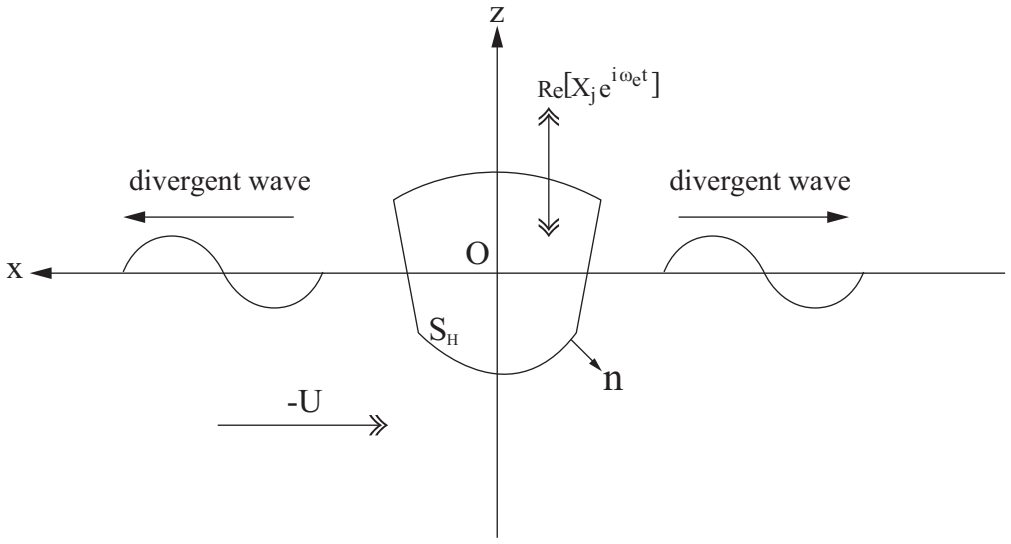

FIGURE 2.4: Concept of radiation problem.

2.5.1 Added Mass and Damping Coefficient

By integrating radiation pressure over ship hull on i-th mode, complex radiation force with time variable can be expressed as $F_i^R = \Re[F_i e^{i\omega_e t}]$, and F_i is the complex amplitude of radiation

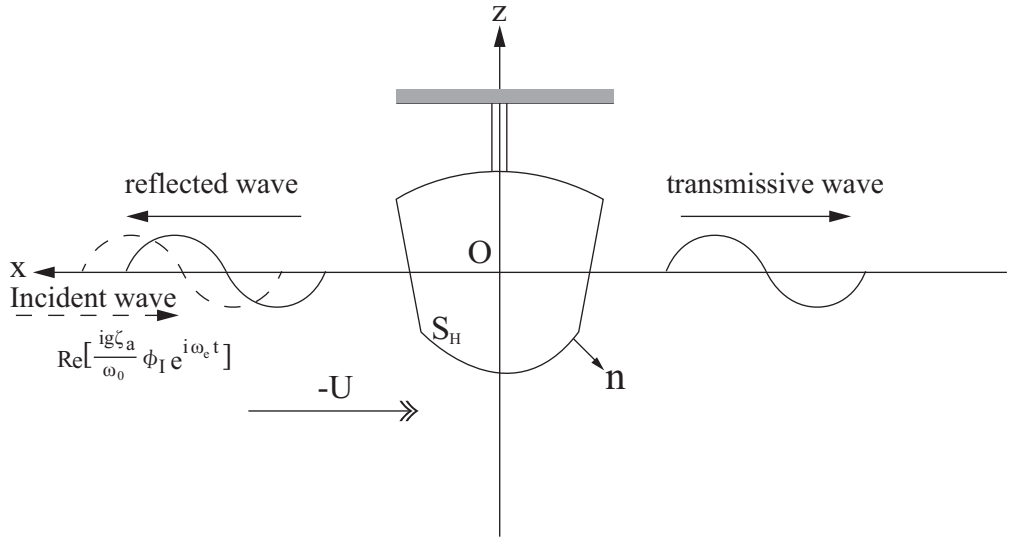

FIGURE 2.5: Concept of diffration problem.

force applying on i-th mode which can be written as

$$F_i = \sum_{j=1}^{N} \boldsymbol{X}_j T_{ij} \quad (i = 1 \sim N), \tag{2.66}$$

where

$$T_{ij} = \rho(i\omega_e)^2 \iint_{S_H} \left\{ \left(1 + \frac{U}{i\omega_e}\boldsymbol{V}\cdot\nabla\right)\phi_j - \frac{1}{2}\left(\frac{U}{\omega_e}\right)^2 (\boldsymbol{h}^j\cdot\nabla)(\boldsymbol{V}\cdot\boldsymbol{V}) \right\} \widetilde{n}_i dS. \tag{2.67}$$

T_{ij} is the radiation force acting on i-th mode caused by j-th mode obtained from integrating $P^{(1)}$ over ship hull on i-th mode. It is noted that the direction of pressure is opposite to the normal vector of the hull surface, so there is a minus mark when integration.

Complex radiation force also can be expressed as the sum of the part (called added mass) proportional to acceleration $(i\omega_e)^2\boldsymbol{X}_j$ and the part (damping coefficient) proportional to velocity $i\omega_e\boldsymbol{X}_j$. Radiation force on i-th mode can be rewritten by using added mass a_{ij} and damping coefficient b_{ij}:

$$F_i^R \equiv -\sum_{j=1}^{N}[a_{ij}\ddot{\xi}_j + b_{ij}\dot{\xi}_j] = \Re\left\{-\sum_{j=1}^{N}\boldsymbol{X}_j[(i\omega_e)^2 a_{ij} + i\omega_e b_{ij}]e^{i\omega_e t}\right\}, \tag{2.68}$$

and

$$F_i = -\sum_{j=1}^{N}\boldsymbol{X}_j[(i\omega_e)^2 a_{ij} + i\omega_e b_{ij}]. \tag{2.69}$$

Combining Eqs.(4.12), (2.67) and (2.69), added mass and damping coefficient can be written as

$$a_{ij} = \Re\left[\frac{T_{ij}}{\omega_e^2}\right], \quad b_{ij} = -\Im\left[\frac{T_{ij}}{\omega_e}\right], \tag{2.70}$$

where "$\Im$" means the imaginary part of complex.

2.5.2 Wave-exciting Force

In the same way, wave-exciting force on i-th mode in diffraction problem can be expressed as $F_i^W = \Re[E_i e^{i\omega_e t}]$, and complex amplitude E_i is shown as

$$E_i = -\rho g \zeta_a \frac{\omega_e}{\omega_0} \iint_{S_H} \left(1 + \frac{U}{i\omega_e} \boldsymbol{V} \cdot \nabla\right) (\phi_I + \phi_S) \widetilde{n}_i dS. \tag{2.71}$$

2.6 Rankine Panel Method

Green function method is widely used due to fewer unknowns in computation by integrating only on ship hull and to automatically satisfy the complicated radiation conditions. However, Green function method can only treat the situation of uniform flow as basis flow and there are some onerous formulae that need to be calculation.

In order to overcome the above shortcomings, Rankine panel method or Rankine source method is adopted to express and solve the potential flow mentioned above. For the purpose of obtaining an equivalent solution of kernel function $1/r$ of Green function method, Rankine panel method cannot satisfy the strict physical meaning at infinity like Green function method. Setting Rankine source not only on ship hull but also on the free surface surrounding it and applying Reyleigh's artificial friction coefficient or computational technique like panel shift method to satisfy numerically radiation boundary condition is necessary for computational processing. Because the additional Rankine sources are applied on the free surface, the disadvantage of a large amount of calculation cannot be avoided compared to Green's function method. However, Rankine panel method could calculate the response of ship with forward in the case of double-body flow as basis flow more rigorously and accurately.

To gain a solution of the velocity potential, so-called indirect Rankine panel method (RPM) is adopted, in which the velocity potential of unsteady flow ϕ_j (or ϕ_S) is expressed by a source distribution σ_j (or σ_S) over the body surface S_H and the free surface S_F, with the Rankine source used as the kernel function. Namely, the velocity potential can be written as follows:

$$\phi_j(P) = \iint_{S_H + S_F} \sigma_j(Q) G(P;Q) dS(Q), \tag{2.72}$$

where $P = (x, y, z)$ denotes a field point in the fluid and $Q = (x', y', z')$ an integration point on the boudary surface, and

$$G(P;Q) = \begin{cases} G_0(P;Q) + G_0'(P;Q) & \text{when} \quad Q \quad \text{on} \quad S_H \\ G_0(P;Q) & \text{when} \quad Q \quad \text{on} \quad S_F \end{cases}, \tag{2.73}$$

where,

$$G_0(P;Q) = -\frac{1}{4\pi r}, \quad G_0'(P;Q) = -\frac{1}{4\pi r'}, \tag{2.74}$$

$$\begin{cases} r = \sqrt{(x-x')^2 + (y-y')^2 + (z-z')^2} \\ r' = \sqrt{(x-x')^2 + (y-y')^2 + (z+z')^2} \end{cases}. \tag{2.75}$$

Note that $G_0'(P;Q)$ is the mirror image of $G_0(P;Q)$ reflected in the undisturbed free surface $z = 0$ and hence $G_0(P;Q) + G_0'(P;Q)$ satisfies the rigid-wall boundary condition on $z = 0$, which is to satisfied by the double-body flow velocity potential used as the steady basis flow in this paper. When the field point P is located on the boundary S_H or S_F and considered the singularity of $1/r$, the normal derivative of Eq.(2.72) takes the following form

$$\frac{\partial \phi_j(P)}{\partial n_P} = \frac{1}{2}\sigma_j(P) + \iint_{S_F+S_H} \sigma_j(Q)\frac{\partial G(P;Q)}{\partial n_P})dS(Q). \tag{2.76}$$

The left-hand side of Eq.(2.76) can be specified with the boundary conditions when P is located on S_H from Eq.(2.57) and on S_F from Eq.(2.36). To make the solution unique, the radiation condition must be imposed, which is numerically satisfied in the RPM by the so-called panel shift method (RSM), shifting collocation points by one panel upstream on the free surface. More details on the numerical procedure can be referred to Iwashita et al. (2016) [30] and Yasuda et al. (2016) [31] from which several numercial techniques to handle infinty boundary condition are introduced and its effectiveness is proven.

In the same way for basis flow, potential ϕ_D can be presented in the form of Rankine source over ship hull as well as free surface:

$$\phi_D(P) = \iint_{S_H+S_F} \sigma_D(Q)G(P;Q)dS(Q), \tag{2.77}$$

and substituting above equation into Eq.(2.12), the source strength σ_D of ϕ_D over ship hull and free surface can be confirmed. Then, the double-body flow potential can be got.

To apply Rankine source into boundary conditions for the purpose of solving source strength to present velocity potential, boundary conditions should be discretized for numerical computation.

Velocity potential of j-th motion in Eq.(2.72) can be rewritten as discretized form as

$$\begin{aligned}\phi_j(P_i) &= \sum_{n=1}^{NH} \sigma_j(Q_n)\{G_0(P_i,Q_n) + G_0'(P_i,Q_n)\}\Delta S(Q_n) \\ &+ \sum_{n=NH+1}^{NH+NF} \sigma_j(Q_n) G_0(P_i,Q_n)\Delta S(Q_n), \end{aligned} \tag{2.78}$$

where NH is the meshing number of ship hull we set and NF is free surface. The specific data is shown in the result section. Annotation 'i' is the position information of wanted velocity potential of j-th motion and 'n' is the position information for source strength. The figure 2.6 shows the concept of Rankine sources over ship hull and free surface, and illustrates the position information.

To begin with, for radiation problem, if the potential position P_i locates on the ship hull, the ship hull condition Eq.(2.57) can be shown as

$$\begin{aligned}\widetilde{n}_j(P_i) + \frac{U}{i\omega_e}\widetilde{m}_j(P_i) &= \sum_{n=1}^{NH} \sigma_j(Q_n)\frac{\partial}{\partial n}\{G_0(P_i,Q_n) + G_0'(P_i,Q_n)\}\Delta S(Q_n) \\ &+ \sum_{n=NH+1}^{NH+NF} \sigma_j(Q_n)\frac{\partial}{\partial n} G_0(P_i,Q_n)\Delta S(Q_n) \quad \text{on} \quad S_H \quad . \end{aligned} \tag{2.79}$$

Then, if the position location is on the free surface, its boundary condition Eq.(2.36) is applied and can be discretized as

$$
\begin{aligned}
&\sum_{n=1}^{NH} \sigma_j(Q_n)\Big[K_e\{G_0(P_i,Q_n)+G_0'(P_i,Q_n)\} \\
&-\left\{2i\tau\frac{\partial\Phi_D(P_i)}{\partial x}+\frac{2}{K_0}\left(\frac{\partial\Phi_D(P_i)}{\partial x}\frac{\partial^2\Phi_D(P_i)}{\partial x^2}+\frac{\partial\Phi_D(P_i)}{\partial y}\frac{\partial^2\Phi_D(P_i)}{\partial x\partial y}\right)\right\}\times\left\{\frac{\partial G_0(P_i,Q_n)}{\partial x}+\frac{\partial G_0'(P_i,Q_n)}{\partial x}\right\} \\
&-\left\{2i\tau\frac{\partial\Phi_D(P_i)}{\partial y}+\frac{2}{K_0}\left(\frac{\partial\Phi_D(P_i)}{\partial x}\frac{\partial^2\Phi_D(P_i)}{\partial x\partial y}+\frac{\partial\Phi_D(P_i)}{\partial y}\frac{\partial^2\Phi_D(P_i)}{\partial y^2}\right)\right\}\times\left\{\frac{\partial G_0(P_i,Q_n)}{\partial y}+\frac{\partial G_0'(P_i,Q_n)}{\partial y}\right\} \\
&-\frac{2}{K_0}\frac{\partial\Phi_D(P_i)}{\partial x}\frac{\partial\Phi_D(P_i)}{\partial y}\left\{\frac{\partial^2 G_0(P_i,Q_n)}{\partial x\partial y}+\frac{\partial^2 G_0'(P_i,Q_n)}{\partial x\partial y}\right\} \\
&-\frac{1}{K_0}\frac{\partial\Phi_D(P_i)}{\partial x}\frac{\partial\Phi_D(P_i)}{\partial x}\left\{\frac{\partial^2 G_0(P_i,Q_n)}{\partial x^2}+\frac{\partial^2 G_0'(P_i,Q_n)}{\partial x^2}\right\} \\
&-\frac{1}{K_0}\frac{\partial\Phi_D(P_i)}{\partial y}\frac{\partial\Phi_D(P_i)}{\partial y}\left\{\frac{\partial^2 G_0(P_i,Q_n)}{\partial y^2}+\frac{\partial^2 G_0'(P_i,Q_n)}{\partial y^2}\right\}-\left\{\frac{\partial G_0(P_i,Q_n)}{\partial z}+\frac{\partial G_0'(P_i,Q_n)}{\partial z}\right\}\Big]\Delta S(Q_n) \\
&+\sum_{n=NH+1}^{NH+NF}\sigma_j(Q_n)\,[K_eG_0(P_i,Q_n) \\
&-\left\{2i\tau\frac{\partial\Phi_D(P_i)}{\partial x}+\frac{2}{K_0}\left(\frac{\partial\Phi_D(P_i)}{\partial x}\frac{\partial^2\Phi_D(P_i)}{\partial x^2}+\frac{\partial\Phi_D(P_i)}{\partial y}\frac{\partial^2\Phi_D(P_i)}{\partial x\partial y}\right)\right\}\frac{\partial G_0(P_i,Q_n)}{\partial x} \\
&-\left\{2i\tau\frac{\partial\Phi_D(P_i)}{\partial y}+\frac{2}{K_0}\left(\frac{\partial\Phi_D(P_i)}{\partial x}\frac{\partial^2\Phi_D(P_i)}{\partial x\partial y}+\frac{\partial\Phi_D(P_i)}{\partial y}\frac{\partial^2\Phi_D(P_i)}{\partial y^2}\right)\right\}\frac{\partial G_0(P_i,Q_n)}{\partial y} \\
&-\frac{2}{K_0}\frac{\partial\Phi_D(P_i)}{\partial x}\frac{\partial\Phi_D(P_i)}{\partial y}\frac{\partial^2 G_0(P_i,Q_n)}{\partial x\partial y}-\frac{1}{K_0}\frac{\partial\Phi_D(P_i)}{\partial x}\frac{\partial\Phi_D(P_i)}{\partial x}\frac{\partial^2 G_0(P_i,Q_n)}{\partial x^2} \\
&-\frac{1}{K_0}\frac{\partial\Phi_D(P_i)}{\partial y}\frac{\partial\Phi_D(P_i)}{\partial y}\frac{\partial^2 G_0(P_i,Q_n)}{\partial y^2}-\frac{\partial G_0(P_i,Q_n)}{\partial z}\Big]\Delta S(Q_n)=0 \quad \text{on} \quad S_F \quad ,
\end{aligned}
\tag{2.80}
$$

where $K_e = \omega_e^2/g$ and KeL is called nondimensional wavenumber, $K_0 = g/U^2$ is Kelvin wave's wavenumber, and nondimensional value $\tau = U\omega_e/g$ called Hanaoka's parameter which dominates the unsteady flow.

Furthermore, for diffraction problem, the discretized ship hull boundary condition can be expressed as following equation from Eq.(2.54) if P_i locating on ship hull.

$$
\begin{aligned}
-\frac{\partial\phi_I(P_i)}{\partial n} &= \sum_{n=1}^{NH}\sigma_S(Q_n)\frac{\partial}{\partial n}\left\{G_0(P_i,Q_n)+G_0'(P_i,Q_n)\right\}\Delta S(Q_n) \\
&+ \sum_{n=NH+1}^{NH+NF}\sigma_S(Q_n)\frac{\partial}{\partial n}G_0(P_i,Q_n)\Delta S(Q_n) = \quad \text{on} \quad S_H \quad .
\end{aligned}
\tag{2.81}
$$

The last situation is P_i is on free surface in diffraction problem, the discretized equation is similar to Eq.(2.80) as long as change σ_j to σ_S shown as

$$
\begin{aligned}
&\sum_{n=1}^{NH} \sigma_S(Q_n)\Big[K_e\{G_0(P_i,Q_n)+G_0'(P_i,Q_n)\} \\
&-\left\{2i\tau\frac{\partial\Phi_D(P_i)}{\partial x}+\frac{2}{K_0}\left(\frac{\partial\Phi_D(P_i)}{\partial x}\frac{\partial^2\Phi_D(P_i)}{\partial x^2}+\frac{\partial\Phi_D(P_i)}{\partial y}\frac{\partial^2\Phi_D(P_i)}{\partial x\partial y}\right)\right\}\times\left\{\frac{\partial G_0(P_i,Q_n)}{\partial x}+\frac{\partial G_0'(P_i,Q_n)}{\partial x}\right\} \\
&-\left\{2i\tau\frac{\partial\Phi_D(P_i)}{\partial y}+\frac{2}{K_0}\left(\frac{\partial\Phi_D(P_i)}{\partial x}\frac{\partial^2\Phi_D(P_i)}{\partial x\partial y}+\frac{\partial\Phi_D(P_i)}{\partial y}\frac{\partial^2\Phi_D(P_i)}{\partial y^2}\right)\right\}\times\left\{\frac{\partial G_0(P_i,Q_n)}{\partial y}+\frac{\partial G_0'(P_i,Q_n)}{\partial y}\right\} \\
&-\frac{2}{K_0}\frac{\partial\Phi_D(P_i)}{\partial x}\frac{\partial\Phi_D(P_i)}{\partial y}\left\{\frac{\partial^2 G_0(P_i,Q_n)}{\partial x\partial y}+\frac{\partial^2 G_0'(P_i,Q_n)}{\partial x\partial y}\right\} \\
&-\frac{1}{K_0}\frac{\partial\Phi_D(P_i)}{\partial x}\frac{\partial\Phi_D(P_i)}{\partial x}\left\{\frac{\partial^2 G_0(P_i,Q_n)}{\partial x^2}+\frac{\partial^2 G_0'(P_i,Q_n)}{\partial x^2}\right\} \\
&-\frac{1}{K_0}\frac{\partial\Phi_D(P_i)}{\partial y}\frac{\partial\Phi_D(P_i)}{\partial y}\left\{\frac{\partial^2 G_0(P_i,Q_n)}{\partial y^2}+\frac{\partial^2 G_0'(P_i,Q_n)}{\partial y^2}\right\}-\left\{\frac{\partial G_0(P_i,Q_n)}{\partial z}+\frac{\partial G_0'(P_i,Q_n)}{\partial z}\right\}\Big]\Delta S(Q_n) \\
&+\sum_{n=NH+1}^{NH+NF}\sigma_S(Q_n)\,[K_eG_0(P_i,Q_n) \\
&-\left\{2i\tau\frac{\partial\Phi_D(P_i)}{\partial x}+\frac{2}{K_0}\left(\frac{\partial\Phi_D(P_i)}{\partial x}\frac{\partial^2\Phi_D(P_i)}{\partial x^2}+\frac{\partial\Phi_D(P_i)}{\partial y}\frac{\partial^2\Phi_D(P_i)}{\partial x\partial y}\right)\right\}\frac{\partial G_0(P_i,Q_n)}{\partial x} \\
&-\left\{2i\tau\frac{\partial\Phi_D(P_i)}{\partial y}+\frac{2}{K_0}\left(\frac{\partial\Phi_D(P_i)}{\partial x}\frac{\partial^2\Phi_D(P_i)}{\partial x\partial y}+\frac{\partial\Phi_D(P_i)}{\partial y}\frac{\partial^2\Phi_D(P_i)}{\partial y^2}\right)\right\}\frac{\partial G_0(P_i,Q_n)}{\partial y} \\
&-\frac{2}{K_0}\frac{\partial\Phi_D(P_i)}{\partial x}\frac{\partial\Phi_D(P_i)}{\partial y}\frac{\partial^2 G_0(P_i,Q_n)}{\partial x\partial y}-\frac{1}{K_0}\frac{\partial\Phi_D(P_i)}{\partial x}\frac{\partial\Phi_D(P_i)}{\partial x}\frac{\partial^2 G_0(P_i,Q_n)}{\partial x^2} \\
&-\frac{1}{K_0}\frac{\partial\Phi_D(P_i)}{\partial y}\frac{\partial\Phi_D(P_i)}{\partial y}\frac{\partial^2 G_0(P_i,Q_n)}{\partial y^2}-\frac{\partial G_0(P_i,Q_n)}{\partial z}\Big]\Delta S(Q_n)=0 \quad \text{on} \quad S_F \quad . \qquad (2.82)
\end{aligned}
$$

Combining the above boundary conditions expressed as discretized form, the Rankine source strength σ_j or σ_S over ship hull and free surface could be solvable, then the velocity potential for general motion can be obtained finally by Eq.(2.72).

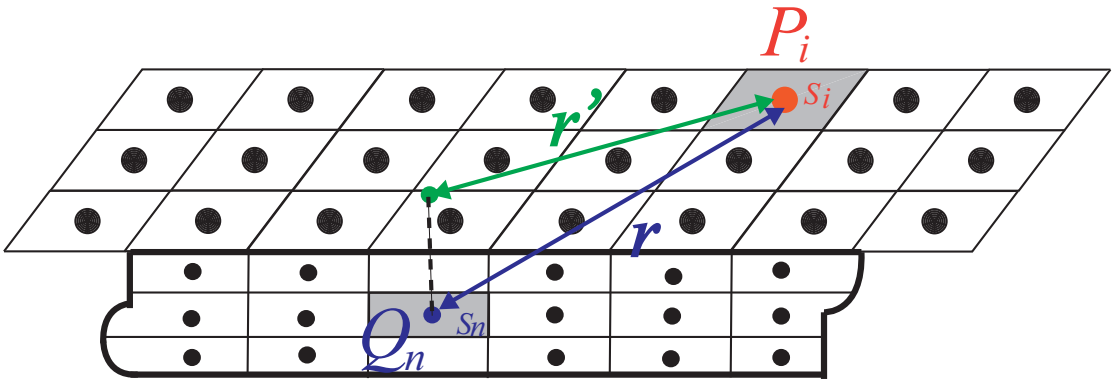

FIGURE 2.6: Concept of Rankine panel method.

2.7 Conclusion

This section defined two kinds of velocity potentials, steady and unsteady, based on whether varies with time. The pressure field was decided by Bernoulli's equation derived from Euler's equation and continuity equation. The free-surface boundary conditions were obtained through the fact that wave pressure on free-surface should be atmosphere pressure and the substantial derivative of pressure on free-surface equals zero. Substantial derivative to ship hull could get the ship hull boundary conditions for general motions and export the general n-term and m-term. For unsteady pressure, it was separated into radiation problem and diffraction problem according to the ship motion. Rankine panel method was used to express the source strength and decide the velocity potential.

Chapter 3

Mode Functions

In Chapter 3, it is elucidated that the deduction of natural modes of Timoshenko beam with concerning about shearing force and introduction of several numerical orthogonal polynomials to replace of natural modes reasonably. The orthogonality of natural modes of Timoshenko beam is discussed compared with Euler beam and orthogonal polynomials like Legendre and Chebyshev polynomials. Cubic B-spline methods including modal analysis method and direct method are also adopted to prove the correct conclusion even the dry modes are presented as piecewise curve using cubic B-spline basis functions.

3.1 Natural Modes of Timoshenko Beam

A theoretical analysis of the effect of transverse shear and rotary inertia on the natural frequencies of a uniform beam is presented. There are common frequencies between the calculated and the observed values of the natural frequency when considering the Euler-Bernoulli beam that tends to overestimate the natural frequencies of elastic motions and this problem is exacerbated for higher elastic modes. Taking secondary effects of shear lag and deformation of a beam by transverse shear and rotary inertia into account, the Timoshenko beam is adopted as a more advanced model and provides a better prediction, especially for a blunt ship. The effect of shear lag and deformation is to increase the flexibility of the beam because of the additional deflection that is introduced. The effect of rotary inertia is to increase the dynamic loading on the beam because of the additional inertia loading due to the rotational acceleration of the differential elements of the beam.

The Timoshenko beam proposed a beam theory by adding the effects of shear distortion and rotary inertia to the Euler-Bernoulli model. In the Timoshenko beam theory, Bernoulli's assumption that plane cross-sections remain perpendicular to the neutral axis of the beam is replaced

by the assumption that the angle between the neutral axis and the normal of the cross-section is proportional to the shear force. Figure 3.1 illustrates the concept of Timoshen beam and Euler Bernoulli beam.

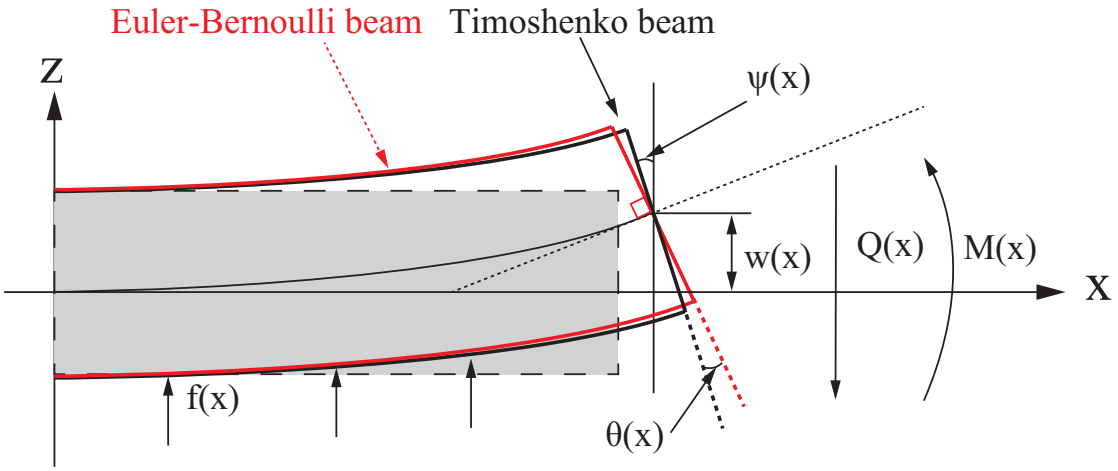

FIGURE 3.1: Concept map of Timoshenko beam and Euler-Bernoulli beam.

Consider a beam with Length L ($L = 2$ by default in this paper, $x = -L/2m$ is ship stern and $x = L/2$ is bow), the modulus of elasticity $E(x)$, the mass per unit of length $m(x)$, the moment of inertia $I(x)$, the cross-section area $A(x)$. It is noteworthy that the ship is treated as a uniform beam, parameters $E(x)$, $m(x)$, $A(x)$ do not change with the location in theory for brevity so that constant values E, m, A are used in the following content and these can be shifted out of the integration. The linear transverse deflection of beam is the same as vertical deflection $H_z(x;t)$ mentioned in Eq.(2.38). Let $\psi(x;t)$ be the angle which the cross-section of the beam forms with the y-axis (downward is positive direction) when only bending is considered and $\partial H_z(x;t)/\partial x = \psi(x;t)$ due to assumption in Bernoulli beam theory. If the cress-section is subsequently exposed to shear, it does not rotate further but the neutral axis changes its angle with x-axis by the angle $\theta(x;t)$. Then, the relation by further assumption can be expressed as

$$\frac{\partial H_z(x;t)}{\partial x} = \psi(x;t) + \theta(x;t). \tag{3.1}$$

The constitutive equations within linear elasticity are

$$\begin{cases} M(x;t) = -EI\dfrac{d\psi(x;t)}{dx} \\ Q(x;t) = k'\theta(x;t)GA = k'\left(\dfrac{\partial H_z(x;t)}{\partial x} - \psi(x;t)\right)GA \end{cases}, \tag{3.2}$$

where, $M(x;t)$ is bending moment, $Q(x;t)$ is shearing force, G is shearing modulus and k' is correction factor dependent on cross-section geometry.

The inertia moment M_I due to rotary using same moment I is

$$M_I(x;t) = \rho_s I \frac{\partial^2 \psi(x;t)}{\partial t^2}, \tag{3.3}$$

where, ρ_s is the density of beam per unit length and $\rho_s = m/A$.

Considering the balance of moments of beam on small scale length dx, the balance equation can be expressed as

$$-\frac{\partial M(x;t)}{\partial x}dx + Q(x;t)dx = \rho_s I \frac{\partial^2 \psi(x;t)}{\partial t^2}dx. \tag{3.4}$$

Substituting Eq.(3.2) into above equation, we can obtain:

$$EI\frac{\partial^2 \psi(x;t)}{\partial x^2} + k'\left(\frac{\partial H_z}{\partial x} - \psi(x;t)\right)GA - \rho_s I\frac{\partial^2 \psi(x;t)}{\partial t^2} = 0. \tag{3.5}$$

Then, the equilibrium equation of force balance can be gained by the same way in the form of

$$\frac{\partial Q(x;t)}{\partial x}dx + f(x;t)dx = m\frac{\partial^2 H_z}{\partial t^2}dx, \tag{3.6}$$

where, $f(x;t)$ is the distribution of external force by flow. Substituting Eq.(3.2) into above equation, the equilibrium equation can be rewritten as

$$m\frac{\partial^2 H_z(x;t)}{\partial t^2} - k'\left(\frac{\partial^2 H_z(x;t)}{\partial x^2} - \frac{\partial \psi(H;t)}{\partial x}\right)GA = f(x;t). \tag{3.7}$$

Differentiate Eq.(3.5) with respect to x, equation can be derived to

$$EI\frac{\partial^3 \psi(x;t)}{\partial x^3} + k'\left(\frac{\partial^2 H_z(x;t)}{\partial x^2} - \frac{\partial \psi(x;t)}{\partial x}\right)GA - \rho_s I\frac{\partial^3 \psi(x;t)}{\partial t^2 \partial x} = 0. \tag{3.8}$$

The vibration equation can be obtained as follows by combinating Eqs.(3.7),(3.8) and cancelling the terms about $\psi(x;t)$:

$$\begin{aligned} m\frac{\partial^2 H_z(x;t)}{\partial t^2} + EI\frac{\partial^4 H_z(x;t)}{\partial x^4} - \left(\rho_s I + \frac{mEI}{k'GA}\right)\frac{\partial^4 H_z(x;t)}{\partial x^2 \partial^2 t} + \rho_s I\frac{m}{k'GA}\frac{\partial^4 H_z(x;t)}{\partial t^4} \\ = f(x;t) - \frac{mEI}{k'GA}\frac{\partial^2 f(x;t)}{\partial x^2} + \frac{\rho_s I}{k'GA}\frac{\partial^2 f(x;t)}{\partial t^2}. \end{aligned} \tag{3.9}$$

Here, the effect of rotary inertia is neglected for simplicity by setting $\rho_s I = 0$ and because the effect is believed to be small. The equilibrium equation can be simplified further as

$$m\frac{\partial^2 H_z(x;t)}{\partial t^2} + \frac{\partial^2}{\partial x^2}\left\{EI\frac{\partial^2 H_z(x;t)}{\partial x^2}\right\} - \frac{\partial^2}{\partial x^2}\left\{\frac{mEI}{k'GA}\frac{\partial^2 H_z(x;t)}{\partial^2 t}\right\} = f(x;t) - \frac{\partial^2}{\partial x^2}\left\{\frac{mEI}{k'GA}f(x;t)\right\}. \tag{3.10}$$

It is the equation of elastic motion in the time domain of the Timoshenko beam. This formula also applies the cases of parameters like EI or $mEI/k'GA$ are functions with respect to x rather than constant. The first term of the above equation is inertia force, the second term is restoring force by the beam (different with restoring force by flow) and the third term is called shearing force which is a new term after considering the shear. The second term on the right-hand side of Eq.(3.10) is also an added term due to shear and it can be understood as a new force by the beam (called shear-deformation force in the paper) due to shear effect contrast to an external force by the flow.

To obtain the dry eigen-mode functions of the Timoshenko beam, let us consider the homogeneous equation with the right-hand side of Eq.(3.9) equal to zero, and a uniform beam with m, EI, $k'GA$ treated as constant. In the case of dry eigen-mode, let the vertical displacement is expressed as n-th mode shape for now:

$$H_z(x;t) = \Re\left\{w_n(x)e^{i\sigma_n t}\right\}, \tag{3.11}$$

where σ_n denotes the natural frequency of dry mode which is different with ω_e. Applying the variable-separation method with the time-dependent part, the homogeneous equation for the x-dependent vertical deflection of the uniform Timoshenko beam can be written as follows:

$$\frac{1}{\kappa_n^4}\frac{d^4 w_n(x)}{dx^4} + \gamma^2\frac{d^2 w_n(x)}{dx^2} - w_n(x) = 0, \quad \kappa_n^4 = \frac{m}{EI}\sigma_n^2, \quad \gamma^2 = \frac{EI}{k'GA}, \tag{3.12}$$

where κ_n denotes the n-th eigen-value associated with the dry-mode natural frequency σ_n, $w_n(x)$ is the corresponding n-th dry eigen-mode function of the vertical deflection, and γ^2 is the ratio of flexural rigidity with shear rigidity which determines the amount of contribution of shear effect.

Considering the free-free beam satisfying Eq.(3.12) and the free-end boundary conditions, we can obtain analytical solutions expressed in the form as follows. The specific steps and explanation refer to Appendix A.

$$w_{n+5}(x) = Y_n(q) = \begin{cases} \dfrac{1}{1+(\alpha_n/\beta_n)^2}\left[\dfrac{\cos(\kappa_n\alpha_n q)}{\cos(\kappa_n\alpha_n)} + \dfrac{\cosh(\kappa_n\beta_n q)}{\cosh(\kappa_n\beta_n)}\dfrac{\alpha_n^2}{\beta_n^2}\right] & \text{for} \quad n = 2l \\ \dfrac{1}{1+(\alpha_n/\beta_n)^2}\left[\dfrac{\sin(\kappa_n\alpha_n q)}{\sin(\kappa_n\alpha_n)} + \dfrac{\sinh(\kappa_n\beta_n q)}{\sinh(\kappa_n\beta_n)}\dfrac{\alpha_n^2}{\beta_n^2}\right] & \text{for} \quad n = 2l+1 \end{cases}, \tag{3.13}$$

where

$$\alpha_n = \sqrt{\frac{\sqrt{(\kappa_n\gamma)^4+4}+(\kappa_n\gamma)^2}{2}}, \quad \beta_n = \sqrt{\frac{\sqrt{(\kappa_n\gamma)^4+4}-(\kappa_n\gamma)^2}{2}}, \tag{3.14}$$

and $n = 2, 3, \ldots, q = x/(L/2)$ (with L the beam length); $n = 2l$ is an even number and $n = 2l+1$ is an odd number for $l = 1, 2, \ldots$ and κ_n, α_n, β_n denote the values satisfying the following eigen-value equation:

$$\begin{cases} \alpha_n \tan(\kappa_n\alpha_n) + \beta_n \tanh(\kappa_n\beta_n) = 0, & \text{for} \quad n = 2l \\ \beta_n \tan(\kappa_n\alpha_n) - \alpha_n \tanh(\kappa_n\beta_n) = 0, & \text{for} \quad n = 2l+1 \end{cases}, \tag{3.15}$$

Note that $w_n(x)$ is an even or odd function of x according to as n is even or odd number, which is obvious from Eq.(3.13), and with the ratio γ^2 changing, the eigen-values change automatically, influencing the homogeneous solutions eventually. These dry modes of the Timoshenko beam satisfy the physically relevant free-end boundary conditions but they are not orthogonal unfortunately because of the existence of shear effect. It can be easily confirmed that the homogenous equations and resulting solutions of the Euler beam can be retrieved when γ^2 becomes zero. Then, these solutions of Euler beam can be retarded from above equations by $\alpha = \beta = 1$ in the form as follows.

$$w^E_{n+5}(x) = Y^E_n(q) = \begin{cases} \frac{1}{2}\left[\frac{\cos(\kappa^E_n q)}{\cos(\kappa^E_n)} + \frac{\cosh(\kappa^E_n q)}{\cosh(\kappa^E_n)}\right], & \text{for} \quad n = 2l \\ \frac{1}{2}\left[\frac{\sin(\kappa^E_n q)}{\sin(\kappa^E_n)} + \frac{\sinh(\kappa^E_n q)}{\sinh(\kappa^E_n)}\right], & \text{for} \quad n = 2l+1 \end{cases}, \tag{3.16}$$

and the eigen-value equation are

$$\begin{cases} \tan\kappa^E_n + \tanh\kappa^E_n = 0, & \text{for} \quad n = 2l \\ \tan\kappa^E_n - \tanh\kappa^E_n = 0, & \text{for} \quad n = 2l+1 \end{cases}. \tag{3.17}$$

Superscript "E" is attached here for values of Euler beam to distinguish between two beams. Natural modes of Euler beam is widely used by researchers due to their unique advantages which are orthogonality of mass and stiffness matrices as

$$\begin{cases} \int_{-1}^{1} Y^E_m(q) Y^E_n(q) dq = \frac{1}{2}\delta_{mn} \\ \int_{-1}^{1} \frac{d^2Y^E_m(q)}{dq^2}\frac{d^2Y^E_n(q)}{dq^2} dq = \frac{1}{2}(k^E_n)^4\delta_{mn} \end{cases}. \tag{3.18}$$

It is convenient and fast to calculate the mass matrix and stiffness matrix by these relations in computation. However, there are no such same neat relations in the case of Timoshenko beam when shear effect is considered. It must be reminded that Timoshenko beam is announced to be

non-orthogonal for deformation of free-free beam in integration. In fact, there is different form or definition in the technical term of "orthogonality" which is discussed in Appendix A. There is no such relation of this kind that can be used because of free-free end conditions.

From Eq.(3.15) and Eq.(3.17), the natural frequencies of dry modes σ_n for the Timoshenko beams ($\gamma^2 = 3.6 \times 10^{-3}$ for example in paper) and Euler beam ($\gamma^2 = 0$) can be calculated in the condition of $m/EI = 0.5833$ and the result is shown in Table 3.1. The Euler beam model tends to give slightly higher natural frequencies as compared to the Timoshenko beam, and this tendency becomes prominent for the natural frequencies of higher modes. The Timoshenko beam could predict more precise ship motions at higher encounter wave frequencies for a blunt ship where the shear effect cannot simply be neglected.

TABLE 3.1: Dry mode frequencies comparsion between Euler beam ($\gamma^2 = 0$) and Timoshenko beam ($\gamma^2 = 3.6 \times 10^{-3}$) with parameters $m/EI = 0.5833$.[unit rad/s].

$n+5$	Euler beam	Timoshenko beam
7	23.163	21.314
8	63.851	49.274
9	125.173	80.041
10	209.917	110.597
11	309.098	140.586

3.2 Orthogonal Polynomials

In this paper, an even simpler representation for elastic mode functions is studied in terms of orthogonal polynomials, despite the fact that these functions are just mathematical and hence lack a physical basis and do not satisfy appropriate free-end boundary conditions.

At the first example of orthogonal polynomials, the Legendre polynomials $P_n(q)$ are applied as elastic modes of the Timoshenko beam. In mathematics, the Legendre polynomials are solutions to Legendre's differential equation. A compact expression for the Legendre polynomials is given by Rodrigues' formula:

$$w_{n+5}(x) = P_n(q) = \frac{1}{2^n n!}\frac{d^n}{dq^n}(q^2-1)^n \quad n = 2, 3, 4, \ldots \tag{3.19}$$

An important property of the Legendre polynomials is that they are orthogonal with respect to the interval $-1 \leq q \leq 1$ and its result can be expressed as

$$\int_{-1}^{1} P_m(q)P_n(q)dq = \frac{2}{2n+1}\delta_{mn} \quad . \tag{3.20}$$

As the next exampe of orthogonal polynomials, we consider the Chebyshev polynomials, which include the first kind denoted as $T_n(q)$ and the second kind denoted as $U_n(q)$. They are expressed as follows:

$$w_{n+5}(x) = \begin{cases} T_n(\cos\Theta) = \cos n\Theta \\ U_n(\cos\Theta) = \dfrac{\sin(n+1)\Theta}{(n+1)\sin\Theta} \end{cases}, \tag{3.21}$$

where $q = \cos\Theta$ and $n = 2, 3, \ldots$. It should be noted that the second kind $U_n(q)$ is modified from the original definition by dividing with $n+1$ so that $U_n(q=1) = 1$.

$T_n(q)$ and $U_n(q)$ are orthogonal in terms of the weight funtion $(1-q^2)^{-\frac{1}{2}}$ and $(1-q^2)^{\frac{1}{2}}$, respectively, over the interval $-1 \le q \le 1$:

$$\begin{cases} \displaystyle\int_{-1}^{1} T_m(q)T_n(q)\frac{1}{\sqrt{1-q^2}}dq = \frac{\pi}{2}\delta_{mn} \\ \displaystyle\int_{-1}^{1} U_m(q)U_n(q)\sqrt{1-q^2}dq = \frac{\pi}{2}\frac{1}{(n+1)^2}\delta_{mn} \end{cases}. \tag{3.22}$$

Notably, these orthogonality relations of Chebyshev polynomials cannot be applied to the computation of the mass matrix and also the stiffness matrix to be explained later, due to the weight functions shown in Eq.(3.22). Therefore it is worth noting that there is coupling in the mass matrix for all even or odd modes, including the coupling of rigid modes of heaven and pitch with the corresponding symmetric or antisymmetric polynomials for elastic modes. The mode

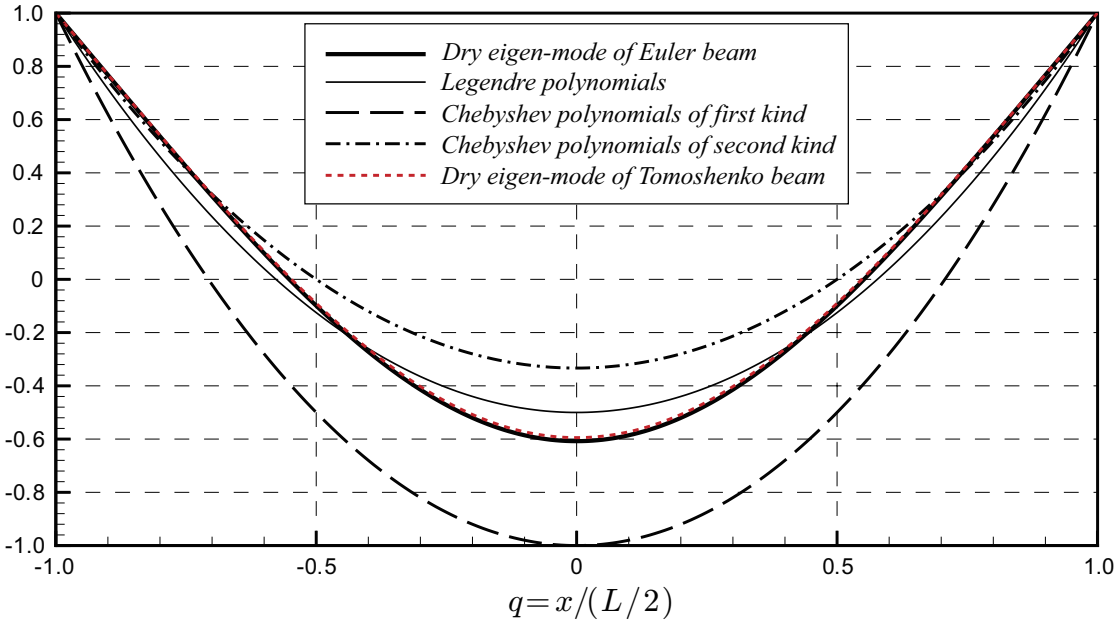

FIGURE 3.2: The first elastic mode shapes ($j = 7$) of mode functions used.

functions for the first five elastic modes ($j = 7 \sim 11$) of motion using Legendre and two kinds of

TABLE 3.2: Comparison between Legendre and Chebyshev polynomials.

$n+5$	$P_n(q)$	$T_n(q)$	$U_n(q)$
7	$(3q^2-1)/2$	$2q^2-1$	$(4q^2-1)/3$
8	$(5q^3-3q)/2$	$4q^3-3q$	$(8q^3-4q)/4$
9	$(35q^4-30q^2+3)/8$	$8q^4-8q^2+1$	$(16q^4-12q^2+1)/5$
10	$(63q^5-70q^3+15q)/8$	$16q^5-20q^3+5q$	$(32q^5-32qx^3+6q)/6$
11	$(231q^6-315q^4+105q^2-5)/16$	$32q^6-48q^4+18q^2-1$	$(64q^6-80q^4+24q^2-1)/7$

Chebyshev polynomials are compared in Table 3.2. Here, the profiles of the first elastic bending mode (j=7) of these polynomials are illustrated as Fig.3.2, in which the free-free beam modes of Euler beam and Timoshenko beam are included for comparison. The curves of Euler and Timoshenko beams just have a slight difference, which is caused by the shear effect. Note that only the dry modes of Euler beam and the Legendre polynomials can be zero when the proposed mode functions are integrated over the interval $-1 \leq q \leq 1$, from which no coupling terms exist between rigid and elastic motions in the mass matrix if these two mode functions are used in the subsequent hydroelastic analysis.

3.3 B-spline Element Methods

Another modal analysis method is provided for supplement by using the cubic B-spline element in this study for estimating the hydroelastic responses of ships with forward speed in waves. B-spline methods are widely used in computer-aided geometric design and the field of ship hull design. It has minimal support with respect to a given degree, smoothness, and domain partition. Any spline function of a given degree can be expressed as a linear combination of B-splines of that degree. Following this idea, according to the objects, total deformation or dry modes, the studies on this topic can be classified into two categories, the "direct method" and "modal analysis method". Clearly, no matter which method you choose, the curve order is depended on the B-spline basis function like the cubic B-spline function used in the paper is third order. That means the curves represented as cubic B-spline function has third-order on each partition and second-order continuous on the joint of partitions.

3.3.1 Modal Analysis Algorithm

In modal analysis algorithm, the dry modes are represented as the combination of cubic B-spline basis function in the process of solving dry modes and eigen-value equations. The j-th natural

modes of Euler beam can be expressed as

$$w_j^E(x) = \sum_{k=1}^{NX+3} \alpha_k^j N_k^3(x), \quad u \in [a_k, a_{k+1}) \tag{3.23}$$

where, $U = \{a_0, a_1, a_2, \cdots, a_m\}$ be a nondecreasing sequence of real number. NX is the number of panel division in the x-direction. Since one cubic spline function extends its influence over four panels, the number of total unknows is $NX+3$. The a_i are called knots and U is knot vector. The i-th B-spline basis function of p-degree (order $p+1$), denoted by N_i^n with knots. Here $N_k^3(x)$ is called cubic B-spline basis function and simplied as $N_k(x)$ for breivty in the following content. α_k^j is k-th control point (or control strength is more suitable in paper) to deciding j-th natural mode of Euler beam. n-th degree B-splines can be calculated by using recursion formula called de Boor, Cox recursion formula:

$$N_i^0 = \begin{cases} 1 & u \in [a_k, a_{k+1}) \\ 0 & \text{otherwise} \end{cases}, \tag{3.24}$$

and

$$N_k^n(u) = a_k^{n-1} N_k^{n-1}(u) + (1 - a_{i+k}^{n-1}) N_{k+1}^{n-1}(u), \tag{3.25}$$

where

$$a_k^{n-1} = (u - a_k)/(a_{k+n} - a_k). \tag{3.26}$$

The uniform slender ship is divided into 10 panel divisions and let sequence U be uniformed from ship stern to bow like $U = \{-1, -0.8, \cdots, 0.8, 1\}$. The uniform cubic B-spline basis functions are illustrated in Fig.3.3. Substituting Eq.(3.23) into spatial vertial deflection of Euler beam (shear effect is neglected here for better explanation) as

$$-\omega_j^2 m w_j(x) + \frac{d^2}{dx^2}\left\{EI\frac{d^2 w_j(x)}{dx^2}\right\} = 0. \tag{3.27}$$

It turns to expressions of matrices form as the following equation with $[M]$ and $[D]$ after integrating over ship hull with weight $N_i(x)$. M_{ij} and D_{ij} are mass matrix and stiffness matrix.

$$(-\kappa_j^4[M] + [D])\{\alpha^j\} = \{0\}, \qquad \kappa_j^4 = \frac{m\omega_j^2}{EI}, \tag{3.28}$$

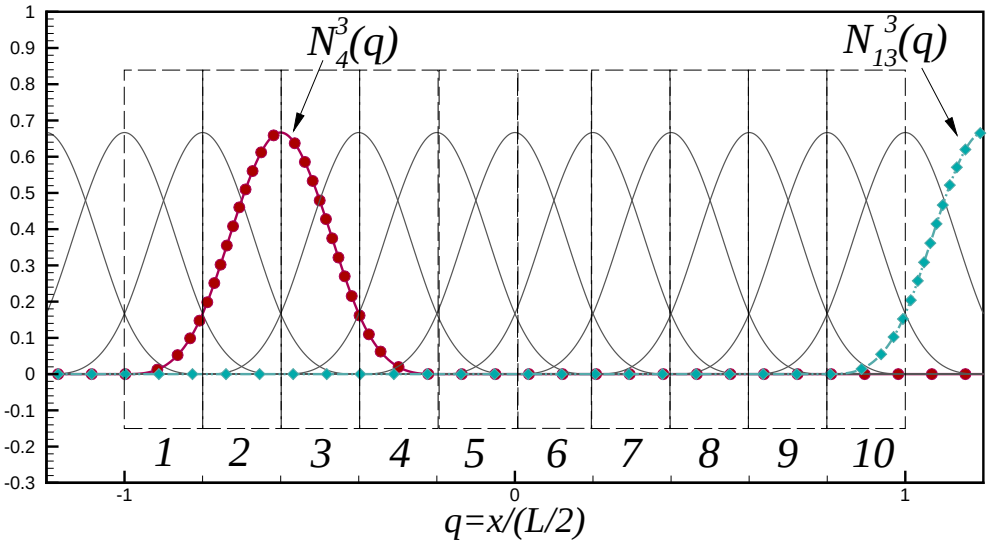

FIGURE 3.3: The uniform cubic B-spline basis functions.

and

$$\begin{cases} M_{ij} = L/2 \int_{-1}^{1} N_i(q) N_j(q) dq \\ D_{ij} = L/2 \int_{-1}^{1} \frac{d^2 N_i(q)}{dq^2} \frac{d^2 N_j(q)}{dq^2} dq \end{cases}. \tag{3.29}$$

Then, multiplying both sides of the formula by the inverse mass matrix $[M]^{-1}$ can obtain the eigenvectors $\{\alpha^j\}$ and eigenvalues κ_j^4:

$$\left(-[M]^{-1}[D]\right)\{\alpha^j\} = \kappa_j^4 \{\alpha^j\}. \tag{3.30}$$

Eigenvalues correspond to the natural frequency of Euler beam while eigenvectors correspond to mode shapes. Frequencies of dry modes are compared between dry modes of Euler beam and calculated by cubic B-spline function in Tab.3.3. Since $NX + 3 = 13$, it should have 11 frequencies for elastic modes shown in the table and two zero for rigid motions. It is clear that the B-spline method can calculate dry frequencies precisely up to $j = 15$ when $NX = 10$ judging from error compared with dry modes of Euler beam.

After knowing eigenvectors α^j, the mode shapes can be calculated but still need to be normalized to make sure that $w(q = 1) = 1$. Then, the mode shapes using cubic B-spline basis function can be expressed as

$$w_j(x) = q_j \sum_{k=1}^{NX+3} \alpha_k^j N_k(x) = \sum_{k=1}^{NX+3} \alpha_k^j N_k(x). \tag{3.31}$$

TABLE 3.3: Frequency comparison between dry modes and B-spline method.

Mode	Dry mode	B-spline	error %
7	2.3650	2.3648	−0.0093
8	3.9266	3.9271	0.0144
9	5.4978	5.5016	0.0691
10	7.0680	7.0840	0.2187
11	8.6390	8.6882	0.5650
12	10.2102	10.3375	1.2467
13	11.7810	12.0500	2.2830
14	13.3518	13.7553	3.0218
15	14.9226	15.1659	1.6301
16	16.4934	26.2236	58.9942
17	21.2058	26.2992	24.0187

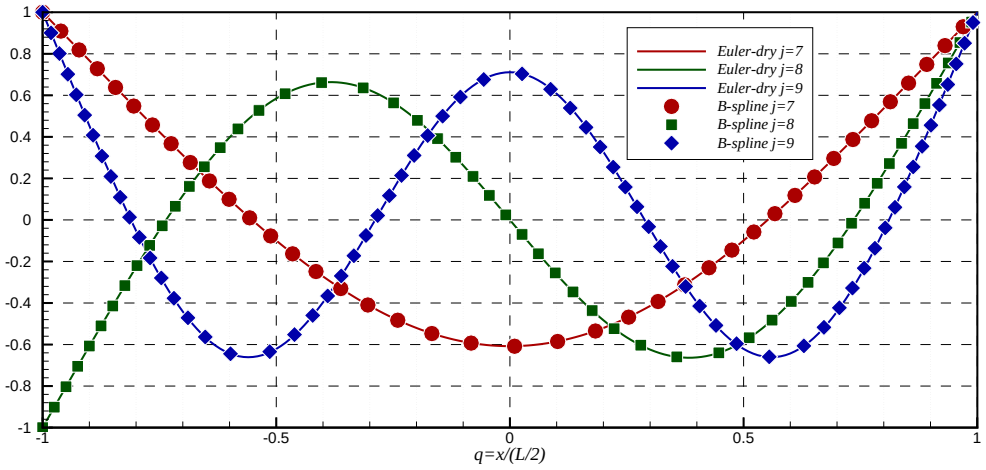

FIGURE 3.4: Mode shapes comparison between dry modes and B-spline method.

where constant q_j can be attached into eigenvectors α^j directly. The curves calculated by using the B-spline method are shown in Fig.3.4. In other words, the so-called modal analysis method is that the continuous modeshapes of dry modes are expressed in the form of segment lines with fourth-order using cubic B-spline basis functions. Higher-order elastic bending modes demand more divisions to achieve accurate fitting. This method has no essential difference from the method solving dry modes, which does not make any difference in the final numerical results. Thus, the total vertical deflection can be expressed as

$$H_z(x) = \Re\left[\sum_{j=1}^{N} X_j w_j(x) e^{i\omega_e t}\right] = \Re\left[\sum_{j=1}^{N} X_j \sum_{k=1}^{NX+3} \alpha_k^j N_k(x) e^{i\omega_e t}\right]. \tag{3.32}$$

where α_k^j is known and X_j is what we need to solve.

If the effect of shear is included, the spatial vertical deflection of Timoshenko beam is expressed as

$$-\omega_j^2 m w_j(x) + \frac{d^2}{dx^2}\left\{EI\frac{d^2 w_j(x)}{dx^2}\right\} + m\omega_j^2\gamma^2\frac{d^2}{dx^2}\left\{w_j(x)\right\} = 0, \tag{3.33}$$

and the expression of matrices form as

$$\left(-\kappa_j^4[M] + [D] + \gamma^2\kappa_j^4[S]\right)\{\alpha^j\} = \{0\}, \qquad \kappa_i^4 = \frac{m\omega_j^2}{EI}. \tag{3.34}$$

Then, the above equation can be rewritten as

$$\left(-\kappa_j^4\left\{[M] - \gamma^2[S]\right\} + [D]\right)\{\alpha^j\} = \{0\}, \quad S_{ij} = L/2\int_{-1}^{1} N_i(q)\frac{d^2 N_j(q)}{dq^2}dq \quad , \tag{3.35}$$

and when combinating matrices $[M]$ and $[S]$ as one matrix $[M'] = [M] - \gamma^2[S]$, it becomes same expression as Eq.(3.30). Consequently, eigenvalue and eigenvector are related to parameter γ which dominates the contribution of shear effect.

3.3.2 Direct Method Algorithm

The second algorithm is that we only consider or focus on the totally coupled deformation like in the real case instead of decomposing it into rigid modes and elastic modes since the cubic B-spline curve can draw random curves. In other words, cubic B-spline basis function is treated as kind of mode function. The deformation that do not care about any modes just the final one can be presented as

$$H_z(x) = \Re\left[\sum_{k=1}^{NX+3}\alpha_k N_k(x)e^{i\omega_e t}\right]. \tag{3.36}$$

This method skips the process of modal analysis, whose results should same as the modal analysis one. Observing from Eq.(3.32), it is essentially the same as Eq.(3.36) if we set $(\sum_{j=1}^{N} X_j\alpha_k^j) = \alpha_k$ as shown in following equation:

$$\sum_{j=1}^{N} X_j w_j(x) = \sum_{j=1}^{N} X_j \sum_{k=1}^{NX+3}\alpha_k^j N_k(x) = \sum_{k=1}^{NX+3}\left(\sum_{j=1}^{N} X_j\alpha_k^j\right)N_k(x) = \sum_{k=1}^{NX+3}\alpha_k N_k(x). \tag{3.37}$$

3.4 Conclusion

This section deduced the equilibrium equation of elastic motion in the time domain of the Timoshenko beam through force analysis on the Timoshenko beam which considers shear effect.

Then, the homogenous equation for the x-dependent vertical deflection of the uniform Timoshenko beam and its analytical solutions can be obtained. Also, the solution in the case of Euler beam is easy to gain as long as set parameter $\gamma^2 = 0$ which means no shear effect. Some orthogonal polynomials are presented as optional mode functions to take place, like Legendre polynomials and Chebyshev polynomials of two kinds. Not only the dry modes of Euler beam or Timoshenko beam but also the natural frequency can be calculated perfectly using the B-spline element method.

Chapter 4

Motion Equations

Chapter 4 describes the formulation of motions of Timoshenko beam including rigid and elastic modes using the mode expansion method by integration over ship hull with weights into matrix form. Appropriate boundary conditions are induced and adopted into the stiffness matrix to obtain the final conventional motion equations. The spatial part of the distribution of external force acting on a transverse cross-section of the ship is used which is analyzed in Chapter 2 and the shear-deformation force is added here. The matrices of mass, stiffness, and shearing are denoted and the form of restoring force is derived.

4.1 Mode Expansion Method

The Timoshenko beam model incorporates the effects of shear distortion and rotary inertia in the Euler beam model. In the Timoshenko beam theory, Bernoulli's assumption that plane cross-sections remain orthogonal to the neutral axis of the beam is replaced by the assumption that the angle between the neutral axis and the normal of the cross-section is proportional to the shearing force. The linear vertical deflection of the beam neutral axis can be divided into contributions due to bending moment and shearing force. By neglecting the effect of rotary inertia, the time-domain motion equation of a Timoshenko beam can be written as shown in Eq.(3.10). Then, separating the time dependency $e^{i\omega_e t}$ with an assumption of time-harmonic external force and resulting oscillation of a ship, the spatial part of the vertical deflection, denoted as $w(x)$, is governed by the beam equation affected by the shearing force:

$$-\omega_e^2 m w(x) + \frac{d^2}{dx^2}\left\{EI\frac{d^2 w(x)}{dx^2}\right\} + \omega_e^2 \frac{d^2}{dx^2}\left\{m\gamma^2 w(x)\right\} = f(x) - \frac{d^2}{dx^2}\left\{\gamma^2 f(x)\right\}, \tag{4.1}$$

where $\gamma^2 = EI/k'GA$ as defined in Eq.(3.12) and $f(x)$ is the spatial part of the distribution of external local pressure force acting on a transverse cross-section of the ship, and the second term

on the right-hand side of Eq.(4.1) may be written as

$$f^S(x) = -\frac{d^2}{dx^2}\left\{\gamma^2 f(x)\right\}. \tag{4.2}$$

This term is the second-order derivative of the external local force $f(x)$ in the x-direction which is a new term added to the case of Euler beam when the shear effect is considered. Thus, $f^S(x)$ is functionally treated as the shear-deformation force.

Since both ends of he ship are free, the appropriate boundary conditions to be satisfied free-end boundary condition as

$$EI\frac{d^2w(x)}{dx^2} = 0, \quad \frac{d}{dx}\left\{EI\frac{d^2w(x)}{dx^2}\right\} = 0, \quad \text{at} \quad x = \pm\frac{L}{2}, \tag{4.3}$$

where L is the ship length.

The time-independent vertical deflection $w(x)$ may be expanded in an appropriate set as modes like Eq.(2.38), in the form

$$w(x) = \sum_{j=1}^{N} X_j w_j(x), \tag{4.4}$$

where the complex amlitude X_j of each mode is unknown at this stage. Substituting Eq.(4.4) into Eq.(4.3) and writing the result with the normalized coordinate $q = x/(L/2)$, the free-end boundary conditoins can be written as follows:

$$\sum_{j=1}^{N} X_j EI\frac{d^2w_j(q)}{dq^2} = 0, \quad \sum_{j=1}^{N} X_j \frac{d}{dq}\left\{EI\frac{d^2w_j(q)}{dq^2}\right\} = 0, \quad \text{at} \quad q = \pm 1. \tag{4.5}$$

With the method of weighted residuals, Eq.(4.1) is multiplied by $w_i(x)$, $i = 1 \sim N$, and integrated over the length of beam. Then, we obtain a linear system of simultaneous equations for determining the unknown complex amplitude X_j in the form

$$\sum_{j=1}^{N} X_j \int_{-L/2}^{L/2} w_i(x)\left[-\omega_e^2 m w_j(x) + \omega_e^2 \frac{d^2}{dx^2}\left\{m\gamma^2 w_j(x)\right\} + \frac{d^2}{dx^2}\left\{EI\frac{d^2w_j(x)}{dx^2}\right\}\right]dx$$
$$= \int_{-L/2}^{L/2} w_i(x)\left\{f(x) + f^S(x)\right\}dx. \tag{4.6}$$

In terms of matrix coefficients, these can be briefly rewritten in the form

$$\sum_{j=1}^{N} X_j\left[-\omega_e^2 M_{ij} + \omega_e^2 S_{ij} + D_{ij}\right] = \Gamma_i + \Gamma_i^S \quad \text{for} \quad i = 1 \sim N, \tag{4.7}$$

where the matrix coefficients M_{ij}, S_{ij}, and D_{ij} on the left-hand side are mass matrix, shear matrix, and the stiffness matrix, respectively. With the normalized coordinate q, these matrix coefficients are written as

$$M_{ij} = \frac{L}{2}\int_{-1}^{1} m w_i(q) w_j(q) dq, \tag{4.8}$$

$$S_{ij} = \frac{L}{2}\int_{-1}^{1} w_i(q)\frac{d^2}{dq^2}\left\{m\gamma^2 w_j(q)\right\} dq, \quad S_{ij} \neq S_{ji}, \tag{4.9}$$

$$D_{ij} = \frac{L}{2}\int_{-1}^{1} w_i(q)\frac{d^2}{dq^2}\left\{EI\frac{d^2 w_j(q)}{dq^2}\right\} = \frac{L}{2}\int_{-1}^{1} EI\frac{d^2 w_i(q)}{dq^2}\frac{d^2 w_j(q)}{dq^2} dq. \tag{4.10}$$

For the stiffness matrix D_{ij} defined above, the mid term in Eq.(4.10) including the fourth-order differentiation of $w_j(q)$ is transformed into the right term using the partial integration twice. However, this transformation is correct if and only if each mode function $w_j(q)$ satisfies the free-end boundary conditions of Eq.(4.3). If the mathematical orthogonal functions (like Legendre and Chebyshev polynomials) are used in place of the dry eigen-modes of Euler or Timoshenko beam, we must enforce the free-end boundary conditions not to each mode function but to the sum of mode functions as shown in Eq.(4.5). The transformation incorporating the free-end boundary conditions of Eq.(4.5) can be made using partial integration twice, the result of which is described explicitly as follows:

$$\begin{aligned}
\sum_{j=1}^{N} X_j D_{ij} &= \frac{L}{2}\int_{-1}^{1} w_i(q)\sum_{j=1}^{N} X_j\frac{d^2}{dq^2}\left\{EI\frac{d^2 w_j(q)}{dq^2}\right\} dq \\
&= \frac{L}{2}\left[w_i(q)\sum_{j=1}^{N} X_j\frac{d}{dq}\left\{EI\frac{d^2 w_j(q)}{dq^2}\right\} + \frac{dw_i(q)}{dq}\sum_{j=1}^{N} X_j EI\frac{d^2 w_j(q)}{dq^2}\right]_{-1}^{1} \\
&+ \frac{L}{2}\int_{-1}^{1}\frac{d^2 w_i(q)}{dq^2}\sum_{j=1}^{N} X_j EI\frac{d^2 w_j(q)}{dq^2} dq \\
&= \frac{L}{2}\sum_{j=1}^{N} X_j\int_{-1}^{1} EI\frac{d^2 w_i(q)}{dq^2}\frac{d^2 w_j(q)}{dq^2} dq.
\end{aligned} \tag{4.11}$$

Namely, it is the total deflection rather than each mode function that satisfies the free-end conditions and the two terms in the second line of Eq.(4.11) should be equal to zero because of the free-end boundary conditions specified by Eq.(4.5). In other words, notwithstanding the fact that orthogonal polynomials have no physical meaning and generally each polynomial function does not satisfy the free-end boundary conditions, the combination of them using the superposition method can conform to the specified boundary conditions and also the beam equation.

4.2 Conventional Motion Equation

The right-hand side of Eq.(4.7) is the integration of external local force acting on a transverse cross-section over ship hull and external local force $f(x)$ is analysed in Chapter 2 (shown as $P(x)$). It includes contributions of linearized pressure force as the diffraction, radiation and restoring forces. These forces are defined as

$$\Gamma_i = \int_{-L/2}^{L/2} w_i(x) f(x) dx = E_i + \sum_{j=1}^{N} X_j(\omega_e^2 a_{ij} - i\omega_e b_{ij} - C_{ij}), \tag{4.12}$$

where, E_i, a_{ij},b_{ij}, and C_{ij} indicate the exciting force, added mass, damping coefficient, and restoring force coefficient, respectively. Similarly, the integration of shear-deformation force can be expanded or expressed in the same form with corresponding symbols with superscript "S" as

$$\Gamma_i^S = \int_{-L/2}^{L/2} w_i(x) f^S(x) dx = E_i^S + \sum_{j=1}^{N} X_j(\omega_e^2 a_{ij}^S - i\omega_e b_{ij}^S - C_{ij}^S). \tag{4.13}$$

Then, E_i^S, a_{ij}^S, b_{ij}^S, and C_{ij}^S are exciting force, added mass, damping coefficient and restoring force coefficient due to shear-deformation force and can be calculated numerically as

$$T_{ij}^S = \rho(i\omega_e)^2 \iint_{S_H} -\frac{d^2}{dx^2}\left[\gamma^2\left\{\left(1 + \frac{U}{i\omega_e}\boldsymbol{V}\cdot\nabla\right)\phi_j - \frac{1}{2}\left(\frac{U}{\omega_e}\right)^2 (\boldsymbol{h}^j\cdot\nabla)(\boldsymbol{V}\cdot\boldsymbol{V})\right\}\right]\widetilde{n}_i dS. \tag{4.14}$$

and

$$a_{ij}^S = \Re\left[\frac{T_{ij}^S}{\omega_e^2}\right], \quad b_{ij}^S = -\Im\left[\frac{T_{ij}^S}{\omega_e}\right]. \tag{4.15}$$

Then,

$$E_i^S = -\rho g \zeta_a \frac{\omega_e}{\omega_0} \iint_{S_H} -\frac{d^2}{dx^2}\left[\gamma^2\left(1 + \frac{U}{i\omega_e}\boldsymbol{V}\cdot\nabla\right)(\phi_I + \phi_S)\widetilde{n}_i\right] dS. \tag{4.16}$$

Restoring force is provided by the integration of the variance of hydrostatic pressure. For elastic bodies, although seemingly different expressions have been discussed, e.g. Newman [18], Malenica [3, 32, 33], their equivalence was proven by Malenica (2009) [34]. It was proven with the rigorous mathematical transformation that the results of seemingly different expressions must be the same, from which the restoring force coefficient C_{ij} considering the effect of elastic deformation is expressed as:

$$C_{ij} = C_{ij}^H + C_{ij}^m, \tag{4.17}$$

$$C_{ij}^S = C_{ij}^{HS} + C_{ij}^{mS}, \tag{4.18}$$

where

$$
\begin{aligned}
C_{ij}^{H} &= \rho g \iint_{S_H} h_z^j \widetilde{n}_i dS \\
&+ \rho g \iint_{S_H} z \left\{ \frac{\partial h_k^j}{\partial x_k} \widetilde{n}_i + \left(h_k^j \frac{\partial h_l^i}{\partial x_k} - h_k^i \frac{\partial h_l^i}{\partial x_k} \right) \widetilde{n}_l \right\} dS, \qquad (4.19) \\
C_{ij}^{m} &= g \iiint_{V} \left(h_x^j \frac{\partial h_z^i}{\partial x} + h_y^j \frac{\partial h_z^i}{\partial y} + h_z^j \frac{\partial h_z^i}{\partial z} \right) dm, \qquad (4.20) \\
C_{ij}^{HS} &= \rho g \iint_{S_H} -\frac{d^2}{dx^2} \left[\gamma^2 h_z^j \widetilde{n}_i \right] dS \\
&+ \rho g \iint_{S_H} -\frac{d^2}{dx^2} \left[\gamma^2 z \left\{ \frac{\partial h_k^j}{\partial x_k} \widetilde{n}_i + \left(h_k^j \frac{\partial h_l^i}{\partial x_k} - h_k^i \frac{\partial h_l^i}{\partial x_k} \right) \widetilde{n}_l \right\} \right] dS, \qquad (4.21) \\
C_{ij}^{mS} &= g \iiint_{V} -\frac{d^2}{dx^2} \left[\gamma^2 \left(h_x^j \frac{\partial h_z^i}{\partial x} + h_y^j \frac{\partial h_z^i}{\partial y} + h_z^j \frac{\partial h_z^i}{\partial z} \right) \right] dm. \qquad (4.22)
\end{aligned}
$$

Then restoring forces F_i^H and F_i^{HS} caused by shear effect are presented already in Eqs.(4.12) and (4.13) as

$$
\begin{aligned}
F_i^H &= -\sum_{j=1}^{N} X_j C_{ij} \quad , \qquad (4.23) \\
F_i^{HS} &= -\sum_{j=1}^{N} X_j C_{ij}^S \quad . \qquad (4.24)
\end{aligned}
$$

The specific steps to obtain restoring force coefficient and its explanation refer to Appendix B.

Substituting Eqs.(4.12) and (4.13) and transposing the radiation and restoring force coefficients to the left-hand side of Eq.(4.7), we have a conventional set of motion equations in the form

$$
\begin{aligned}
&\sum_{j=1}^{N} X_j \left[-\omega_e^2 (M_{ij} + a_{ij} + a_{ij}^S) + i\omega_e (b_{ij} + b_{ij}^S) + \omega_e^2 S_{ij} + D_{ij} + (C_{ij} + C_{ij}^S) \right] \\
&\qquad = E_i + E_i^S \quad \text{for} \quad i = 1 \sim N. \qquad (4.25)
\end{aligned}
$$

We note that the modes of motion to be induced in head waves include surge, heave, pitch, and structural deflections. As mentioned above, the dry eigen-modes of the Timoshenko beam are not orthogonal and thus, the computation for the Timoshenko beam will not be easy as that for the Euler beam when adopting the method of weighted residuals.

Chapter 5

Results and Discussion

Chapter 5 describes the convergence study at forward speed for a total displacement of a ship by a superposition of all modes of motion. Modified Wigley model is used as a calculated object in Rankine panel method. The figures of non-dimensional added mass, damping coefficient, and exciting force are illustrated and compared with different mode functions. The values are defined to check the convergence of total deflection of the ship displacement at the ship bow. The reason for the different speeds of convergence is discussed. Supplementary proof of convergence using Legendre polynomials is raised through analyzing the satisfied boundary condition to prove five bending modes are enough from which the number of the demanded bending mode can be decreased. The effect of shearing force in Timoshenko beam is studied by changing the ratio of flexural and shear rigidities artificially. The merits and demerits for each mode function are analyzed.

5.1 Convergence Study at Forward Speed

The total displacement of a ship must be computed, which can be accomplished by a superposition of all modes of motions as shown in Eq.(2.38), where each mode is the product of the amplitude computed and the mode function assumed. The effectiveness of each of the mode functions adopted must be indicated by checking not only the amplitude of the j-th mode $|X'_j|$ but also the convergence in the sum of all assumed modes representing the total magnitude of the deflection. The parameters with the prime mean the non-dimensional values, for example, $X'_j = X_j/\zeta_a$.

As a reference point for the deflection of the ship, we consider the bow ($q = 1$) in this paper, where we note that $w_j(q = 1) = 1$ for all kinds of mode functions. In fact, due to limitations in the experiment, the wave frequency is limited to a range of relatively low frequencies where

TABLE 5.1: Principal dimensions of modified Wigley model.

Principal dimensions	value [unit]
Ship length: L	2.0 $[m]$
Ship breadth: B	0.3 $[m]$
Draft: d	0.125 $[m]$
Displacement:V	0.0425 $[m^3]$
Height of the ceter of gravity:KG	0.0404 $[m]$
Radius of gyration:κ_{yy}/L	0.248
Froude number:Fn	0.200
Flexural rigidity:EI	360.5257 $[Nm^2]$
Rigidity ratio for Timoshenko beam:γ^2	0.0036

rigid vibration mode is dominant. In order to better verify the applicability of Legendre and Chebyshev polynomials as the mode functions and the accuracy of computed results at higher frequencies, numerical computations using the RPM for the forward speed case are implemented for a modified Wigley model, expressed mathematically as follows:

$$\eta = (1-\zeta^2)(1-\xi^2)(1+0.2\xi^2) + \zeta^2(1-\zeta^8)(1-\xi^2)^4, \tag{5.1}$$

where $\xi = x/(L/2)$, $\eta = y/(B/2)$ and $\zeta = z/d$. The principal dimensions including L, B, d are shown in Table 5.1 and its 3-dimensional figure is shown as Fig.5.1. In Eq.(5.1), x, y, z are the coordinates of the grid points on the hull surface and ξ, η, ζ are the corresponding dimensionless values. Figure 5.2 illustrates the location relations between the modified Wigley model and free surface. Mesh in red is the top view of the modified Wigley model (discretized into 1080 panels), blue is the free surface mesh in the range $-5 < x < 2$ (discretized into 5320 panels), and green mesh is a slightly shifted mesh of free surface using panel shift method to satisfy the radiation boundary condition on infinity. These meshes move to upstream and upward in z-direction slightly.

Numercial computations were performed for the Froude number $F_n = 0.2$, the incident-wave amplitude $\zeta_a = 0.02m$, the flexutral rigidity $EI = 360.5257Nm^2$, and $\gamma^2 = 3.6 \times 10^{-3}$.

The values of non-dimensional added mass and damping coefficient for elastic modes are defined as

$$a'_{ij} = \frac{a_{ij}}{\rho V} \quad \text{for} \quad i = 7 \sim N \quad j = 7 \sim N, \tag{5.2}$$

$$b'_{ij} = \frac{b_{ij}}{\rho V \omega_e} \quad \text{for} \quad i = 7 \sim N \quad j = 7 \sim N. \tag{5.3}$$

where V here is ship displacement. The non-dimensional added mass for first five elastic modes are illustrated as Figs.5.3 to 5.7. Then, non-dimensional damping coefficient are Figs.5.8 to 5.12.

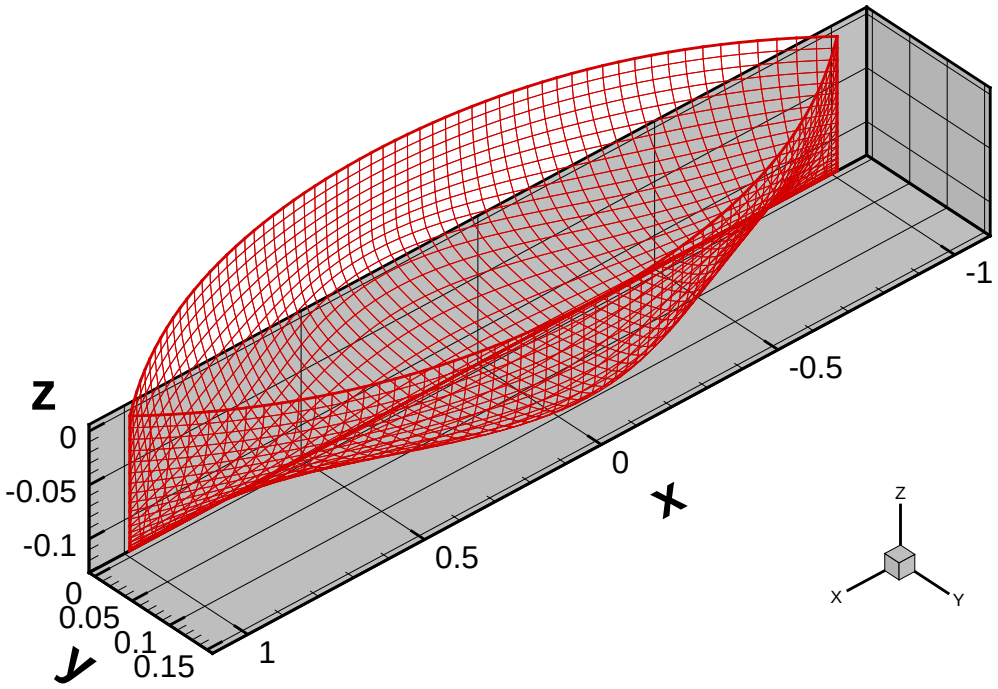

FIGURE 5.1: 3-dimensional modified Wigley model

For reference, computed results shown in these figures are the ones using Legendre polynomials (in red dashed line), both kinds of Chebyshev polynomials (in yellow diamond and green circle), and the dry eigen-modes of the Timoshenko beam (in black line). The abscissa KL is the non-dimensional wavenumber of encountered wave frequency ($KL = \omega_e^2 L/g$). By observing four curves in figures of non-dimensional added mass, it can be found that the amplitudes of added

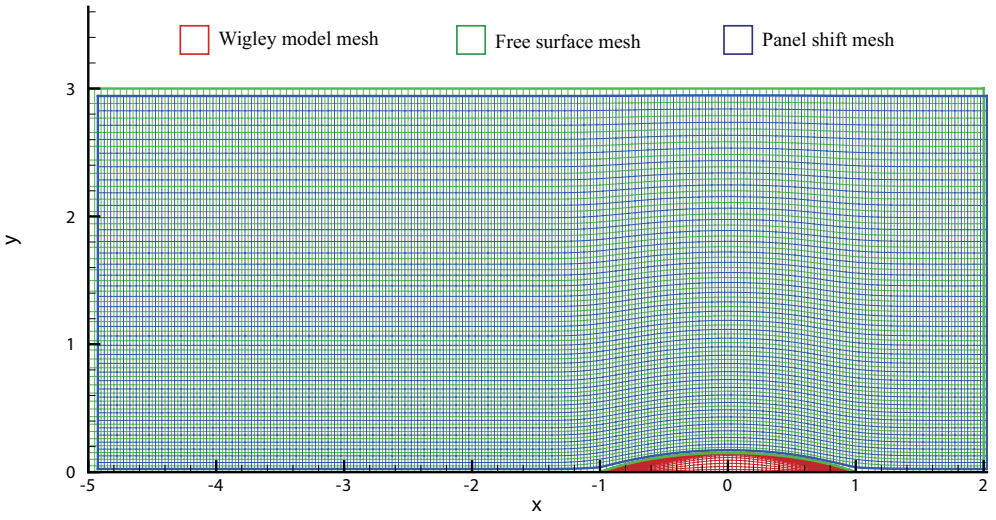

FIGURE 5.2: Meshes of modified Wigley model and free surface in Rankine panel method

mass basically maintain constant values in a relatively large frequency range and the added mass does not change so much when the bending mode turns higher. There is a sharp increasing trend in the range of low frequencies which can be speculated that the program using RPM loses its effectiveness gradually at very low frequencies. What's more, the amplitudes of curves using Chebyshev polynomials of the first kind are largest and almost two or three times as large as the others, because the amplitude of the mode shapes themselves are larger as can be seen from Fig.3.2. Since the amplitude of Chebyshev polynomials of the second kind is the smallest, there is no surprise that no matter the non-dimensional added mass or damping coefficient is the smallest which is almost zero. For the non-dimensional damping coefficient, the four curves show a slow decline to a constant as the encountered frequency increases. The damping coefficient using dry modes and the second kind Chebyshev polynomials are almost zero in large frequency range for higher bending modes.

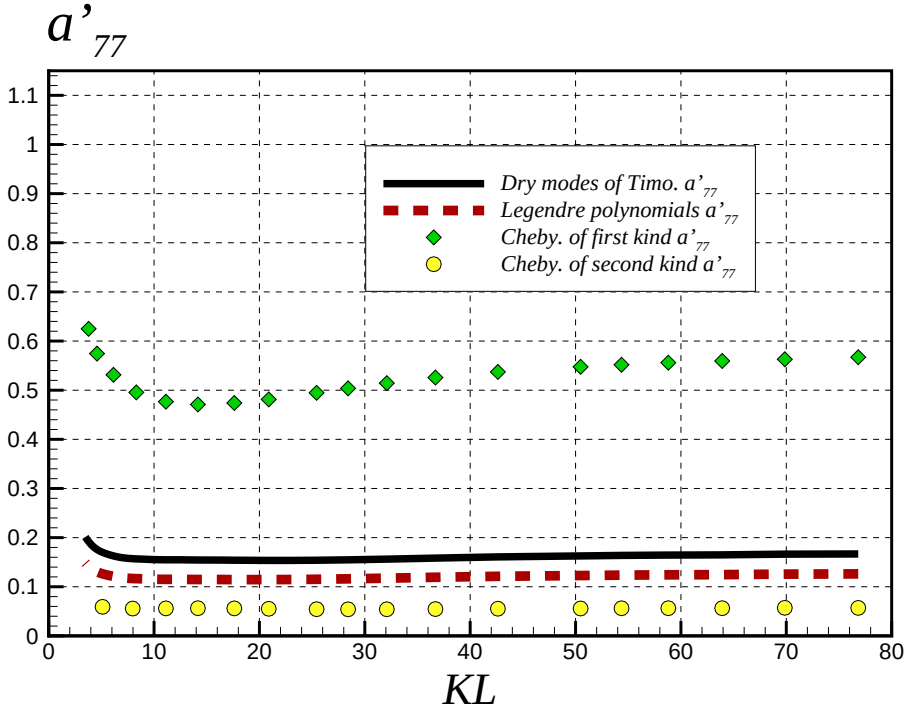

FIGURE 5.3: Non-dimensional added mass a'_{77}.

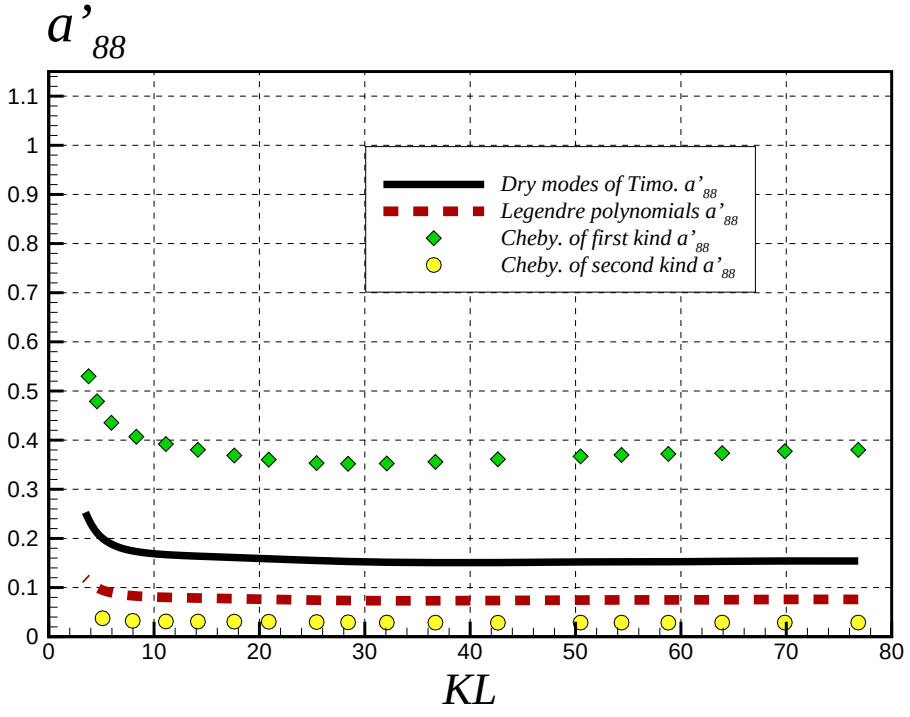

FIGURE 5.4: Non-dimensional added mass a'_{88}.

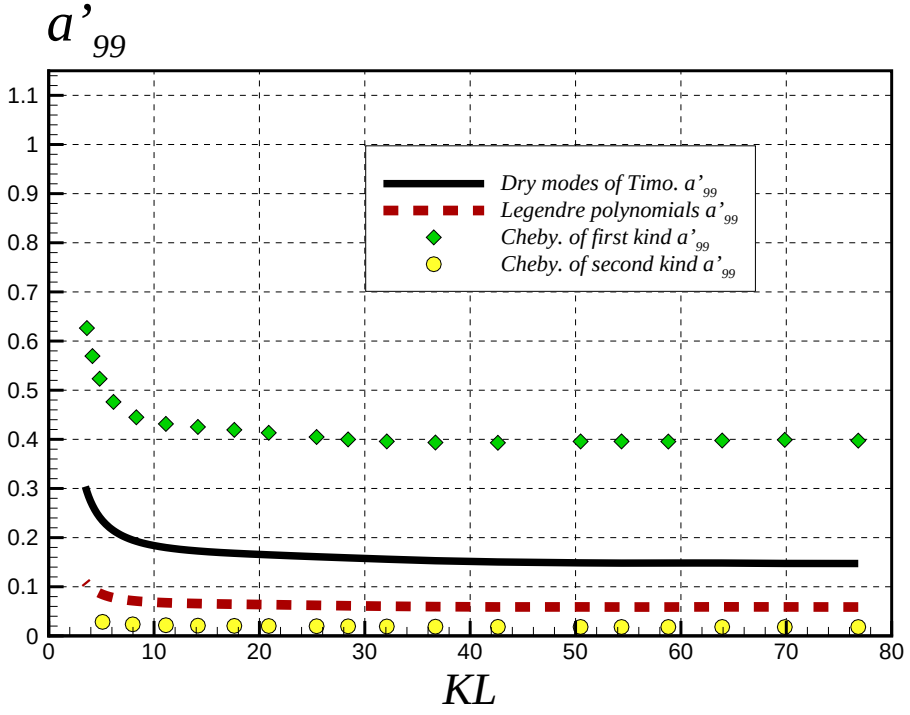

FIGURE 5.5: Non-dimensional added mass a'_{99}.

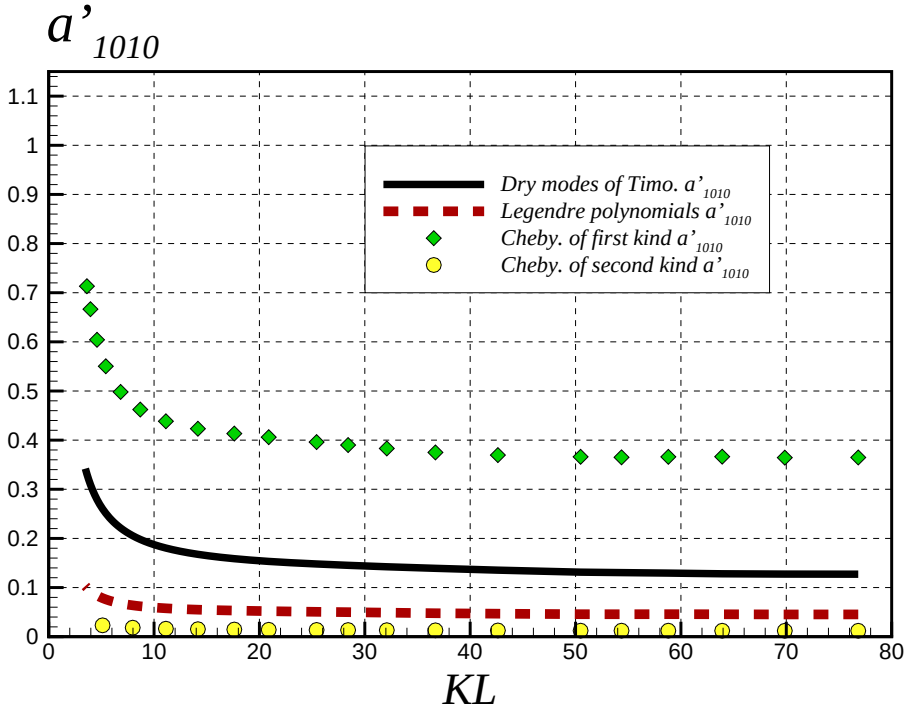

FIGURE 5.6: Non-dimensional added mass a'_{1010}.

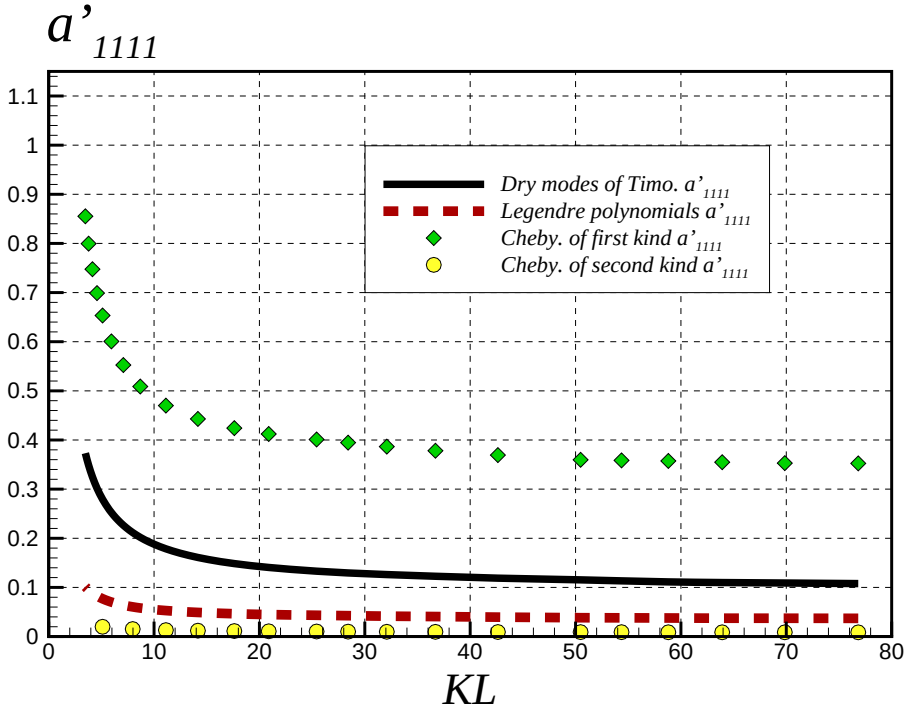

FIGURE 5.7: Non-dimensional added mass a'_{1111}.

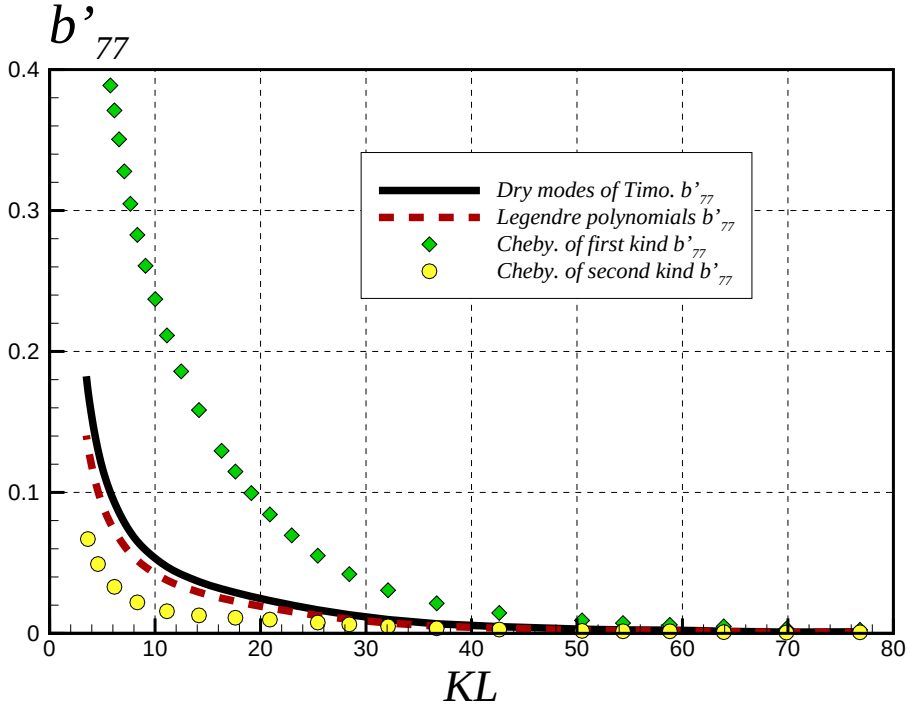

FIGURE 5.8: Non-dimensional damping coefficient b'_{77}.

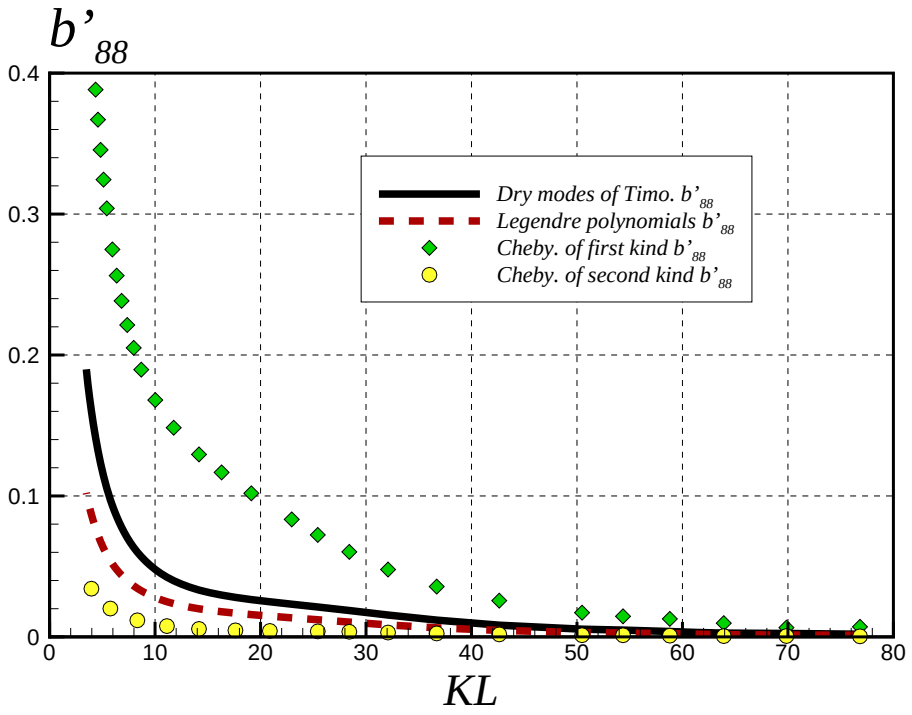

FIGURE 5.9: Non-dimensional damping coefficient b'_{88}.

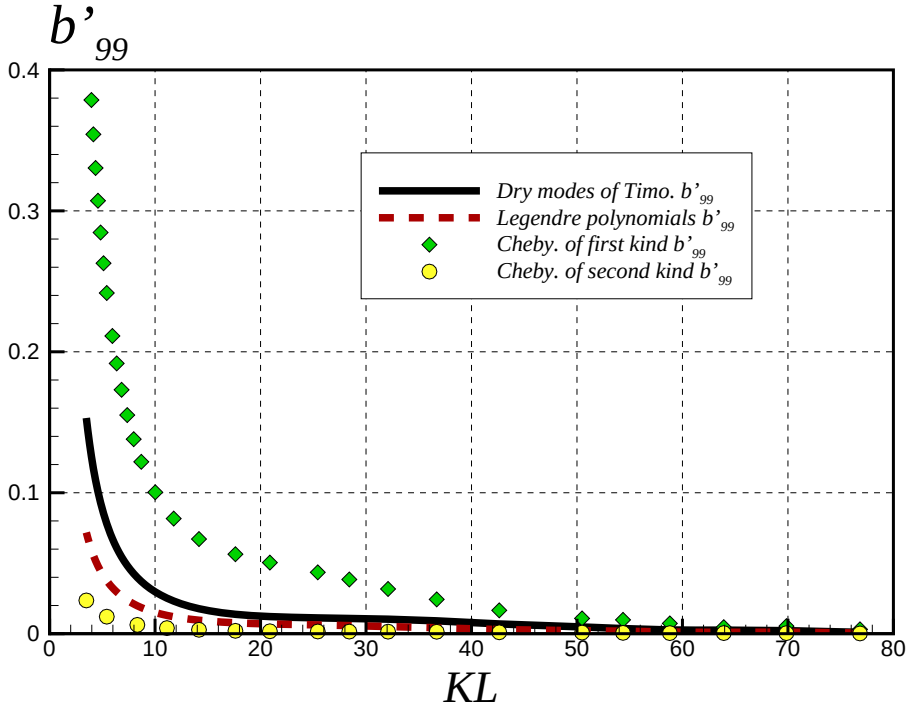

FIGURE 5.10: Non-dimensional damping coefficient b'_{99}.

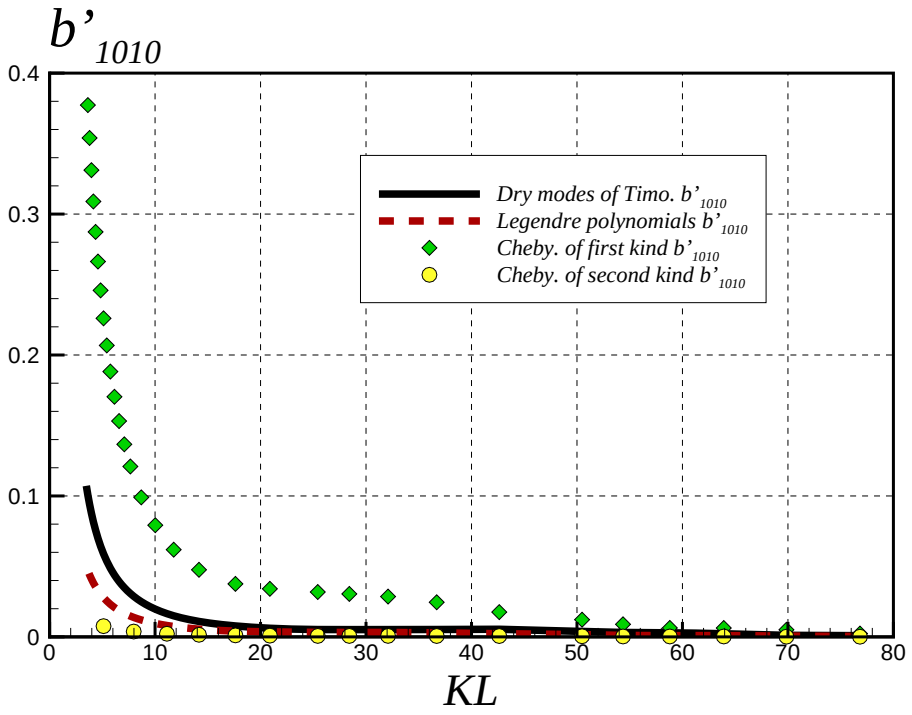

FIGURE 5.11: Non-dimensional damping coefficient b'_{1010}.

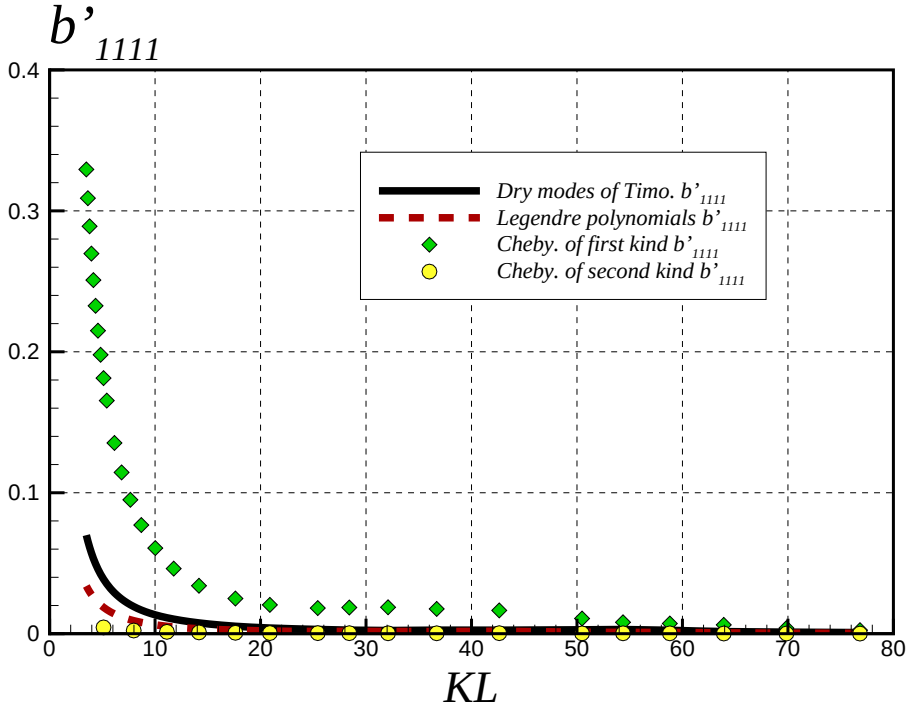

FIGURE 5.12: Non-dimensional damping coefficient b'_{1111}.

Then, the value of non-dimensional exciting force for elastic modes is defined as

$$E_i' = \frac{E_i}{\rho\omega_e^2\zeta_a} \quad \text{for} \quad i = 7 \sim N. \tag{5.4}$$

Since E_i' is a complex value, the amplitude $|E_i'|$ and phase of non-dimensional exciting force for first five elastic motions are illustrated in Figs.5.13 to 5.17. The abscissa λ/L is the ratio of wavelength and ship length from which the scale relationship can be imagined at ease. It can be seen from these figures that the non-dimensional exciting force has one or two peaks at a certain frequency. The wavelength corresponding to the first peak (the highest one) decreases as the order of elastic modes increases. That is, higher-order modes corresponding to the first peaks require higher encounter frequencies. It can be observed E_7' from Fig.5.13 that the second peak appears around $\lambda/L = 0.35$, from which it is referred that the wavelength required for the second peak of higher-order modes is shorter. Similar to added mass or damping coefficient, the amplitudes of curves using different mode functions are positively relative to its amplitudes of mode shapes. Phases for the first three elastic modes match well.

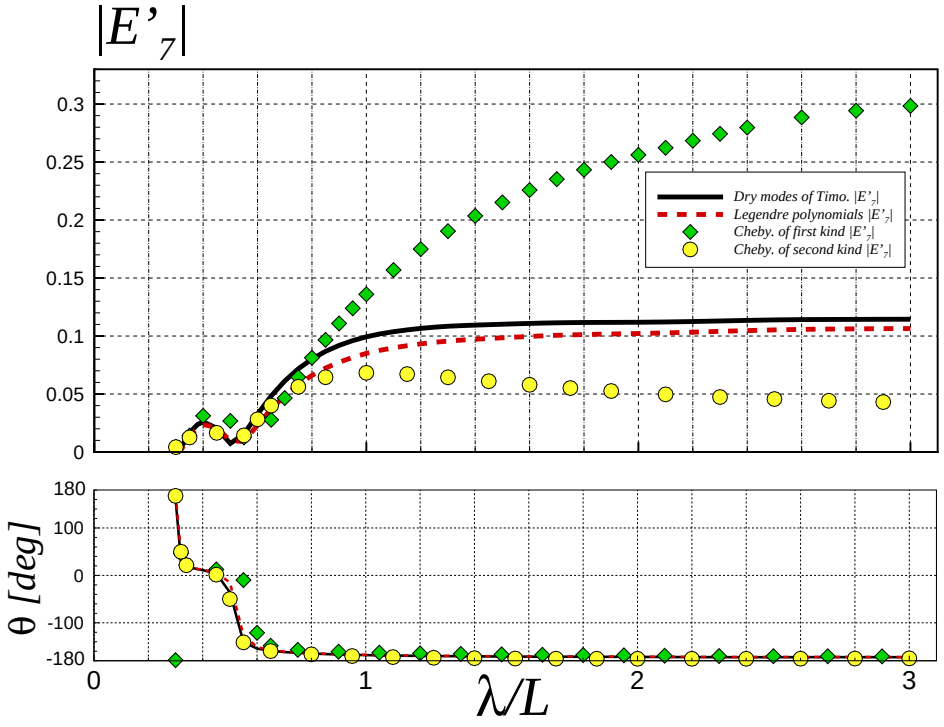

FIGURE 5.13: Non-dimensional exciting force E_7'.

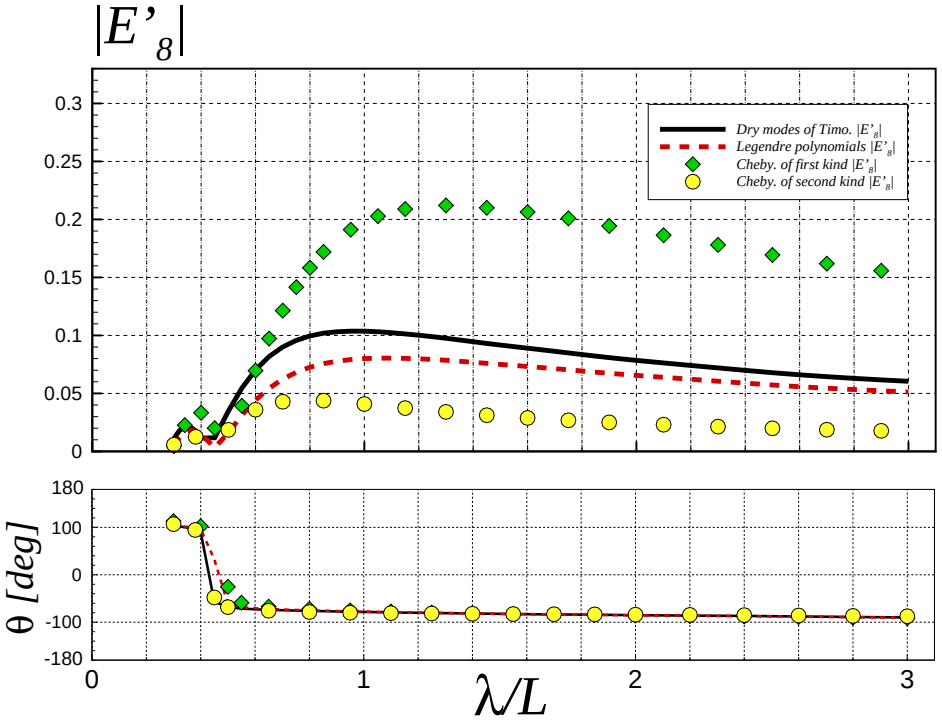

FIGURE 5.14: Non-dimensional exciting force E'_8.

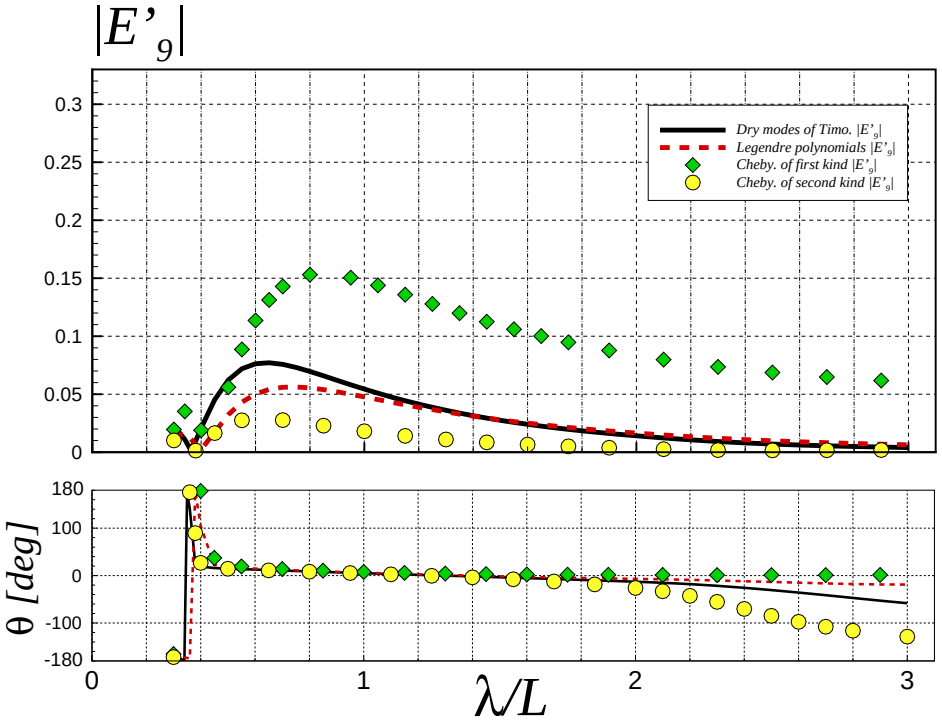

FIGURE 5.15: Non-dimensional exciting force E'_9.

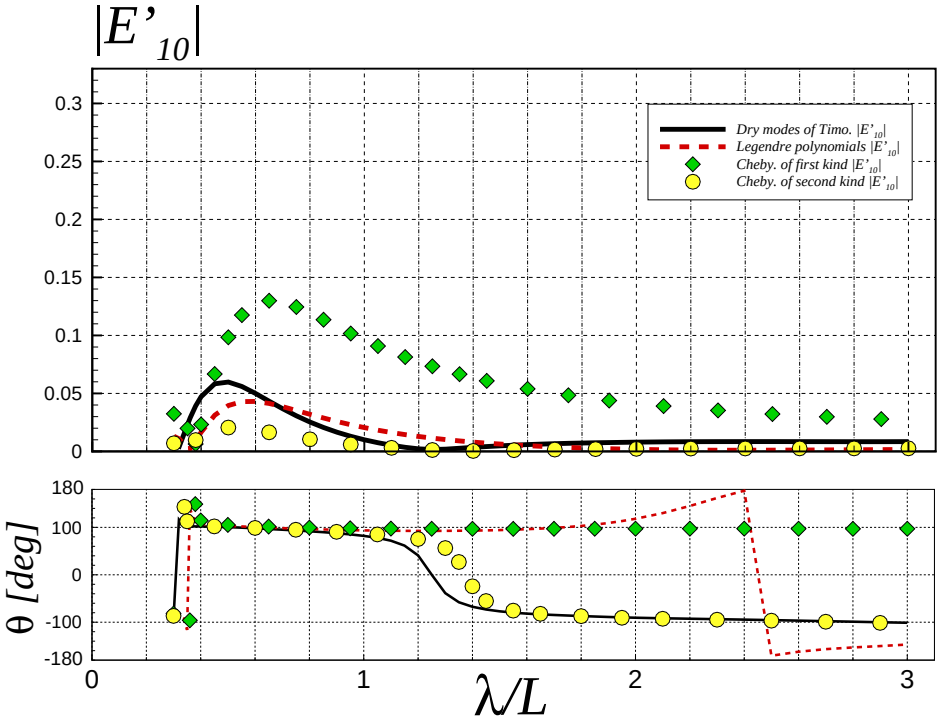

FIGURE 5.16: Non-dimensional exciting force E'_{10}.

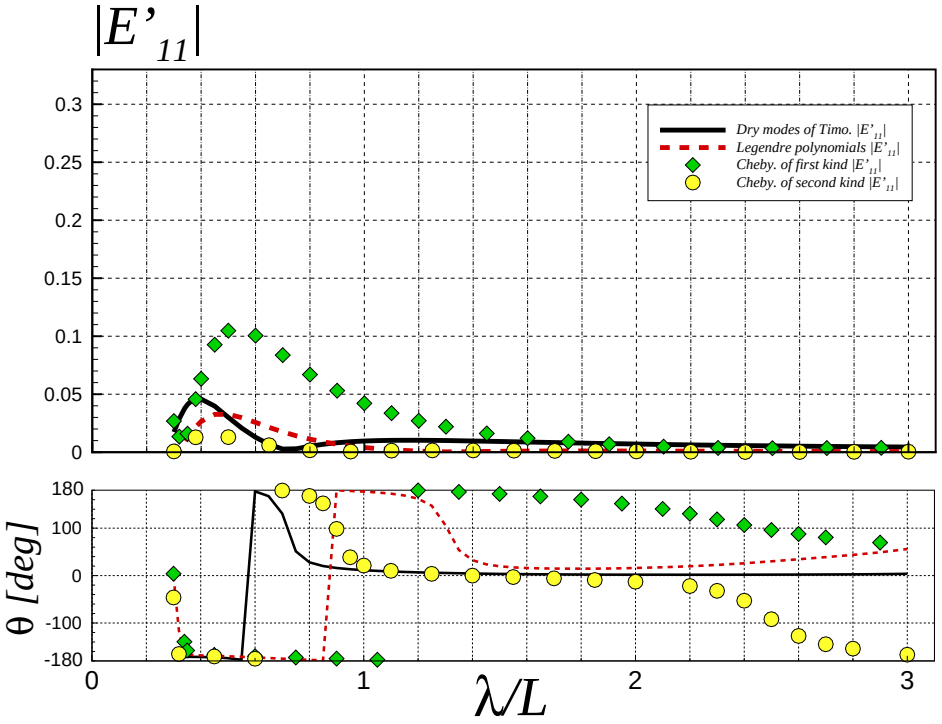

FIGURE 5.17: Non-dimensional exciting force E'_{11}.

To see the convergence in the total deflection of the ship displacement particularly at the bow ($q = 1$), the now values are defined as follows:

$$|X'_{Tj}| = \begin{cases} \left| X'_3 + X'_5 + \sum_{i=7}^{6+j} X'_j \right|, & j \geq 1 \\ \left| X'_3 + X'_5 \right|, & j = 0 \end{cases} , \tag{5.5}$$

which means not only the elastic but also rigid motion is considered here, and the final results are shown in Figs.5.18-5.23. For instance, the value $|X'_{T0}|$ means only the vertical amplitude of rigid motion (heave and pitch) included, and with subscript j increasing, more elastic bending modes are added to present the total vertical deflection.

For rigid motions shown in Fig.5.18, the results of using the Legendre polynomials and the dry eigen-modes of Timoshenko beam are in virtually perfect agreement, since all coupling coefficients of the matrix between the rigid and elastic motion modes are basically zero, although there are significant coupling terms for dry eigen-value owing to the shear effect, which is negligible judging from this figure.

On the other hand, when using the Chebyshev polynomials of the first kind and also of the second kind, we can see a clear difference from the other results in a range of higher frequency because of relatively large values in the coupling matrix coefficients. This is because the Chebyshev polynomials, $T_n(x)$ or $U_n(x)$, are simply used as the mode functions in computing the matrix coefficients of Eqs.(4.8)-(4.10), without the weight functions appearing in Eq.(3.22) in the orthogonal relations.

Fig.5.19 includes the first elastic bending mode X_7, in which a noticeable difference exists in the results between mathematical polynomials and the dry eigen-modes, implying that the convergence in the mode-expansion series is not achieved yet. With the increase in the number of elastic bending modes, we can see convergence in the total deflection at the bow. In fact, in Fig.5.21 adding up to three elastic modes, there is no visible difference in the results between Legendre polynomials and dry eigen-modes. However, we can see still a slight difference in Fig.5.21 when using the Chebyshev polynomials as the mode functions.

By increasing the number of modes up to five elastic modes, as shown in Fig.5.23, the results using the Chebyshev polynomials of the second kind are in virtually perfect agreement with those of the dry eigen-modes and the Legendre polynomials. Whereas the results using the Chebyshev polynomials of the first kind are still slightly different from the other converged results, although that difference is practically negligible.

In summary, the Legendre polynomials may be able to provide better results than the Chebyshev polynomials of the second kind in terms of the rate of convergence with the increase in the number of modes. When using the Chebyshev polynomials, the first kind is commonly and widely

used but a problem in this hydroelasticity analysis is that some of the coupling coefficients in the mass matrix take negative values, as shown explicitly in Table 5.2. As mentioned already, the reason for nonzero off-diagonal values in the mass matrix is that the orthogonal relation shown in Eq.(3.22) is not used but the Chebyshev polynomials are simply used as the mode functions in Eq.(4.8).

From the results described above, it can be concluded that any arbitrary polynomial functions can be applied as the mode functions in the modal superposition method to represent the total deflection. However, the use of Legendre polynomials is highly recommended in terms of simplicity, orthogonality, relatively fast convergence, and hence high precision in obtained results. In addition, since there are no coupling matrix coefficients between the rigid and elastic modes, the elastic deflection can be separated from the rigid-motion modes and associated analyses would be easier.

In this theory, it is rarely possible to range the experiment that ship deforms at forward speed with set elasticity. Besides, our goal is to prove the effectiveness of orthogonal polynomials to replace dry modes. There is no experimental data that can be collected for comparison. Consequently, in order to compare or match with existing experimental data, computed results at zero speed as a validation process of the proposed method are compared with measured results from the experiment conducted by Malenica et al. (2003) [3] and numerical results obtained by Kim et al.(2009) [10, 11]. The detailed results are presented in paper written by Hong et al. (2021) [35] and also illustrated in Appendix C.

The results of elastic modes and total deformation also are obtained by the modal analysis method using the cubic B-spline element method for the supplement. Since the mode shapes between dry modes and B-spline method are almost the same judging from Fig.3.4, there is no surprise for matched results as shown in Figs.5.24-5.25. It is notable that the first comparison for a single elastic mode cannot be calculated by the direct method.

TABLE 5.2: Mass matrix of Chebyshev polynomials of first kind.

M_{ij}	$j=3$	$j=5$	$j=7$	$j=8$	$j=9$	$j=10$
$i=3$	$0.42E-1$	0.0	$-0.14E-1$	0.0	$-0.25E0$	0.0
$i=5$	0.0	$0.14E-1$	0.0	$-0.84E-2$	0.0	$-0.20E-2$
$i=7$	$-0.14E-1$	0.0	$0.19E-1$	0.0	$-0.76E-2$	0.0
$i=8$	0.0	$-0.84E-2$	0.0	$0.20E-1$	0.0	$-0.73E-2$
$i=9$	$-0.28E-2$	0.0	$-0.76E-2$	0.0	$0.20E-1$	0.0
$i=10$	0.0	$-0.2E-2$	0.0	$-0.73E-2$	0.0	$0.20E-1$

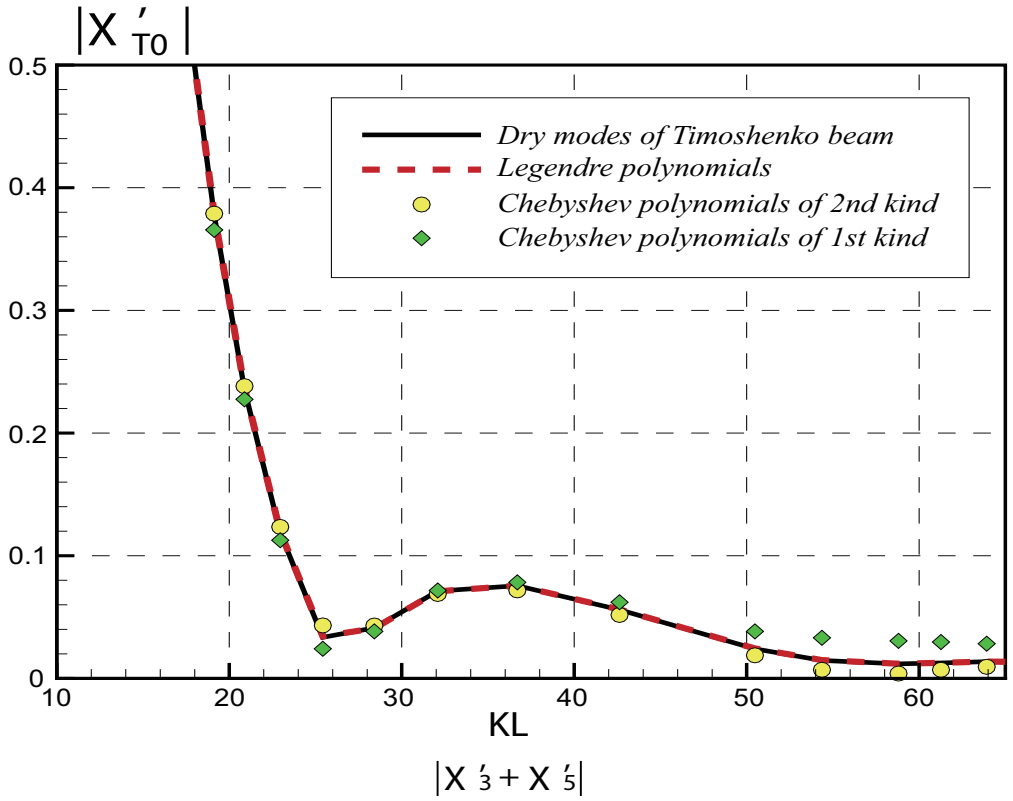

FIGURE 5.18: Non-dimensional deflection amplitude $|X'_{T0}|$.

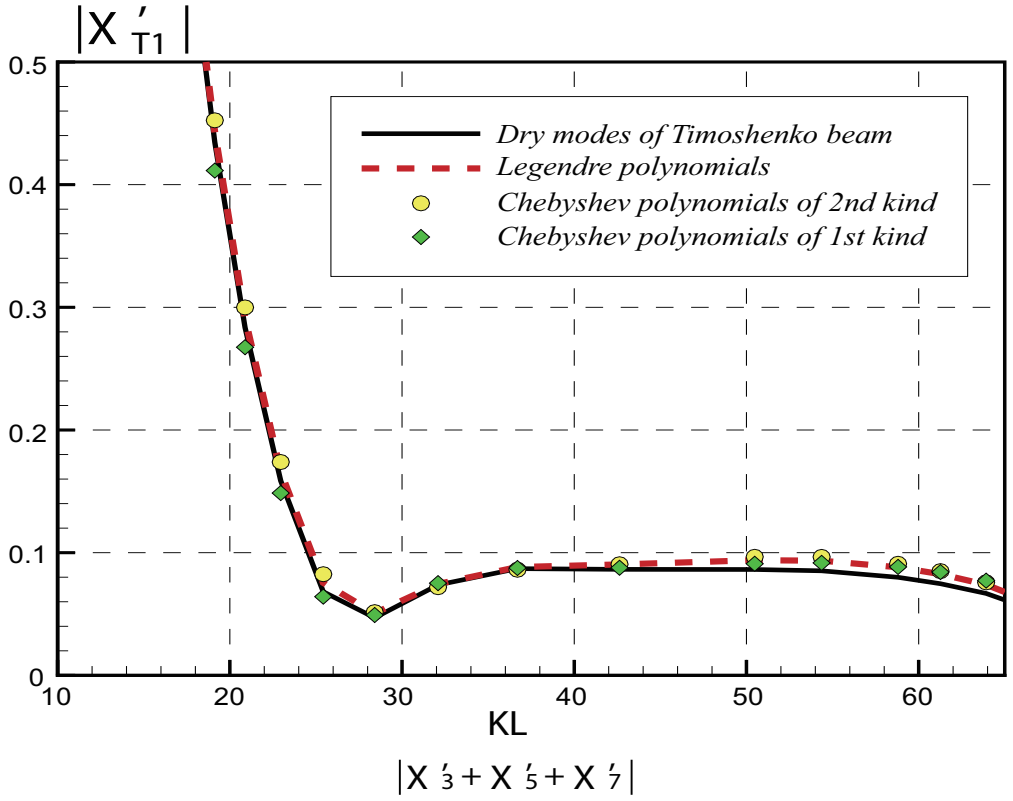

FIGURE 5.19: Non-dimensional exciting force $|X'_{T1}|$.

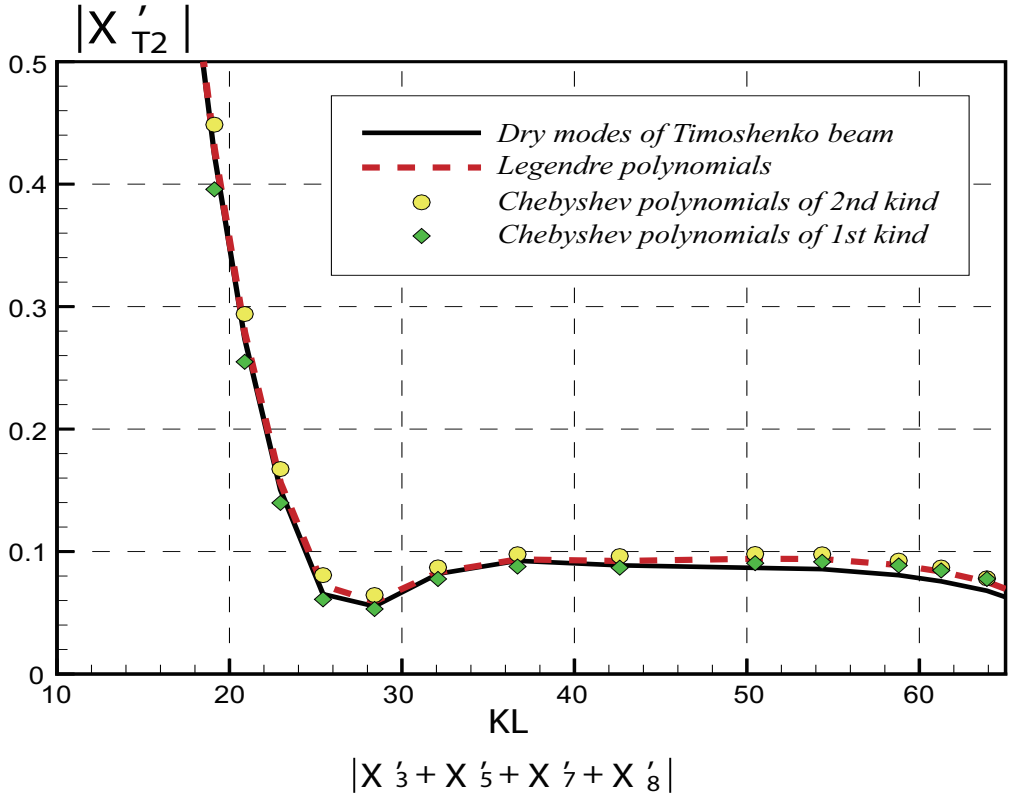

FIGURE 5.20: Non-dimensional exciting force $|X'_{T2}|$.

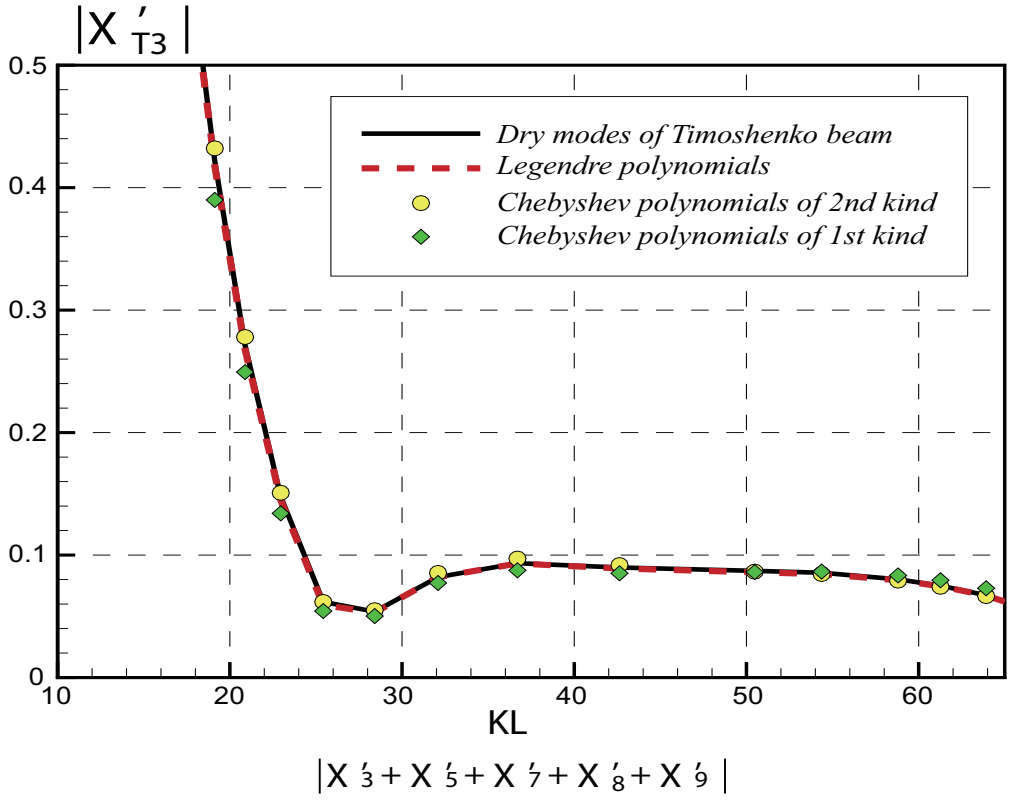

FIGURE 5.21: Non-dimensional exciting force $|X'_{T3}|$.

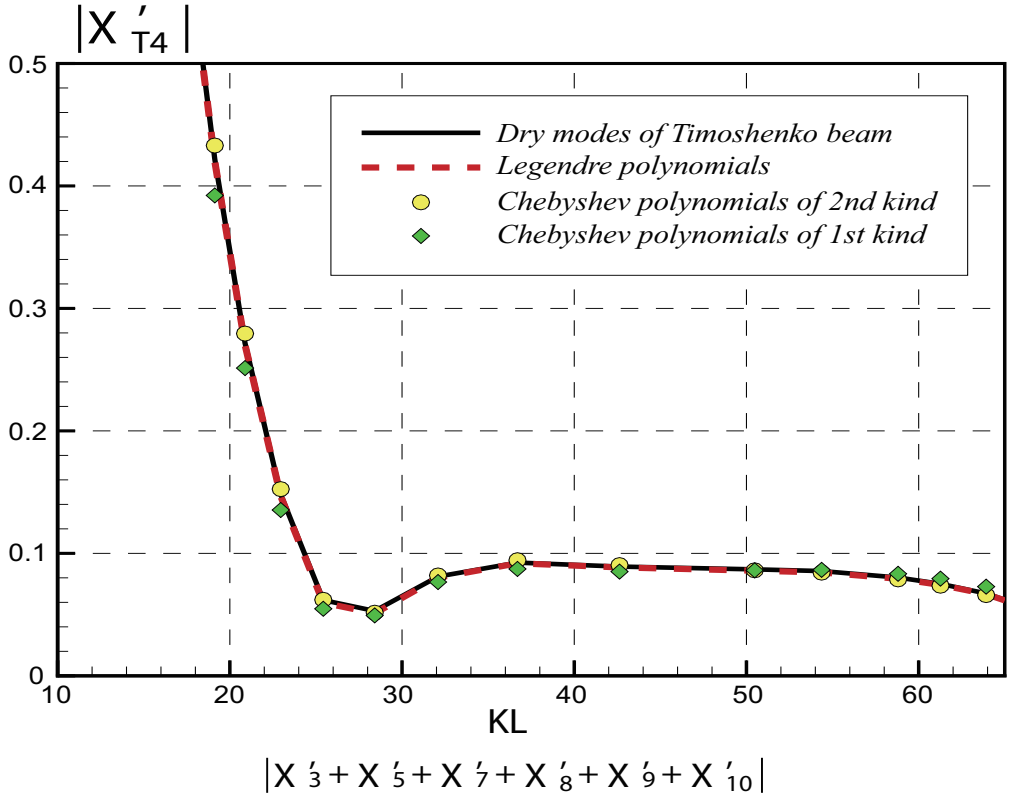

FIGURE 5.22: Non-dimensional exciting force $|X'_{T4}|$.

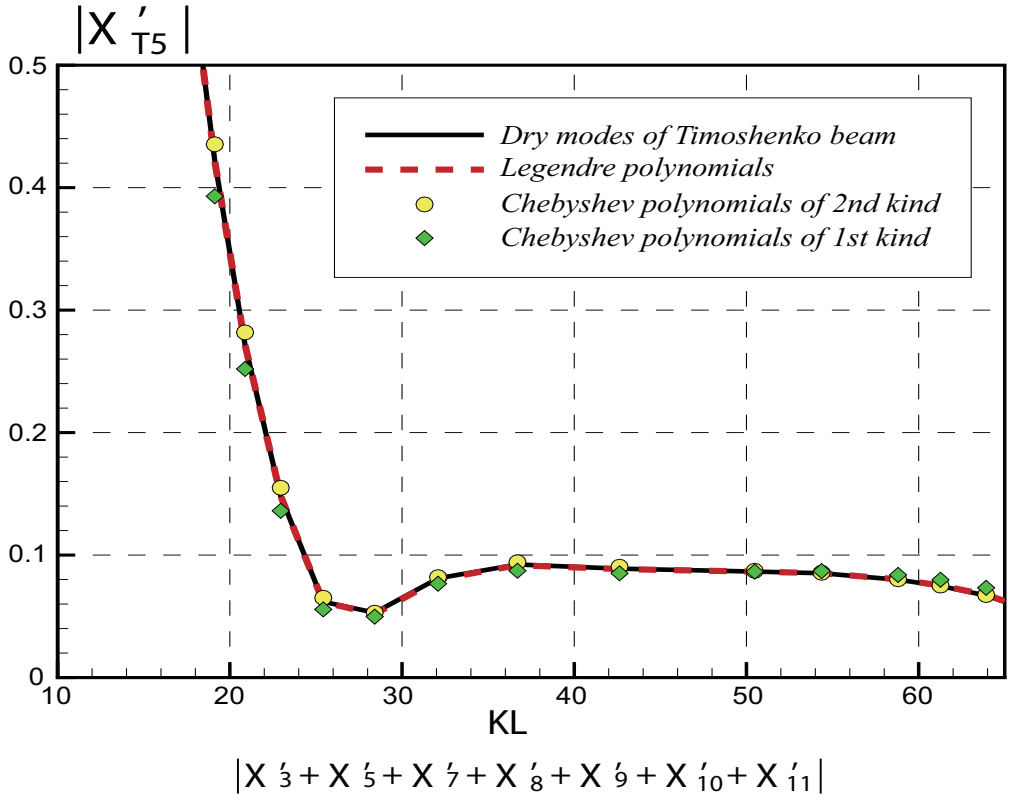

FIGURE 5.23: Non-dimensional exciting force $|X'_{T5}|$.

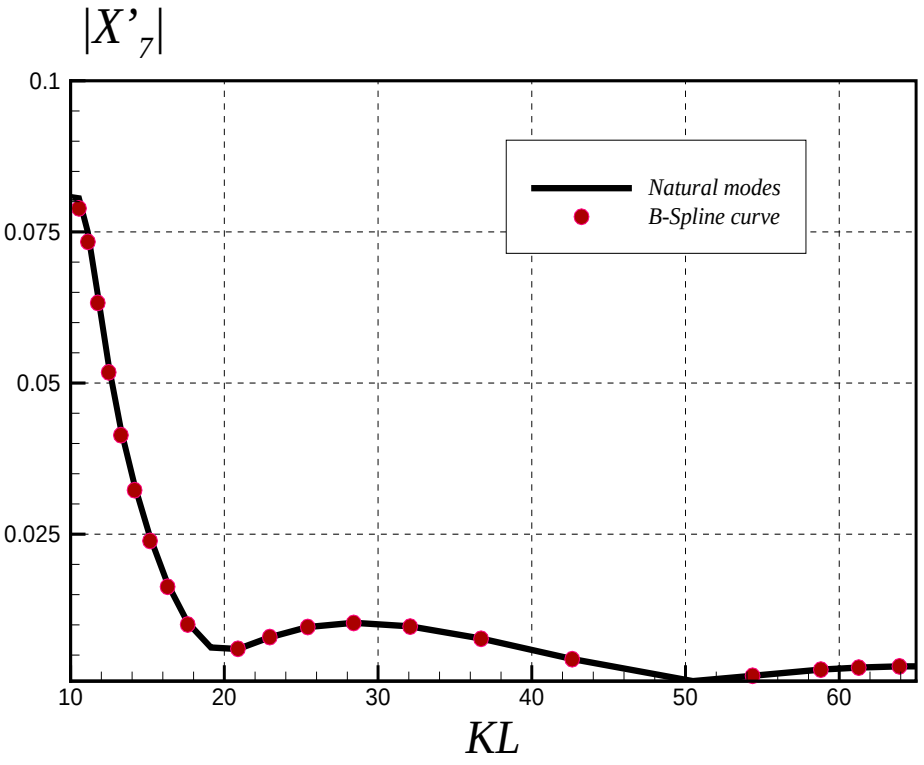

FIGURE 5.24: Comparison of first elastic mode $|X'_7|$ between dry modes and B-spline method for Euler beam.

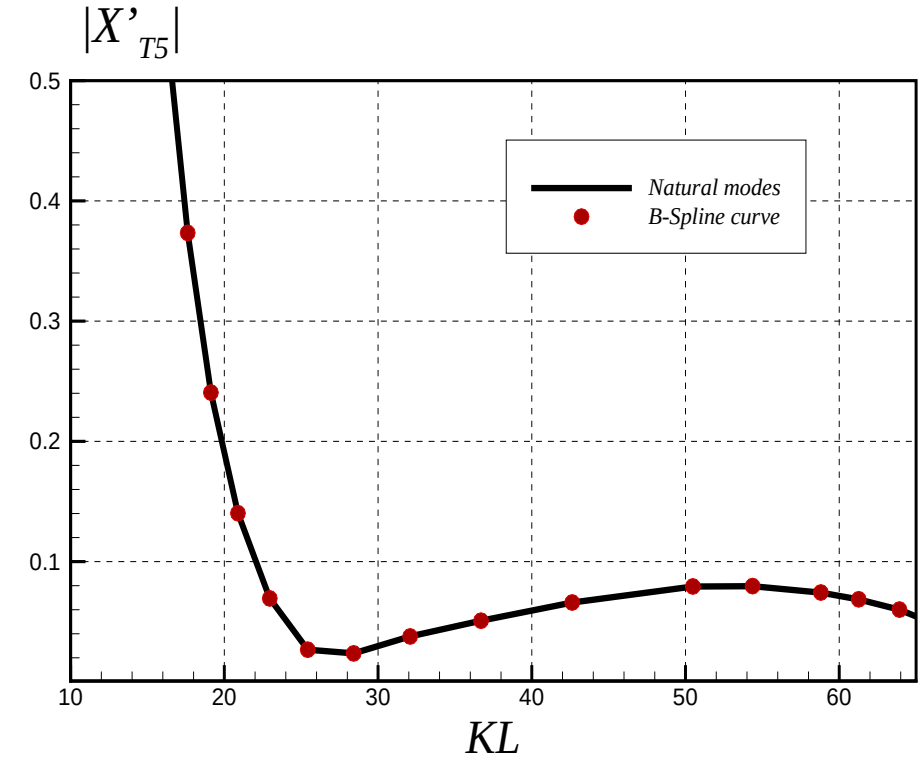

FIGURE 5.25: Comparison of total deflection $|X'_{T5}|$ between dry modes and B-spline method for Euler beam.

5.2 Supplementary Proof of Convergence

5.2.1 Legendre Polynomials

It is proven and seen from the results in the previous section that orthogonal polynomials like Legendre polynomials can substitute dry modes of Timoshenko beam as long as enough modes are applied but the question is whether these modes satisfy the boundary condition already.

To answer this question, one of the boundary conditions of Eq.(4.5) at ship bow can be rewritten as follows by neglecting constant EI:

$$\sum_{j=7}^{11} X_j \frac{d^2 w_j(q)}{dq^2} = -\sum_{j=12}^{N} X_j \frac{d^2 w_j(q)}{dq^2} \approx 0 \quad \text{at} \quad q = 1. \tag{5.6}$$

The new values x_{Ri} and x_{Ii} are defined to present the real part and imaginary part of value in above equations as

$$\begin{aligned} x_{Ri} &= \Re\left[\sum_{j=7}^{7+i} X_j \frac{d^2 w_j(q=1)}{dq^2}\right], \\ x_{Ii} &= \Im\left[\sum_{j=7}^{7+i} X_j \frac{d^2 w_j(q=1)}{dq^2}\right]. \end{aligned} \tag{5.7}$$

Taking Legendre polynomials as example, the second derivative at ship bow can be calculated as

$$\begin{cases} \dfrac{d^2 P_7(q=1)}{dx^2} = 3 \\ \dfrac{d^2 P_8(q=1)}{dx^2} = 15 \\ \dfrac{d^2 P_9(q=1)}{dx^2} = 45 \\ \dfrac{d^2 P_{10}(q=1)}{dx^2} = 105 \\ \dfrac{d^2 P_{11}(q=1)}{dx^2} = 210 \\ \dfrac{d^2 P_{12}(q=1)}{dx^2} = 378 \\ \dfrac{d^2 P_{13}(q=1)}{dx^2} = 630 \end{cases}. \tag{5.8}$$

The number of the second derivative at ship bow using Legendre polynomials turns larger when the order is higher. The results can be illustrated as Figs.5.26 and 5.27. We can see large amplitudes of values both of real and imaginary parts until the fifth bending mode is added. These values can examine or verify the discrepancy intuitively. As the values turn to zero and

the number of the second derivative turn to be larger, it is convenient to estimate the magnitude of the next higher-order motion amplitude like $j = 12$. For instance, $x_{R5} = -0.07$ at the pick when $KL = 30$, the real part of the next higher-order motion amplitude should be less than the value $-0.07/378 \approx -1.85E-4$. In fact, this is a feasible way to prove its convergence rate, and after knowing its convergence rate, we can calculate fewer modes like four modes and use the boundary condition to push back the value of the last one. In Fig.5.26 or 5.27, x_{R5} or x_{I5} is approximated to zero and if we assume it is zero that $x_{R5} = 0$ and $x_{I5} = 0$, the fifth mode amplitude X_{11} can be calculated automatically through relations as

$$X_{11}\frac{d^2P_{11}(q=1)}{dq^2} = -\sum_{j=7}^{10} X_j \frac{d^2P_j(q=1)}{dq^2}. \tag{5.9}$$

In other words, the method using Legendre polynomials as mode functions demands at least four modes in computation to speed up the convergence rate.

5.2.2 Direct Method of Cubic B-spline Function

Although Fig.3.4 illustrates the curves of dry modes of Euler beam and B-spline method matching perfectly well and Tab.3.3 shows the natural frequencies using B-spline method can also be obtained precisely, it is doubtful whether these curves expressed by B-spline method still meet boundary conditions of free-free beam since the endpoint is ruled by only three control points.

From the definition of Eq.(3.31), the second derivative of endpoint (at ship bow) can be expressed as

$$w_j''(q=1) = \sum_{k=1}^{NX+3} \alpha_k^j N_k''(q=1) = \sum_{k=NX+1}^{NX+3} \alpha_k^j N_k''(q=1). \tag{5.10}$$

It is hard to believe that the boundary conditions could be satisfied by only three control points so the Tab.5.3 presents some second and third derivative values to see whether it matches the boundary condition.

Table 5.3: Boundary condition values using Cubic B-spline function at ship bow.

	$j=7$	$j=8$	$j=9$	$j=10$	$j=11$
$w_j(q=1)$	1.0	1.0	1.0	1.0	1.0
$w_j''(q=1)$	−0.0925	−0.6455	−2.2455	−5.3925	−9.9538
$w_j'''(q=1)$	−240.4	−315.6	−379.3	−429.1	−466.4

The table can tell the curve is well-matched exactly on the ship bow as shown in Fig.3.4, and the second derivatives $w_j''(q=1)$ are almost equal to zero and have a tendency of enlarging when the mode order is higher. The third derivatives are far from zero becasue it is the limitation

of the Cubic B-spline function, and it can be improved by adding panels or using higher order B-spline function.

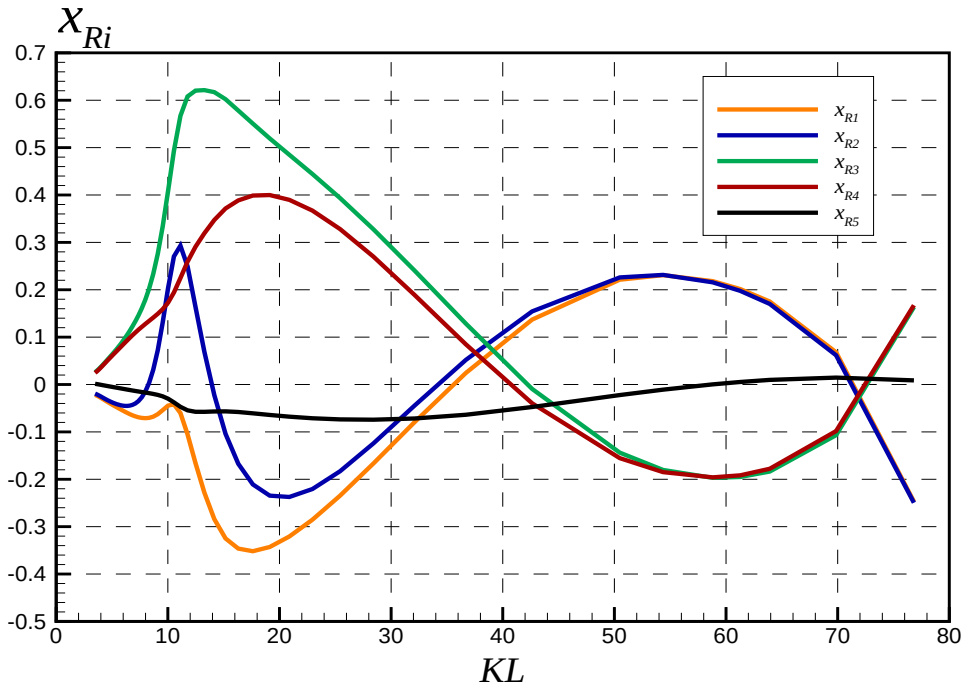

FIGURE 5.26: Real part of boundary condition values using Legendre polynomials at ship bow.

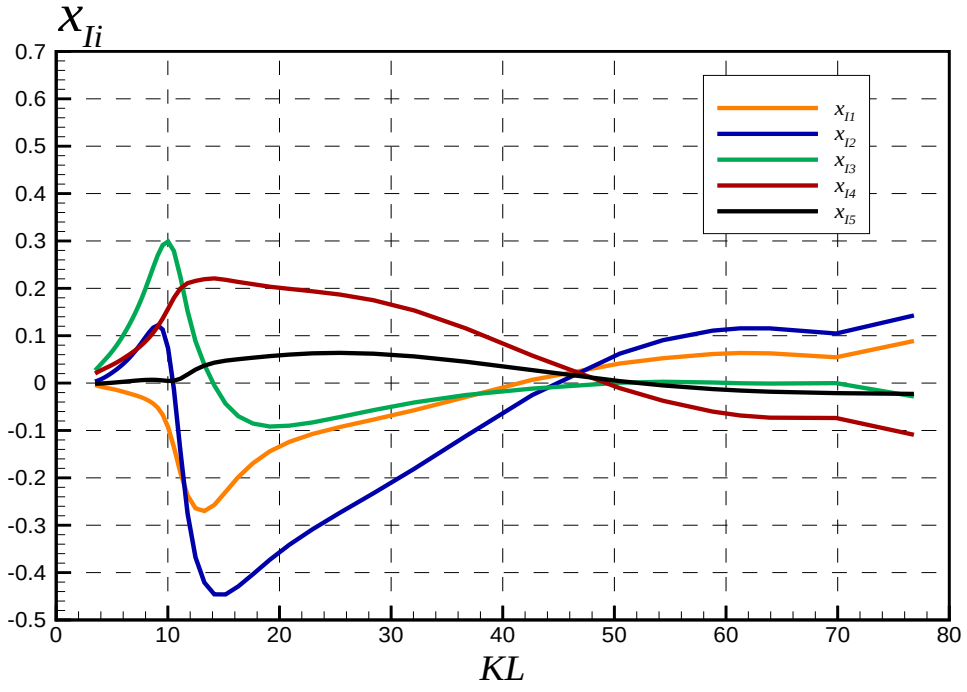

FIGURE 5.27: Imaginary part of boundary condition values using Legendre polynomials at ship bow.

5.3 Effect of Shearing Force

In the present study, the Timoshenko beam model is used, which takes into account the contribution of the shearing force to the vertical elastic deflection. Thus, by changing intentionally the ratio of flexural and shear rigidities γ^2, the shear effect is discussed. In this sensitivity study, the pure elastic deflection should be separated from the rigid motion, since the shear effect affects only the elastic motion, and the amplitude of elastic motion is much smaller than that of rigid motion. For that purpose, the use of Legendre polynomials is recommended particularly in the case of Timoshenko beam approximation.

In order to show converged results of elastic deflection, the amplitude of only the elastic deflection at the bow ($q = 1$) is defined as

$$|X'_{S\,j}| = \left| \sum_{i=7}^{7+j} X'_i \right|. \tag{5.11}$$

Then the value of $j = 4$ (summation of the first five bending modes of the Timoshen beam)

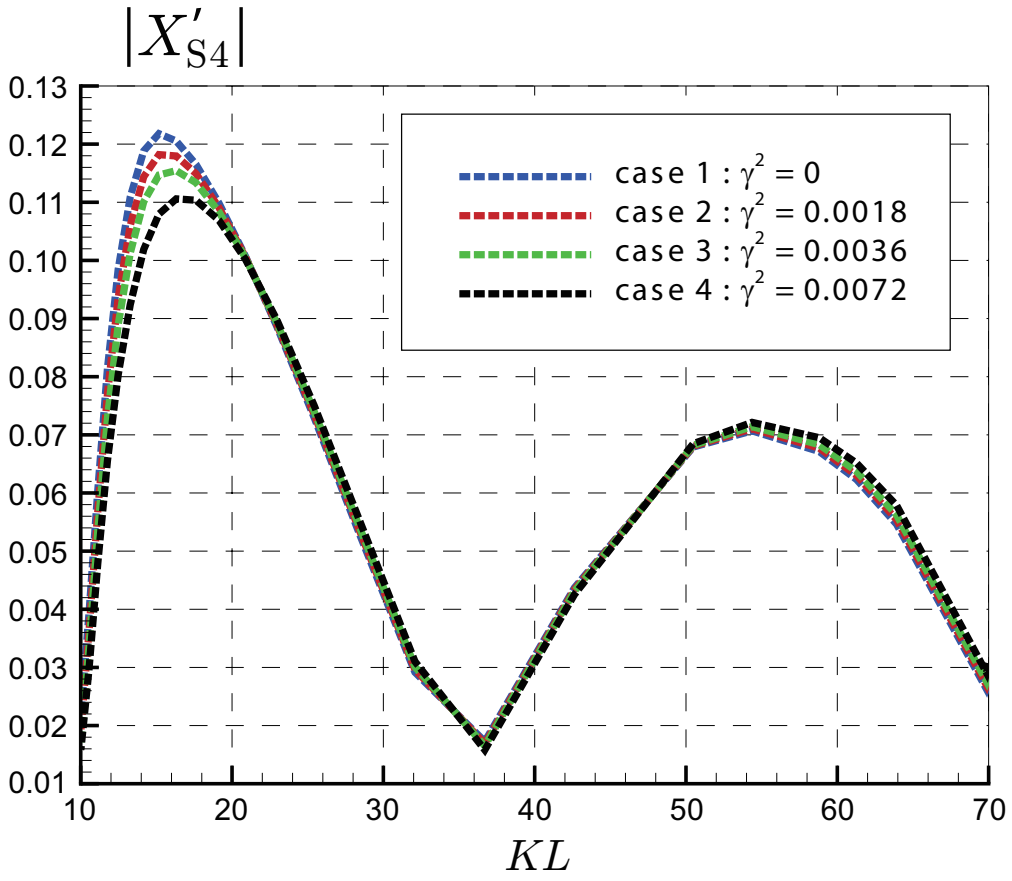

FIGURE 5.28: Comparison of non-dimensional ship-motion deflection between different values of the ratio of flexural and shear rigidities.

is shown in Fig.5.28, where the Legendre polynomials are used as the mode functions with different values of γ^2. The case of $\gamma^2 = 0$ corresponds to no shear effect and hence the results are the same as those for the Euler beam.

It can be seen from Fig.5.28 that the amplitude at the first resonant frequency around $KL = 15$ becomes gradually smaller with γ^2 increasing, while the encountered wave frequency at which the maximal value takes tends to increase slightly. On the contrary, the amplitude at the second resonant frequency around $KL = 55$ increases slightly with γ^2 increasing.

One of the advantages to use the Legendre polynomials in this kind of sensitivity study is that we need not change the Legendre polynomials depending on the values of γ^2 and hence, the resultant amplitudes can be obtained at ease. However, the dry eigen-modes of the Timoshenko beam must be different depending on the values of γ^2, and thus the mass matrix, the shear matrix, and the stiffness matrix will all be changed with γ^2 changing, which may cause additional analysis and computation.

5.4 Discussion

There are several advantages to using the dry eigen-modes of the Timoshenko beam satisfying the free-end boundary conditions for hydroelastic analysis of a ship in waves. One of them is that the eigen-frequencies and corresponding eigen-modes can be analytically obtained, with shear effects taken into account. With this property, the rate of convergence is fast and thus using a few bending modes is enough to obtain converged and accurate results for the wave-induced elastic motion of a ship, which contributes to the reduction of the computation time.

However, as studied by Kashiwagi (1998) [36], once the same idea was extended to the analysis for a pontoon-type VLFS which can be treated as a 2D floating elastic plate with zero thickness, a simple multiplication of the free-free beam dry eigen-modes in both x- and y-axes does not satisfy the governing equation describing the vibration motion of a 2D plate and the free-edge boundary conditions either. Nevertheless, Kashiwagi (1998) adopted a simple multiplication of the free-free beam eigen-modes in both x- and y-axes as the mode functions and the required free-edge boundary conditions could be satisfied by imposing them in the process of partial integration in the transformation of the stiffness matrix. This treatment is equivalent to that the boundary conditions can be satisfied by the sum of mode functions, although each mode function does not satisfy the specified boundary conditions. The resultant stiffness matrix included nonzero off-diagonal elements, but they were obtained by analytical integration, and thus the computation time could be still relatively short.

A similar idea is applied to the ship hydroelastic problem in this paper. Namely, any of the general mode functions may be used to represent the flexural deflection of a ship despite the

fact that each of those functions does not satisfy the required free-end boundary conditions. From viewpoints of relatively fast convergence in the power series of mode functions and also analytical integration for computing the mass, shear, and stiffness matrices, using orthogonal mathematical functions would be preferable and beneficial. A typical example of that kind of orthogonal function system is the Legendre polynomials. Hong et al. (2020) [35, 37, 38] demonstrated that computed results by using the Legendre polynomials were virtually the same as those by using the free-free beam eigen-modes for the whole tested wave-frequency range in the case of Euler beam, and discussed the rationality and consistency of the proposed method.

In the present study, the Timoshenko beam is applied which incorporates the shear effect in the Euler beam. As we can see from Eq.(3.13), the dry eigen-modes are much more complicated than those of the Euler beam. More seriously, the method of weighted residuals cannot bring any advantage to numerical computations, since the eigen-modes of the Timoshenko beam are non-orthogonal. Therefore, we have one more reason to use Legendre polynomials as an alternative in the method of weighted residuals, because they are orthogonal hence the mass matrix has nonzero values only in the diagonal elements and there is no coupling between the rigid motion and elastic bending modes. Although nonzero values in off-diagonal elements (which are analytically given) must be evaluated for the shear and stiffness matrices and more bending modes must be used for sufficient convergence and accuracy, the use of Legendre polynomials is still easier than that using the dry eigen-modes and there is no substantial increase in the computation time. Moreover, due to its orthogonality characteristic, Legendre polynomials can be used to analyze the contribution of shear-deformation force by focusing only on the elastic motion that is separated from the rigid motion, and we need not change any parameters but the ratio γ^2 only. Chebyshev polynomial of the first kind and of the second kind could also be adopted as alternative polynomials but they have a disadvantage in the rate of convergence because of relatively large values in off-diagonal matrix coefficients.

Theoretically, there are two approaches to treating the boundary conditions in mathematical computation: one is to use the eigen-mode functions with physical meaning, and the other is to enforce the boundary conditions as the sum of non-physical mode functions. Each of them can get a consistent result. The latter is recommended here using the orthogonal mode functions like Legendre polynomials since it takes advantage of the method of weighted residuals. Furthermore, it can be applied to represent the shape of elastic deflection in more complicated problems with other boundary conditions and governing motion equations. B-spline methods are also adopted as supplementary including modal analysis method and direct method just for correspondence of the previous two approaches. The modal analysis method fits eigen-modes that satisfy boundary conditions and physical meaning by cubic B-spline basis functions through solving the eigen-value equation and obtains its dry frequencies in the same way. Contrarily, the direct method treats cubic B-spline function in the same way as orthogonal polynomials which has the advantage that the total deflection of a ship can be predicted without computing the

eigen-values and associated eigen-functions but the higher derivatives at the periphery (or ends) of the structure are not accurate enough to satisfy the boundary conditions. Our object in this paper, the ship hull, does not have the same scale as VLFS and considers the forward speed. Therefore, great attention must be paid to the number of partitions. It is necessary to balance the number of grids in each partition is sufficient to ensure the accuracy of the curve since each grid is the point controlling curves in B-spline method, and to prevent the calculation time from being too long due to the increased grids. More importantly, if increasing the number of partitions for accuracy, the consumed time for computation would squarely multiply increase because the matrix size increased. Observing the results, dry modes and orthogonal polynomials commonly need 3 to 5 mode functions whereas cubic needs 10 partitions at least, corresponding to 13 modes. However, In the case of VLFS with no speed, the disadvantage of the cubic B-spline function turns into an advantage because much higher mode functions participated.

Chapter 6

Conclusions

In the present research, the hydroelastic forces on a ship with specified bending mode shapes and resulting flexural deflection of a ship in waves were computed by using the Rankine panel method combined with the modal superposition method in terms of two kinds of mode functions. One is the dry eigen-modes of a uniform Timoshenko beam satisfying the free-end boundary conditions and another kind is the Legendre and Chebyshev polynomials which are mathematically orthogonal but do not satisfy the free-end boundary conditions. Moreover, the Cubic B-spline method was also adopted for providing another idea to express ship deformation since any curve or unknown deformation can be decided if the values of control points are solved.

The accuracy and consistency of the method using Legendre polynomials as alternative mode functions had been demonstrated by comparing with the results using not only dry eigen-modes of the Timoshenko beam in the forward speed case but also the experimental data provided by Malenica et al. (2003) [3] and the numerical results computed with the direct coupling method by Kim et al. (2003) [10, 11] in the zero speed case.

With increasing the number of bending modes, the total deflection of a ship was found to converge and obtained results using Legendre and Chebyshev polynomials were in virtually perfect agreement with the results using the dry eigen-modes of the Timoshenko beam in a wide wave frequency range. It was confirmed that the free-end boundary conditions could be satisfied simplicity by imposing them in the process of partial integration for the transformation of the stiffness matrix. This way of satisfying the boundary conditions is equivalent to that the boundary conditions can be satisfied by the sum of mode functions, although each mode function does not satisfy the specified boundary conditions. For Chebyshev polynomials, the rate of convergence was found to be relatively slow, since the orthogonal relation of Eq.(3.22) which includes the weight function of $1/\sqrt{1-q^2}$ or $\sqrt{1-q^2}$ was not used but the Chebyshev polynomials were used simply as the mode functions in computing the matrix coefficients. Nevertheless, the total

deflection of a ship computed using the Chebyshev polynomials was also in good agreement with other results by taking a sufficient number of mode functions.

Supplementary proof of convergence using Legendre polynomials was raised by analyzing the satisfied boundary conditions to prove five elastic modes are enough. Based on this idea, the number of demanded elastic modes could be decreased to four for speeding up the computation time and the fifth amplitude can be estimated reversely from the boundary condition assuming five bending modes exactly satisfied boundary conditions.

The contribution of the shear effect was discussed by using Legendre polynomials through changing only the ratio of flexural and shear rigidities thanks to the orthogonality characteristic, which could separate the elastic deflection from the rigid motion of a ship. The amplitude of first resonance tends to be smaller and the second is larger when shear effect works. It was confirmed that the effect of shearing force usually was small and practically negligible.

The cubic B-spline method was also adopted for the supplemental explanation including the modal analysis method and direct method to prove this scheme can also present the total deformation of the ship hull. The former one can calculte the natrual frequency and mode shapes precisely while the latter one can calculate the total deflection directly avoding to solve eigenvalue problem. Two methods can be selected flexibly based on purpose. Thses methods hardly satisfy the boudary conditions and needs more unknows that leads to comparely more computation time consuming. Also, it should be balanced that enough grids in each partition ensure precision and the whole number of the grids should be less as possible. The direct method is more lucid and relatively easy in coding the scheme but lack of hydrodynamic force analysis while modal analysis method possesses the results of added mass, damping coefficient of each bending modes, and it needs less computation time because fewer matrices are applied in the final conventional motion equation just like the mode-expansion method. In summary, the cubic B-spline method is more comprehensive and has wider range of applications but may cause much more time for computation.

Euler beam is commonly used for hydroelastic problems no matter on one dimension or two dimensions for its briefness, orthogonality, and following the laws of physics but the shear effect has to be considered further if the research object is not slender enough though its contribution works marginally. However, the dry eigen-modes of the Timoshenko beam and its eigen-value equation turn much more complicated and are sensitive to the ratio of shear rigidity and flexural rigidity. In other words, if the values of shear contribution change, the parameters in the eigen-value equation that are hard to solve should be calculated again, and then the analytical solution calculated again which is the reason why the Legendre polynomials are applied to the study of shear effect contribution, to save steps. What is more essential is dry modes of the Timoshenko beam have no characteristic of orthogonality like the Euler beam that leads to all values in mass matrix existing. Consequently, Legendre polynomials and Chebyshev polynomials are

adopted due to their orthogonal and simplicity. It is noted that there are weights in integration when using Chebyshev polynomials' orthogonality and may cause infinity value in computation. Then, the weights have to be omitted, and use Chebyshev polynomials directly or stiffly when calculating mass matrix. It may one of the reasons causing slightly late convergence. In fact, Chebyshev polynomials, as the fastest polynomials in numerical estimation pointed by Fox and Parker(1968) [39], should convergent faster in the common cases. It should be explained that the amplitude of Legendre polynomials is much closer to dry modes, so Legendre polynomials are more advantageous than Chebyshev polynomials in our special case. The limitation and availability of each mode function were expounded, and it was noted that the Legendre polynomials can be expected to be versatile in the application to a wide range of engineering problems because of its briefness and commonality and it can take advantage of the method of weighted residuals.

Appendix A

Natural modes of Timoshenko beam

This chapter describes how to derive the analytical solution of natural modes of Timoshenko beam. Applying the variable-separation method with the time-dependent part, the homogeneous equation for the x-dependent vertical deflection of the uniform Timoshenko beam can be shown as follows:

$$\frac{1}{\kappa_n^4}\frac{d^4 y_n(x)}{dx^4} + \gamma^2 \frac{d^2 y_n(x)}{dx^2} - y_n(x) = 0, \quad \kappa_n^4 = \frac{m}{EI}\sigma_n^2, \quad \gamma^2 = \frac{EI}{k'GA}, \tag{A.1}$$

where κ_n denotes the n-th eigen-value associated with the dry-mode natural frequency σ_n, $y_n(x)$ is the corresponding n-th dry eigen-mode function of the vertical deflection, and γ^2 is the ratio of flexural rigidity with shear rigidity which determines the amount of contribution of shear effect.

The analytical solution of the differential equation can be written in the form

$$y_n(x) = C_1 \cos(\kappa_n \alpha_n q) + C_2 \cosh(\kappa_n \beta_n q) + C_3 \sin(\kappa_n \alpha_n q) + C_4 \sinh(\kappa_n \beta_n q), \tag{A.2}$$

where $q = x/(L/2)$ is the nondimensional coordinate and

$$\alpha_n = \sqrt{\frac{\sqrt{(\kappa_n\gamma)^4 + 4} + (\kappa_n\gamma)^2}{2}}, \quad \beta_n = \sqrt{\frac{\sqrt{(\kappa_n\gamma)^4 + 4} - (\kappa_n\gamma)^2}{2}}. \tag{A.3}$$

Parameters $C_1 \sim C_4$ are constant values. The first and second terms of Eq.(A.2) are symmetric modes with respect to x or even functions, whereas the third and fourth are odd functions or denote antisymmetric modes. Four boundary conditions equations are demanded to decide these parameters. The slender ship is assumed as a uniform beam floating on the wave with free-end boundary conditions. The moment and shear force on the ends are set to be zero in the form as follows:

$$\frac{d^2 y_n(x)}{dx^2} = 0, \quad \frac{d^3 y_n(x)}{dx^3} = 0, \quad \text{at} \quad x = \pm L/2. \tag{A.4}$$

Substituting analytical solution Eq.(A.2) into above boundary conditions, the second and third derivatives of $w_n(x)$ can be rewritten as

$$\begin{aligned}\frac{d^2y_n(x)}{dx^2} = \; & -C_1\kappa_n^2\alpha_n^2\cos(\kappa_n\alpha_n q) + C_2\kappa_n^2\beta_n^2\cosh(\kappa_n\beta_n q) \\ & -C_3\kappa_n^2\alpha_n^2\sin(\kappa_n\alpha_n q) + C_4\kappa_n^2\beta_n^2\sinh(\kappa_n\beta_n q),\end{aligned} \tag{A.5}$$

$$\begin{aligned}\frac{d^3y_n(x)}{dx^3} = \; & C_1\kappa_n^3\alpha_n^3\sin(\kappa_n\alpha_n q) + C_2\kappa_n^3\beta_n^3\sinh(\kappa_n\beta_n q) \\ & -C_3\kappa_n^3\alpha_n^3\cos(\kappa_n\alpha_n q) + C_4\kappa_n^3\beta_n^3\cosh(\kappa_n\beta_n q).\end{aligned} \tag{A.6}$$

For zero moment force on free ends, Eq.(A.5) can be derived to

$$\begin{cases} -C_1\kappa_n^2\alpha_n^2\cos(\kappa_n\alpha_n) + C_2\kappa_n^2\beta_n^2\cosh(\kappa_n\beta_n) - C_3\kappa_n^2\alpha_n^2\sin(\kappa_n\alpha_n) + C_4\kappa_n^2\beta_n^2\sinh(\kappa_n\beta_n) = 0 \\ -C_1\kappa_n^2\alpha_n^2\cos(\kappa_n\alpha_n) + C_2\kappa_n^2\beta_n^2\cosh(\kappa_n\beta_n) + C_3\kappa_n^2\alpha_n^2\sin(\kappa_n\alpha_n) - C_4\kappa_n^2\beta_n^2\sinh(\kappa_n\beta_n) = 0 \end{cases}. \tag{A.7}$$

Observing the above equation, the relations can be obtained further as

$$\begin{cases} C_1\kappa_n^2\alpha_n^2\cos(\kappa_n\alpha_n) = C_2\kappa_n^2\beta_n^2\cosh(\kappa_n\beta_n) \\ C_3\kappa_n^2\alpha_n^2\sin(\kappa_n\alpha_n) = C_4\kappa_n^2\beta_n^2\sinh(\kappa_n\beta_n) \end{cases}. \tag{A.8}$$

Similarly, for zero shear force on free ends, Eq.(A.6) can be deduced as

$$\begin{cases} C_1\kappa_n^3\alpha_n^3\sin(\kappa_n\alpha_n) + C_2\kappa_n^3\beta_n^3\sinh(\kappa_n\beta_n) - C_3\kappa_n^3\alpha_n^3\cos(\kappa_n\alpha_n) + C_4\kappa_n^3\beta_n^3\cosh(\kappa_n\beta_n) = 0 \\ -C_1\kappa_n^3\alpha_n^3\sin(\kappa_n\alpha_n) - C_2\kappa_n^3\beta_n^3\sinh(\kappa_n\beta_n) - C_3\kappa_n^3\alpha_n^3\cos(\kappa_n\alpha_n) + C_4\kappa_n^3\beta_n^3\cosh(\kappa_n\beta_n) = 0 \end{cases}. \tag{A.9}$$

Then, the other relations can be gained as the same way:

$$\begin{cases} C_1\kappa_n^3\alpha_n^3\sin(\kappa_n\alpha_n) = -C_2\kappa_n^3\beta_n^3\sinh(\kappa_n\beta_n) \\ C_3\kappa_n^3\alpha_n^3\cos(\kappa_n\alpha_n) = C_4\kappa_n^3\beta_n^3\cosh(\kappa_n\beta_n) \end{cases}. \tag{A.10}$$

So far, relations in Eqs.(A.8) and (A.10) still cannot decide parameters $C_1 \sim C_4$.

A.1 Symmetric modes

The first aligned formulae in Eqs.(A.8) and (A.10) are used to solve symmetric modes with respect to C_1 and C_2, so the following equations are obtained as

$$\begin{vmatrix} \kappa_n^2\alpha_n^2\cos(\kappa_n\alpha_n) & -\kappa_n^2\beta_n^2\cosh(\kappa_n\beta_n) \\ \kappa_n^3\alpha_n^3\sin(\kappa_n\alpha_n) & \kappa_n^3\beta_n^3\sinh(\kappa_n\beta_n) \end{vmatrix} \begin{Bmatrix} C_1 \\ C_2 \end{Bmatrix} = \begin{Bmatrix} 0 \\ 0 \end{Bmatrix}. \tag{A.11}$$

Excepting the meaningless values $C_1 = C_2 = 0$, the required condition is necessary that the determinant of matrix (expressed as D) should be zero as the form of

$$D = \kappa_n^5 \alpha_n^2 \beta_n^3 \cos(\kappa_n \alpha_n) \sinh(\kappa_n \beta_n) + \kappa_n^5 \alpha_n^3 \beta_n^2 \sin(\kappa_n \alpha_n) \cosh(\kappa_n \beta_n) = 0. \tag{A.12}$$

Then it can be simplified to frequency equation for solving κ_n of symmetric modes (κ_n is equivalent to dry frequency) as

$$\alpha_n \tan(\kappa_n \alpha_n) + \beta_n \tanh(\kappa_n \beta_n) = 0. \tag{A.13}$$

Proposing the symmetrical parts from Eq.(A.2), the symmetric solution can be deduced with considering the frequency equation as

$$\begin{aligned} y_n(x) &= C_1 \cos(\kappa_n \alpha_n q) + C_2 \cosh(\kappa_n \beta_n q) \\ &= C_1 \left\{ \cos(\kappa_n \alpha_n q) + \frac{\alpha_n^2 \cos(\kappa_n \alpha_n)}{\beta_n^2 \cosh(\kappa_n \beta_n)} \cosh(\kappa_n \beta_n q) \right\} \\ &= C_1 \cos(\kappa_n \alpha_n) \left\{ \frac{\cos(\kappa_n \alpha_n q)}{\cos(\kappa_n \alpha_n)} + \frac{\alpha_n^2}{\beta_n^2} \frac{\cosh(\kappa_n \beta_n q)}{\cosh(\kappa_n \beta_n)} \right\} \end{aligned} . \tag{A.14}$$

$y_n(x)$ is homogenous solution of symmertic modes which cannot determine its unique parameter C_1. To normalize the different alternative polynomials, the mode function should be defaulted as $|y_n(q) = 1|$ at $q = \pm 1$, so that

$$C_1 \cos(\kappa_n \alpha_n q) = \frac{1}{1 + (\alpha_n / \beta_n)^2}, \tag{A.15}$$

and the normalized symmetric solution can be rewritten as

$$y_n(x) = \frac{1}{1 + (\alpha_n / \beta_n)^2} \left\{ \frac{\cos(\kappa_n \alpha_n q)}{\cos(\kappa_n \alpha_n)} + \frac{\cosh(\kappa_n \beta_n q)}{\cosh(\kappa_n \beta_n)} \frac{\alpha_n^2}{\beta_n^2} \right\}. \tag{A.16}$$

$n = 1, 3, 5, \ldots$, and the heave motion is belongs to symmetric rigid motion that is included by setting $n = -1$ as

$$y_{-1}(x) = 1. \tag{A.17}$$

A.2 Antisymmetric modes

In the same way, the second equations in Eqs.(A.8)-(A.10) are combined to deduce antisymmetric modes with respect to C_3 and C_4, the equations can be expressed in the form of matrix:

$$\begin{vmatrix} \kappa_n^2 \alpha_n^2 \sin(\kappa_n \alpha_n) & -\kappa_n^2 \beta_n^2 \sinh(\kappa_n \beta_n) \\ \kappa_n^3 \alpha_n^3 \cos(\kappa_n \alpha_n) & -\kappa_n^3 \beta_n^3 \cosh(\kappa_n \beta_n) \end{vmatrix} \begin{Bmatrix} C_3 \\ C_4 \end{Bmatrix} = \begin{Bmatrix} 0 \\ 0 \end{Bmatrix}. \tag{A.18}$$

Condition $C_3 = C_4 = 0$ is useless and the requirement is that the determinant of matrix is zero as

$$D = -\kappa_n^5 \alpha_n^2 \beta_n^3 \sin(\kappa_n \alpha_n) \cosh(\kappa_n \beta_n) + \kappa_n^5 \alpha_n^3 \beta_n^2 \cos(\kappa_n \alpha_n) \sinh(\kappa_n \beta_n) = 0. \tag{A.19}$$

Then, it can be simplified to frequncy equation of antisymmetric modes in the form

$$\beta_n \tan(\kappa_n \alpha_n) - \alpha_n \tanh(\kappa_n \beta_n) = 0. \tag{A.20}$$

The antisymmetric solution is derived by proposing the antisymmertical parts from Eq.(A.2) as the following form,

$$\begin{aligned} y_n(x) &= C_3 \sin(\kappa_n \alpha_n q) + C_4 \sinh(\kappa_n \beta_n q) \\ &= C_3 \left\{ \sin(\kappa_n \alpha_n q) + \frac{\alpha_n^2 \sin(\kappa_n \alpha_n)}{\beta_n^2 \sinh(\kappa_n \beta_n)} \sinh(\kappa_n \beta_n q) \right\} \\ &= C_3 \sin(\kappa_n \alpha_n) \left\{ \frac{\sin(\kappa_n \alpha_n q)}{\sin(\kappa_n \alpha_n)} + \frac{\alpha_n^2}{\beta_n^2} \frac{\sinh(\kappa_n \beta_n q)}{\sinh(\kappa_n \beta_n)} \right\} \quad . \end{aligned} \tag{A.21}$$

$y_n(x)$ here is homogenous solution of antisymmertic modes and the normalized solution can be rewritten as the similar formula as

$$y_n(x) = \frac{1}{1 + (\alpha_n/\beta_n)^2} \left\{ \frac{\sin(\kappa_n \alpha_n q)}{\sin(\kappa_n \alpha_n)} + \frac{\sinh(\kappa_n \beta_n q)}{\sinh(\kappa_n \beta_n)} \frac{\alpha_n^2}{\beta_n^2} \right\}, \tag{A.22}$$

$n = 2, 4, 6, \ldots$, and the pitch motion is belongs to antisymmetric rigid motion that is included by setting $n = 0$ as

$$y_0(x) = q. \tag{A.23}$$

In conclusion, the complete formula can be expressed as

$$y_n(x) = \begin{cases} \dfrac{1}{1 + (\alpha_n/\beta_n)^2} \left[\dfrac{\cos(\kappa_n \alpha_n q)}{\cos(\kappa_n \alpha_n)} + \dfrac{\cosh(\kappa_n \beta_n q)}{\cosh(\kappa_n \beta_n)} \dfrac{\alpha_n^2}{\beta_n^2} \right] & \text{for} \quad n \quad \text{is odd} \\ \dfrac{1}{1 + (\alpha_n/\beta_n)^2} \left[\dfrac{\sin(\kappa_n \alpha_n q)}{\sin(\kappa_n \alpha_n)} + \dfrac{\sinh(\kappa_n \beta_n q)}{\sinh(\kappa_n \beta_n)} \dfrac{\alpha_n^2}{\beta_n^2} \right] & \text{for} \quad n \quad \text{is even} \end{cases} \tag{A.24}$$

and complete eigen-value equation is presented as:

$$\begin{cases} \alpha_n \tan(\kappa_n \alpha_n) + \beta_n \tanh(\kappa_n \beta_n) = 0 & \text{for} \quad n \quad \text{is odd} \\ \beta_n \tan(\kappa_n \alpha_n) - \alpha_n \tanh(\kappa_n \beta_n) = 0 & \text{for} \quad n \quad \text{is even} \end{cases}, \tag{A.25}$$

where $n = 1, 2, 3, \ldots$. The formation of variable n would be modified slightly in the main body for the purpose of unification.

A.3 Orthogonality of Timoshenko beam

The orthogonality of eigen functions of Timoshenko beam is pointed out by Rensburg and Merwe (2006)[40]. If $[u_1\phi_1]^T$ and $[u_2\phi_2]^T$ correspond to different eigenvalues, then

$$\int_0^1 u_1 u_2 + \frac{1}{\alpha}\int_0^1 \phi_1\phi_2 = 0, \tag{A.26}$$

or

$$\int_0^1 u_1 u_2 = -\frac{1}{\alpha}\int_0^1 \phi_1\phi_2, \tag{A.27}$$

where, u and ϕ are the beam deflection and slope in that paper, respectively.

The relation can be checked by substituting our notations into above equation as

$$\begin{aligned}&\left(\kappa_m^4 - \kappa_n^4\right)\left\{\int_{-1}^1 y_m y_n dq + \gamma^2\int_{-1}^1 \frac{dy_m}{dq}\frac{dy_n}{dq}dq\right\}\\ &= \left[\frac{d^3y_m}{dq^3}q_n - \frac{d^3y_n}{dq^3}q_m - \frac{d^2y_m}{dq^2}\frac{dy_n}{dq} + \frac{d^2y_n}{dq^2}\frac{dy_m}{dq} + \gamma^2\left\{\kappa_m^4\frac{dy_m}{dq}y_n - \kappa_n^4\frac{dy_n}{dq}y_m\right\}\right]_{-1}^1.\end{aligned} \tag{A.28}$$

Therefore, if the eigenfunctions are obtained such that the right-hand side of Eq.(A.28) becomes zero with appropriate boundary conditions imposed, we can say that

$$\left(\kappa_m^4 - \kappa_n^4\right)\left\{\int_{-1}^1 y_m y_n dq + \gamma^2\int_{-1}^1 \frac{dy_m}{dq}\frac{dy_n}{dq}dq\right\} = 0. \tag{A.29}$$

The so-called orthogonality of Timoshenko beam like Eq.(A.27) actually cannot be used in the program since there is no help for calculation so that it is declared that Timoshenko beam is not orthogonal like others. Again, $\gamma = 0$ in the Euler beam can obtain the orthogonality of natural modes of Euler beam.

Appendix B

Restoring Force Coefficient for Elastic Floating Body

This appendix aims to describe how to derive the restoring force coefficient for elastic floating body and its relative explanation.

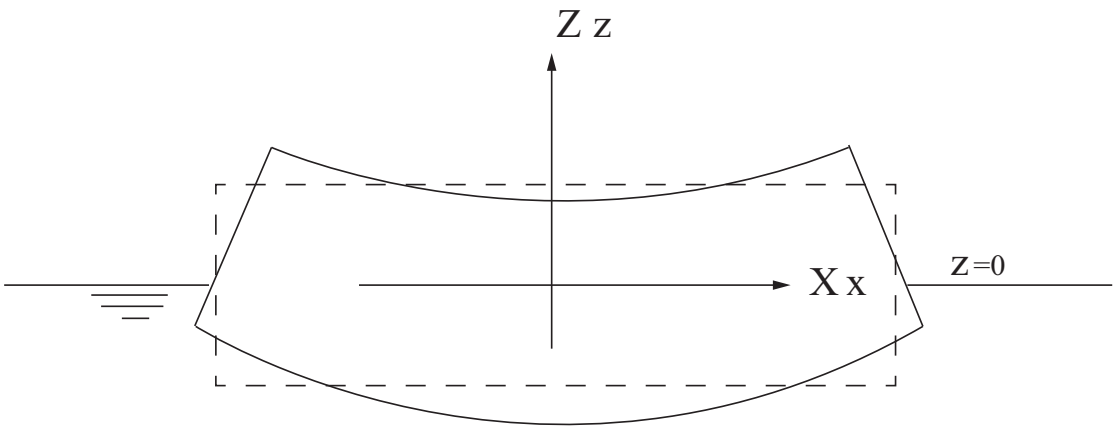

FIGURE B.1: Flexible body motions.

The modal decomposition is assumed for the displacement vector $\boldsymbol{H}$ shown as Eq.(2.38), $\boldsymbol{h}_j$ presented as Eq.(2.40) are the mode shape vectors or mode functions.

B.1 Hydrostatic Pressure Force

The generalized pressure force corresponding to the j-th mode can be expressed as:

$$\boldsymbol{F}_j^H = -\rho g \iint_{\overline{S}_B} z\overline{h}^j \overline{n} dS, \tag{B.1}$$

where the overline "-" sign is used to denote the instantanous value of the corresponding quantity.

Linear theory is assumed to rewrite the above equation on the body position at rest as

$$\boldsymbol{F}_j^H = -\rho g \iint_{\overline{S}_B} (Z + \delta Z)(\boldsymbol{h}^j + \delta \boldsymbol{h}^j)(\boldsymbol{n} + \delta \boldsymbol{n}) dS, \tag{B.2}$$

where δ denotes the change of the corresponding quantity due to rigid or elastic motions. Then, only the linear terms of above equation are extracted to turn in the form of

$$\boldsymbol{F}_j^H = -\rho g \iint_{\overline{S}_B} (\delta Z \boldsymbol{h}^j \boldsymbol{n}) + (Z \delta \boldsymbol{h}^j \boldsymbol{n}) + (Z \boldsymbol{h}^j \delta \boldsymbol{n}) dS = \boldsymbol{F}_j^{Hz} + \boldsymbol{F}_j^{Hh} + \boldsymbol{F}_j^{Hn}. \tag{B.3}$$

Then change of the different quantities can be obtained using the notion of directional derivative which can be written as

$$\delta Z = (\boldsymbol{H}\nabla) Z = \boldsymbol{H}\boldsymbol{k}, \quad \delta \boldsymbol{h}^j = (\boldsymbol{H}\nabla)\boldsymbol{h}^j, \quad \delta N = (\boldsymbol{H}\nabla)\boldsymbol{N}, \tag{B.4}$$

where $\boldsymbol{N} = \boldsymbol{n} dS$ and the operator $\boldsymbol{H}\nabla$ is defined by

$$\boldsymbol{H}\nabla = H_x \frac{\partial}{\partial X} + H_y \frac{\partial}{\partial Y} + H_z \frac{\partial}{\partial Z} = \sum_{j=1}^{N} X_j (h_x^j \frac{\partial}{\partial X} + h_y^j \frac{\partial}{\partial Y} + h_z^j \frac{\partial}{\partial Z}), \tag{B.5}$$

In the case of the normal vector $\boldsymbol{N}$, since the normal vector is unknown in an explicit form, some clarifications are necessary. If the equation of the body surface is written in its parametric form:

$$\boldsymbol{R}(u, v) = X(u, v)\boldsymbol{i} + Y(u, v)\boldsymbol{j} + Z(u, v)\boldsymbol{k}. \tag{B.6}$$

The normal vector direction is defined by the following vertor product:

$$\boldsymbol{N} = \frac{\partial \boldsymbol{R}}{\partial u} \times \frac{\partial \boldsymbol{R}}{\partial v}. \tag{B.7}$$

Knowing that $(\boldsymbol{H}\nabla)\boldsymbol{R} = \boldsymbol{H}$ we deduce:

$$\delta \boldsymbol{N} = \frac{\partial \boldsymbol{H}}{\partial u} \times \frac{\partial \boldsymbol{R}}{\partial v} + \frac{\partial \boldsymbol{R}}{\partial u} \times \frac{\partial \boldsymbol{H}}{\partial v}, \tag{B.8}$$

which can be rewritten in the following form:

$$\begin{aligned}\delta \boldsymbol{N} &= \left[\left(\frac{\partial H_z}{\partial Z}+\frac{\partial H_y}{\partial Y}\right)N_x-\frac{\partial H_y}{\partial X}N_y-\frac{\partial H_z}{\partial X}N_z\right]\boldsymbol{i}\\ &+ \left[-\frac{\partial H_x}{\partial Y}N_x+\left(\frac{\partial H_x}{\partial X}+\frac{\partial H_z}{\partial Z}\right)N_y-\frac{\partial H_z}{\partial Y}N_z\right]\boldsymbol{j}\\ &+ \left[-\frac{\partial H_x}{\partial Z}N_x-\frac{\partial H_y}{\partial Z}N_y+\left(\frac{\partial H_y}{\partial Y}+\frac{\partial H_x}{\partial X}\right)N_z\right]\boldsymbol{k}. \end{aligned} \tag{B.9}$$

Then, using Eqs.(B.4)(B.5) and (B.9), the parts of resoring force coefficient $C_{ij}^{H}=C_{ij}^{Hz}+C_{ij}^{Hh}+C_{ij}^{Hn}$ can be expressed as

$$C_{ij}^{Hz} = \rho g\iint_{S_B} h_z^j(h_x^i n_x+h_y^i n_y+h_z^i n_z)dS, \tag{B.10}$$

$$\begin{aligned}C_{ij}^{Hh} &= \rho g\iint_{S_B} z\left[\left(h_x^j\frac{\partial h_x^i}{\partial x}+h_y^j\frac{\partial h_x^i}{\partial y}+h_z^j\frac{\partial h_x^i}{\partial z}\right)n_x\right.\\ &+ \left(h_x^j\frac{\partial h_y^i}{\partial x}+h_y^j\frac{\partial h_y^i}{\partial y}+h_z^j\frac{\partial h_y^i}{\partial z}\right)n_y\\ &+ \left.\left(h_x^j\frac{\partial h_z^i}{\partial x}+h_y^j\frac{\partial h_z^i}{\partial y}+h_z^j\frac{\partial h_z^i}{\partial z}\right)n_z\right], \end{aligned} \tag{B.11}$$

$$\begin{aligned}C_{ij}^{Hn} &= \rho g\iint_{S_B} z\left\{\left[\left(\frac{\partial h_y^j}{\partial y}+\frac{\partial h_z^j}{\partial z}\right)n_x-\frac{\partial h_y^j}{\partial x}n_y-\frac{\partial h_z^j}{\partial x}n_z\right]h_x^i\right.\\ &+ \left[-\frac{\partial h_x^j}{\partial y}n_x+\left(\frac{\partial h_x^j}{\partial x}+\frac{\partial h_z^j}{\partial z}\right)n_y-\frac{\partial h_z^j}{\partial y}n_z\right]h_y^i\\ &+ \left.\left[-\frac{\partial h_x^j}{\partial z}n_x-\frac{\partial h_y^j}{\partial z}n_y+\left(\frac{\partial h_x^j}{\partial x}+\frac{\partial h_y^j}{\partial y}\right)n_z\right]h_z^i\right\}dS. \end{aligned} \tag{B.12}$$

The resulting expressions are not simple and are rewritten as the following expressions briefly by using Einstein summation convention,

$$\begin{aligned}C_{ij}^{H} &= \rho g\iint_{S_H} h_z^j\widetilde{n}_i dS\\ &+ \rho g\iint_{S_H} z\left\{\frac{\partial h_k^j}{\partial x_k}\widetilde{n}_i+\left(h_k^j\frac{\partial h_l^i}{\partial x_k}-h_k^i\frac{\partial h_l^i}{\partial x_k}\right)\widetilde{n}_l\right\}dS. \end{aligned} \tag{B.13}$$

B.2 Gravity Forces

The gravity force should be taken into account to obtain complete restoring force coefficient for elastic motions. The generalized gravity froce associated with each mode can be defined to

$$\boldsymbol{F}_i^m = -\iiint_V g\delta\boldsymbol{h}^i\boldsymbol{k}dm. \tag{B.14}$$

Then, the correspoding coefficient becomes:

$$C_{ij}^{m} = \iiint_{V} g\left(h_x^j \frac{\partial h_z^i}{\partial x} + h_y^j \frac{\partial h_z^i}{\partial y} + h_z^j \frac{\partial h_z^i}{\partial z}\right) dm. \tag{B.15}$$

Thus, the final expression of restoring force coefficient C_{ij} is

$$C_{ij} = C_{ij}^{Hz} + C_{ij}^{Hh} + C_{ij}^{Hn} + C_{ij}^{m}. \tag{B.16}$$

Appendix C

Comparison with Experiments at Zero Speed

In the present study, the Legendre polynomials and the dry eigen-modes obtained by eigen-value analysis are applied in the numerical computations for both Euler beam and Timoshenko beam. As a validation process of the proposed method, computed results are compared with measured results from the experiment conducted by Malenica et al. (2003) [3] and numerical results obtained by Kim et al. (2009) [10, 11]. The numerical results of Kim et al. are obtained using the direct coupling scheme between the time-domain Rankine panel method and the one-dimensional finite element method (FEM). The experiment measuring the vertical bending of an elastic barge model was conducted in BGO-First (Toulon, France) to validate the developed numerical code for the hydroelastic response (Malenica et al. 2003). The shape of the barge model is shown in Fig.C.1. As shown in this figure, the barge model is composed of several small floaters that have $0.19m$ in length, $0.6m$ in breadth, $0.25m$ in depth, and $0.12m$ in draft. A small gap ($0.015m$) exists between adjacent floaters to prevent the collapse of each body and they are connected by two long plates on the top of the barge that has low flexural rigidity. In the experiment, the optical sensors (KRYPTON system) were installed on the deck of a floater and the vertical motion RAO (Response amplitude operator) was measured at 7 points in head waves, as indicated in Fig.C.1.

The results of RAO at each point (except for No.12) are summarized in Figs.C.2-C.7. Computed resutls in the present study are shown for both approximation using the Euler beam and the Timoshenko beam, and for each approximation of the barge, both legendre polynomials and dry eigen-modes are used independently as the mode functions in the mode-expansion method. The present numerical results are in good agreement with both experimental data and numerical

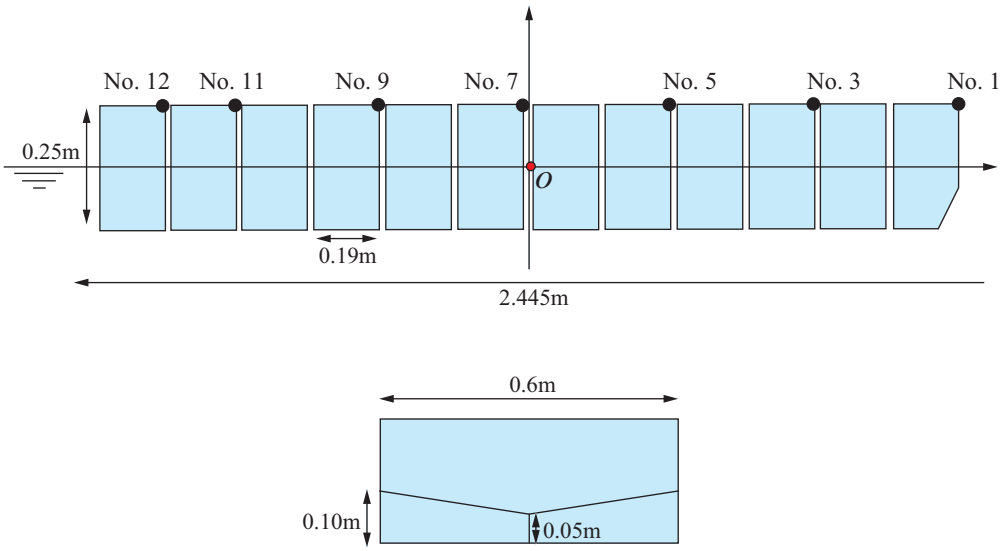

FIGURE C.1: Side view of the barge model used in the experiment.

results by Kim et al. [10, 11]. It is also confirmed that the resulting using the Legendre polynomials agree well with the corresponding results using the dry eigen-modes without substantial difference for both approximations with Euler beam and Timoshenko beam.

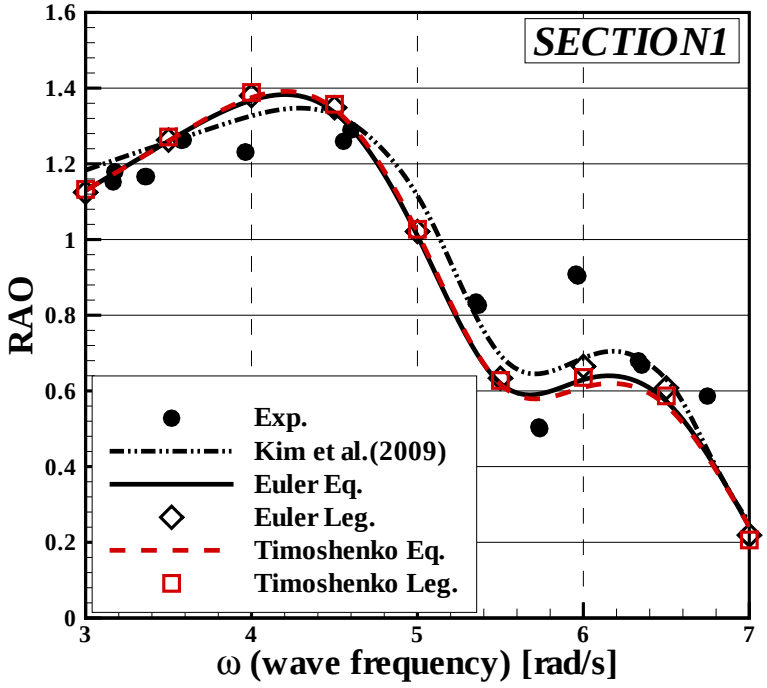

FIGURE C.2: Vertial displacement RAO of a barge model at point 1 in head waves.

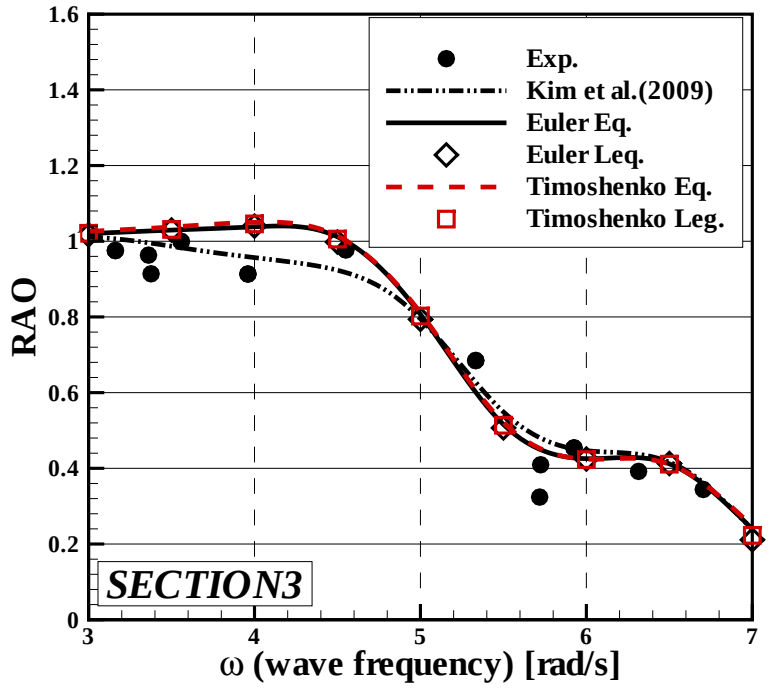

FIGURE C.3: Vertial displacement RAO of a barge model at point 3 in head waves.

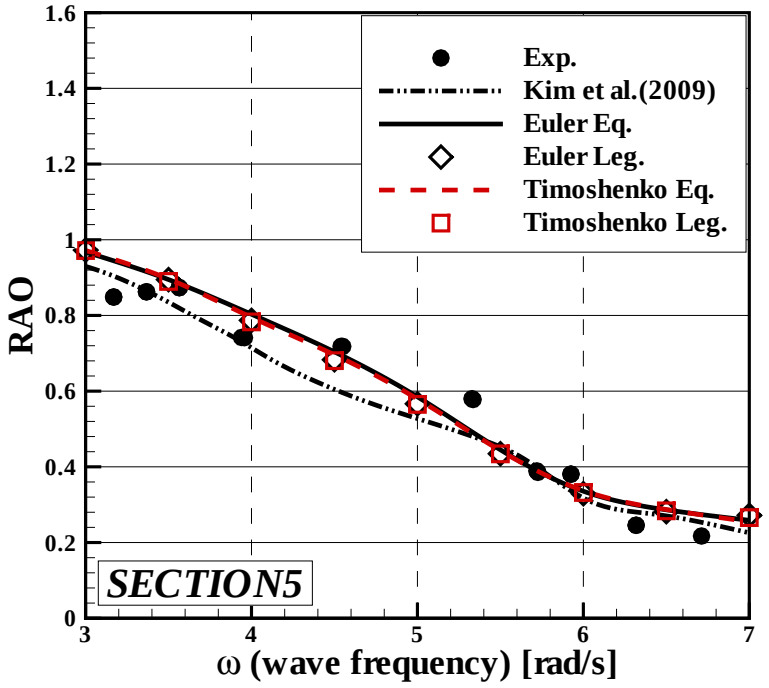

FIGURE C.4: Vertial displacement RAO of a barge model at point 5 in head waves.

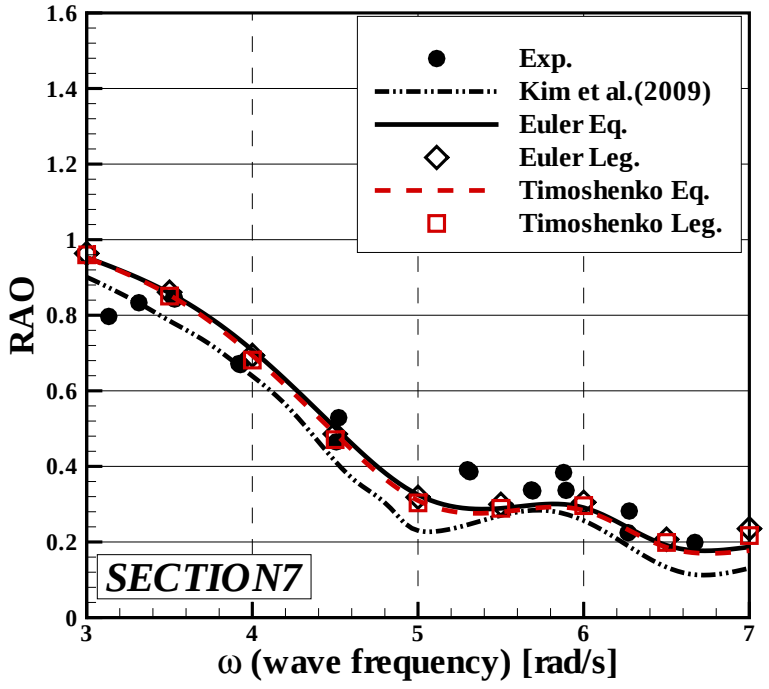

FIGURE C.5: Vertial displacement RAO of a barge model at point 7 in head waves.

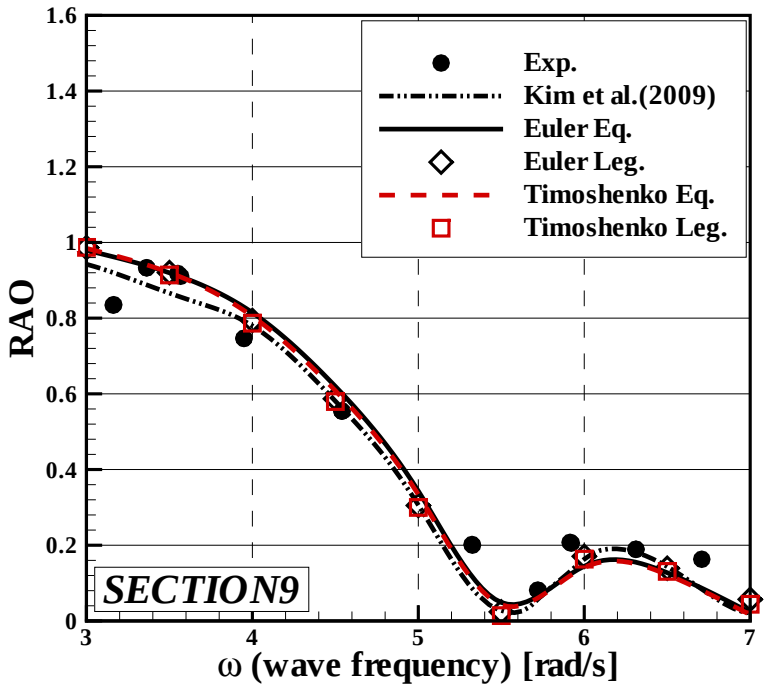

FIGURE C.6: Vertial displacement RAO of a barge model at point 9 in head waves.

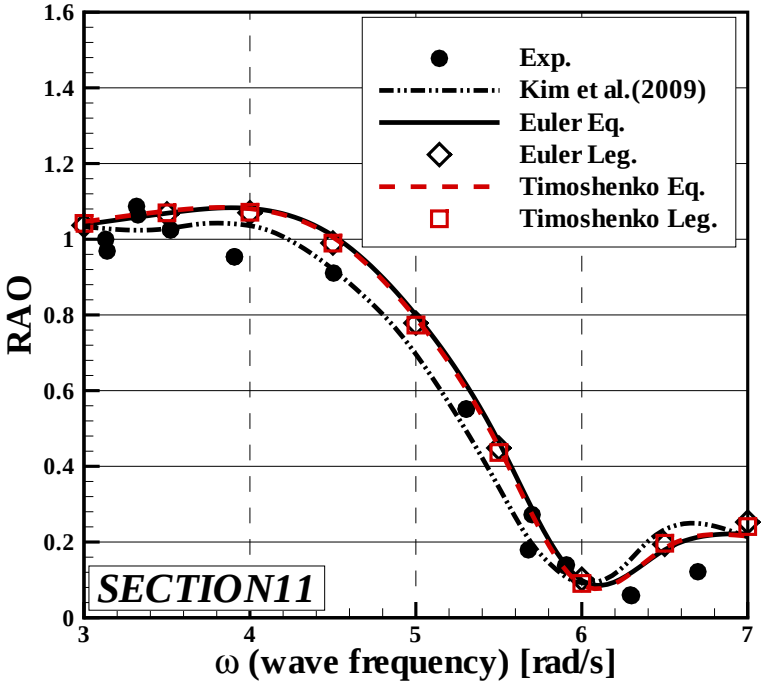

FIGURE C.7: Vertial displacement RAO of a barge model at point 11 in head waves.

Bibliographies

[1] R.E.D. Bishop and W.G. Price. Hydroelasticity of ships. *Cambridge University Press*, 1979.

[2] J.J. Jensen and M. Dogliani. Wave-induced ship full vibrations in stochastic seaways. *Marine Structures*, 9:353–387, 1996.

[3] $\check{S}$. Malenica. Hydroelastic response of a barge to impulsive and non-impulsive wave loads. *Hydroelasticity in Marine Technology, Oxford, UK*, pages 107–115, 2003.

[4] K. Kim and Y. Kim. Numerical analysis on ship hydroelasticity by using 3d rankine panel method and 3d finite element method. *Hydroelasticity in Marine Technology, Tokyo, Japan*, pages 21–40, 2012.

[5] $\check{S}$. Malenica and Q. Derbane. Hydro-elastic issues in the design of ultra large container ships-tulcs project. *Hydroelasticity in Marine Technology, Tokyo, Japan*, pages 233–246, 2012.

[6] Y. Kim and J. Kim. Benchmark study on motions and loads of a 6750-teu containership. *Ocean Engineering*, 119:262–273, 2016.

[7] D.M. Park, J.H. Kim, and Y. Kim. Numerical analysis on added resistance of hydroelastic body in waves. *Proceedings of International Workshop on Water Waves and Floating Bodie, Dalian, China*, pages 165–168, 2017.

[8] J.L. Jiao, Z.Y. Chen, C.H. Chen, and H.L. Ren. Timedomain hydroelastic analysis of nonlinear motions and loads on a large bowfare ship advancing in high irregular seas. *Journal of Marine Science and Technology*, 25:426–454, 2020.

[9] E.N. Dvorkin, D. Celentano, A. Cuitino, and G. Gioia. A vlasov beam element. *Applied Ocean Research*, 33(1):187–196, 1989.

[10] Y. Kim, K.H. Kim, and Y. Kim. Analysis of hydroelasticity of floating shiplike structure in time domain using a fully coupled hybrid bem-fem. *Journal of Ship Research*, 53:31–47, 2009.

[11] Y. Kim, K.H. Kim, and Y. Kim. Springing analysis of a seagoing vessel using fully coupled bem-fem in the time domain. *Ocean Engneering*, 36(11):785–796, 2009.

[12] K.H. Shin, J.W. Hirdaris, S.G. Jeong, and J.B. Park. Two-and three-dimensional springing analysis of a 16,000 teu container ship in regular waves. *Ships and Offshore Sturctures*, 10(5):498–509, 2009.

[13] A. Bokaian. Natural frequencies of beams under compressive axial loads. *Journal of sound and vibration*, 126(1):49–65, 1988.

[14] S.H. Farchaly and M.G. Shebl. Exact frequency and mode shape formulae for studying vibration and stability of timoshenko beam system. *Journal of sound and vibration*, 180(2):205–227, 1995.

[15] L. Majkut. Free and forced vibrations of timoshenko beams described by single difference equation. *Journal of Theoretical and Applied Mechanics*, 47(1):193–210, 2009.

[16] I. Senjanović, N. Vladimir, M. Tomic, N. Hadžić, and Š. Malenica. Global hydroelastic analysis of ultra large container ships by improved beam structural model. *International Journal of Naval Architecture and Ocean Engineering*, 6(4):1041–1063, 2014.

[17] N. Datta and M.A. Siddiqui. Hydroelastic analysis of axially loaded timoshenko beams with intermediate end fixities under hydrodynamic slamming loads. *Ocean Engineering*, 127:124–134, 2016.

[18] J.N. Newman. Wave effects on deformable bodies. *Applied ocean research*, 16(1):47–59, 1994.

[19] D. Zhou, Y.K. Cheung, S.H. Lo, and F.T.K. Au. Threedimensional vibration analysis of rectangular thick plates on pasternak foundation. *International journal for numerical methods in engineering*, 59(10):1313–1334, 2002.

[20] H.K. Kim and M.S. Kim. Vibration of beams with generally restrained boundary conditions using fourier series. *Journal of Sound and Vibration*, 245(5):771–784, 2001.

[21] M. Kashiwagi. A direct method versus a mode-expansion method for calculating hydroelastic response of a vlfs in waves. *The Eighth International Offshore and Polar Engineering Conference*, 1998.

[22] X. Lin and M. Takaki. A b-spline element method for predicting the hydroelastic responses of a very large floating structure in waves. *Journal of the Society of Naval Architects of Japan*, 1998(183):219–225, 1998.

[23] D.C. Hong and S.Y Hong. Hydroelastic responses and drift forces of a very-long floating structure equipped with a pin-connected oscillating-water-column breakwater system. *Ocean engineering*, 34(5-6):696–708, 2007.

[24] J.V. Wehausen and E.V. Laitone. Surface waves. *In Encyclopedia of Physics*, 9, 1960.

[25] C.W. Dawson. A practical computer method for solving ship-wave problems. *Proceedings of 2nd International Conference on Numerical Ship Hydrodynamics, California, Berkeley*, 19:30–38, 1977.

[26] P.D. Sclavounos and D.E. Nakos. Ship motions by a three-dimensional rankine panel method. *Proceedings of 18th Symposium on Naval Hydrodynamics, Ann Arbor*, pages 21–40, 1990.

[27] M.K. Wu and T. Moan. Ship motion by a rankine source method. *Ship Technolog Research*, 37:143–152, 1990.

[28] M. Kashiwagi, S. Kuga, and S. Chimoto. Time-and frequency-domain calculation methods for ship hydroelasticity with forward speed. *Proceedings of the 7th International Conference on Hydroelasticity in Marine Technology, Split, Croatia*, 2015.

[29] K. Heo K and M. Kashiwagi. A numerical study of second-order springing of an elastic body using higher-order boundary element method (hobem). *Applied Ocean Research*, 93:101903, 2019.

[30] H. Iwashita, M. Kashiwagi, Y. Ito, and Y. Seki. Calculations of ship seakeeping in low-speed/low-frequency range by frequency-domain rankine panel methods. *Journal of the Japan Society of Naval Architects and Ocean Engineers*, 24:129–146, 2016.

[31] E. Yasuda, H. Iwashita, and M. Kashiwagi. Improvement of rankine panel method for seakeeping prediction of a ship in low frequency region. *In International Conference on Offshore Mechanics and Arctic Engineering*, 49989:V007T06A001, 2016.

[32] Š. Malenica, I. Senjanović, S. Tomašević, and E. Stumpf. Some aspects of hydroelastic issues in the design of ultra large container ships. *Proceedings of International Workshop on Water Waves and Floating Bodies*, 2007.

[33] I. Senjanović, Š. Malenica, and S. Tomas. Investigation of ship hydroelasticity. *Ocean Engineering*, 35(5–6):523–535, 2008.

[34] Š. Malenica, B. Molin, J.T. Twitman, F. Bigot, and I. Senjanović. Some aspects of hydroelastic restoring for elastic bodies. *Proceedings of International Workshop on Water Waves and Floating Bodies, Saint Petersbourg, Russia*, 2009.

[35] Y. Hong, K. Heo, and M. Kashiwagi. Hydroelastic analysis of a ship with forward speed using orthogonal polynomials as mode functions of timoshenko beam. *Applied Ocean Research*, 112, 2021.

[36] M. Kashiwagi. A b-spline galerkin scheme for calculating the hydroelastic response of a very large floating structure in waves. *Journal of marine science and technology*, 3(1):37–49, 1998.

[37] Y. Hong, M. Kashiwagi, and K. Heo. Numerical calculations of wave-induced hydroelastic response of a ship with forward speed using legendre polynomials as mode functions. *In The 30th International Ocean and Polar Engineering Conference*, 2020.

[38] M. Kashiwagi, Y. Hong, and K. Heo. Ship hydroelasticity analysis with timoshenko-beam approximation using legendre and chebyshev polynomials. *The 36th Intl Workshop on Water Waves and Floating Bodies, Seoul, Korea*, 1000(1):1, 2021.

[39] L. Fox and I.B. Parker. Chebyshev polynomials in numerical analysis[r]. 519.4(F6), 1968.

[40] N.F.J. Van Rensburg and A.J. Van der Merwe. Natural frequencies and modes of a timoshenko beam. *Wave motion*, 127:58–69, 2006.